

1 **Divergent metabolism between *Trypanosoma***  
2 ***congolense* and *Trypanosoma brucei* results in**  
3 **differential drug sensitivity**

4  
5 P. C. Steketee<sup>1\*</sup>, E. A. Dickie<sup>2</sup>, J. Iremonger<sup>1</sup>, K. Crouch<sup>2</sup>, E. Paxton<sup>1</sup>, S. Jayaraman<sup>1</sup>, O. A.  
6 Alfituri<sup>1</sup>, G. Awuah-Mensah<sup>3</sup>, R. Ritchie<sup>2</sup>, A. Schnauffer<sup>4</sup>, H. P. de Koning<sup>5</sup>, C. Gadelha<sup>3</sup>, B.  
7 Wickstead<sup>3</sup>, M. P. Barrett<sup>2,6</sup> and L. J. Morrison<sup>1</sup>

8 <sup>1</sup>The Roslin Institute, Royal (Dick) School of Veterinary Studies, University of Edinburgh,  
9 Edinburgh, UK

10 <sup>2</sup>Wellcome Centre for Integrative Parasitology, Institute of Infection, Immunity and  
11 Inflammation, University of Glasgow, Glasgow, UK

12 <sup>3</sup>School of Life Sciences, University of Nottingham, Nottingham, UK

13 <sup>4</sup>Institute of Immunology and Infection Research, University of Edinburgh, Edinburgh, UK

14 <sup>5</sup>Institute of Infection, Immunity and Inflammation, University of Glasgow, Glasgow, UK

15 <sup>6</sup>Glasgow Polyomics, University of Glasgow, UK

16 \*Corresponding author: [Pieter.Steketee@ed.ac.uk](mailto:Pieter.Steketee@ed.ac.uk)

17

18

## 19 **Abstract**

20 Animal African Trypanosomiasis (AAT) is a debilitating livestock disease prevalent across  
21 sub-Saharan Africa, a main cause of which is the protozoan parasite *Trypanosoma*  
22 *congolense*. In comparison to the well-studied *T. brucei*, there is a major paucity of  
23 knowledge regarding the biology of *T. congolense*. Here, we use a combination of omics  
24 technologies and novel genetic tools to characterise core metabolism in *T. congolense*  
25 mammalian-infective bloodstream-form parasites, and test whether metabolic differences  
26 compared to *T. brucei* impact upon drug sensitivity. Like *T. brucei*, glycolysis plays a major  
27 part in *T. congolense* energy metabolism. However, the rate of glucose uptake is  
28 significantly reduced in *T. congolense*, with cells remaining viable when cultured in  
29 concentrations as low as 2 mM. Instead of pyruvate, the primary glycolytic endpoints are  
30 succinate, malate and acetate. Comparative transcriptomics analysis showed higher levels  
31 of activity associated with the mitochondrial pyruvate dehydrogenase complex, acetate  
32 generation and the succinate shunt in *T. congolense*. However, based on omics analysis  
33 and chemical inhibition, there does not appear to be significant levels of oxidative  
34 phosphorylation. Stable-isotope labelling of glucose enabled the comparison of carbon  
35 usage between *T. brucei* and *T. congolense*, highlighting differences in nucleotide and fatty  
36 acid metabolism. To validate the metabolic similarities and differences, both species were  
37 treated with pharmacological inhibitors, confirming a lack of essential electron transport  
38 chain activity in *T. congolense*, but increased sensitivity to inhibition of mitochondrial  
39 pyruvate import. Strikingly, *T. congolense* exhibited significant resistance to inhibitors of fatty  
40 acid synthesis, including a 780-fold greater EC<sub>50</sub> against the lipase and fatty acid synthase  
41 inhibitor Orlistat, compared to *T. brucei*. These data highlight that bloodstream form *T.*  
42 *congolense* diverges from *T. brucei* in key areas of metabolism, with several features that  
43 are intermediate between bloodstream- and insect-stage *T. brucei*. These results have  
44 implications for drug development, mechanisms of drug resistance and host-pathogen  
45 interactions.

## 46 **Introduction**

47 The hemoflagellate protozoan parasite *Trypanosoma congolense* is a primary causative  
48 agent of animal African trypanosomiasis (AAT), which can also be caused by *T. vivax* and *T.*  
49 *brucei* [1]. AAT accounts for livestock deaths in excess of 3 million annually with up to 120  
50 million cattle at risk [2-4]. Thus, AAT is one of the most important livestock diseases across  
51 sub-Saharan Africa.

52 Current methods of AAT control centre around chemotherapy and prophylaxis (reviewed in  
53 [3]), but the very few available veterinary trypanocidal drugs have been used extensively for  
54 decades, resulting in resistance and inadequate protection against AAT [5-7]. As such, there  
55 is a dire need for the development of new and improved chemotherapeutics to manage AAT  
56 [3, 8].

57 Most of our biological understanding of African trypanosomes derives from studies on *T.*  
58 *brucei*, subspecies of which, *T. b. gambiense* and *T. b. rhodesiense*, cause Human African  
59 Trypanosomiasis (HAT) [9]. The ability to culture both procyclic (PCF; tsetse fly) and  
60 bloodstream (BSF; mammalian) forms of *T. brucei in vitro*, combined with its tractability with  
61 respect to genetic manipulation, have enabled extensive study of this species on a molecular  
62 level [10, 11]. In stark contrast, very few *T. congolense* strains are amenable to continuous  
63 bloodstream form (BSF) culture, with a single strain (IL3000) used in most studies [12].  
64 Whilst genetic modification is possible in *T. congolense* PCF stage, routine BSF transfection  
65 has only recently become possible [13-15]. Additionally, although *T. congolense* exhibits a  
66 superficially similar morphology and life cycle to *T. brucei* [16, 17] emerging evidence  
67 increasingly suggests that *T. brucei*, *T. congolense* and *T. vivax* exhibit some profound  
68 differences at the genomic level [18-22], including in genes and phenotypes of direct  
69 relevance to infection biology and disease epidemiology. However, there is a lack of  
70 understanding to what extent these genetic differences translate into biological differences,  
71 including with respect to metabolism.

72 Understanding metabolism is critical to identifying how pathogens survive and thrive in the  
73 varying host environments they encounter, as well as being a means of elucidating drug  
74 targets, modes of drug action and mechanisms of drug resistance [23-25]. *T. brucei*  
75 metabolism has been extensively studied, aided by the application of technologies such as  
76 liquid chromatography-mass spectrometry (LC-MS) and nuclear magnetic resonance (NMR)  
77 spectroscopy (reviewed in detail by [26, 27]), which enable global profiling of the cellular  
78 metabolome.

79 The BSF stage of *T. brucei* utilizes the high levels of glucose available in the mammalian  
80 bloodstream, and depends almost exclusively on the glycolytic pathway to generate ATP  
81 [28]. The first seven steps of glycolysis are encompassed by a specialized organelle, the  
82 glycosome, which maintains its own ATP/ADP and NAD/NADH balance, allowing glycolysis  
83 to proceed at an extraordinarily high rate in comparison to other eukaryotic cells [29]. The  
84 endpoint of glycolysis, pyruvate, is a primary waste product of *T. brucei*, and excreted from  
85 the cell in large quantities. As a result, only small amounts of pyruvate are further  
86 metabolized in the mitochondrion to acetyl-CoA by pyruvate dehydrogenase (PDH), with

87 acetate the main excretory metabolite in this secondary, yet essential pathway [30]. The  
88 acetyl-CoA generated from this pathway is utilized, at least partially, for the *de novo*  
89 synthesis of fatty acids [31]. Indeed, both BSF and PCF *T. brucei* are highly sensitive to the  
90 lipase and fatty acid synthase inhibitor Orlistat [32].

91 Conversely, in the absence of blood meals, glucose is scarce in the tsetse fly midgut [33],  
92 and the main energy source of PCF *T. brucei* is L-proline, the catabolism of which leads to  
93 production of acetate, succinate and L-alanine through a more developed and active  
94 mitochondrion (including an active respiratory chain capable of generating ATP, as opposed  
95 to the inactive respiratory chain in BSF *T. brucei* [34]). Until recently, it was thought that PCF  
96 *T. brucei* did not exhibit active TCA metabolism, although recent data have shown that TCA  
97 intermediates such as succinate and 2-oxoglutarate can stimulate PCF *T. brucei* growth. [35-  
98 37].

99 Among the glycolytic enzymes, *T. brucei* expresses three isoforms of phosphoglycerate  
100 kinase, which catalyze the conversion of 1,3-bisphosphoglycerate to 3-phosphoglycerate  
101 [38]. These are developmentally regulated, with the major isoform in BSF parasites present  
102 in the glycosome (PGK-C), whilst the primary PCF isoform is found in the cytosol (PGK-B)  
103 [39]. The localization of PGK-B in the PCF cytosol is thought to result in an ATP/ADP  
104 imbalance in the glycosome, which is rectified by upregulating the glycosomal “succinate  
105 shunt”, a pathway that includes the ATP-generating phospho*enol*pyruvate carboxykinase  
106 (PEPCK)- and pyruvate phosphate dikinase (PPDK)-mediated conversion of  
107 phospho*enol*pyruvate (PEP) to oxaloacetate and pyruvate respectively [39, 40]. The  
108 succinate shunt, combined with amino acid metabolism, results in the excretion of high  
109 levels of succinate in PCF *T. brucei* [41].

110 Stable isotope labelling data has revealed that BSF *T. brucei* utilize D-glucose to a greater  
111 extent than first realized, with heavy carbons disseminating into amino acid, lipid and  
112 nucleotide metabolism [42]. This study also showed that some of the succinate and malate  
113 excreted from BSF parasites originates from glycolysis and, unexpectedly, inhibition of  
114 PEPCK is lethal at this life-cycle stage [42]. It has also been shown that acetate production  
115 is essential to BSF *T. brucei*, in particular for the synthesis of fatty acids (FAs) [30].  
116 However, acetate excretion, as well as that of succinate and malate, is negligible in BSF *T.*  
117 *brucei* compared to that of pyruvate and L-alanine.

118 In contrast to *T. brucei*, the literature on metabolism in *T. congolense* is scarce. More than  
119 half a century ago it was suggested that BSF *T. congolense* has a significantly lower rate of  
120 glucose consumption compared to BSF *T. brucei* [43]. Furthermore, pyruvate is not the main  
121 glycolytic end product and instead, acetate and succinate are excreted at high levels,

122 indicative of metabolism more akin to PCF *T. brucei* [43]. Further work has revealed  
123 additional differences that support this hypothesis [44-46]. For example, BSF *T. congolense*  
124 primarily expresses cytosolic PGK-C, rather than glycosomal PGK-B [46]. Microscopy has  
125 also revealed a more developed mitochondrion in BSF *T. congolense*, with visible cristae,  
126 suggesting that mitochondrial energy metabolism could play a more prominent role in BSF *T.*  
127 *congolense* [47]. The high levels of acetate excretion first shown by Agosin & Von Brand [43]  
128 are consistent with this hypothesis. However, other studies have shown that BSF *T.*  
129 *congolense* is sensitive to inhibitors of Trypanosome Alternative Oxidase (TAO), including  
130 salicylhydroxamide (SHAM); and is insensitive to cyanide, suggesting that, as for BSF *T.*  
131 *brucei*, TAO is the sole terminal oxidase, responsible for reoxidising glycerol 3-phosphate, in  
132 BSF *T. congolense* [48-51]. Notably, nitroblue tetrazolium staining of BSF *T. congolense*  
133 does indicate the presence of NADH dehydrogenase (complex I) activity [48]. However, to  
134 date, no studies have assessed BSF *T. congolense* sensitivity to chemical inhibition of the  
135 electron transport chain, or the F<sub>1</sub>F<sub>0</sub>-ATPase.

136 Post-genomic technologies allow for the generation of large datasets that enable analysis of  
137 cellular processes on a systems scale, including metabolomics and transcriptomics.  
138 Integration of these data can provide a detailed snapshot of cell metabolism at the transcript  
139 and metabolite levels and help to dissect differences between species or conditions in  
140 unprecedented detail [52]. Furthermore, this knowledge can aid in predication and  
141 understanding of drug efficacy and mode of action

142 This study aimed to generate the first comprehensive overview of the metabolome of  
143 bloodstream-form *T. congolense* IL3000 parasites, allowing a global metabolic comparison  
144 of differences between *T. congolense* and *T. brucei*. Glycolytic metabolism in BSF *T.*  
145 *congolense* appears to be similar to PCF *T. brucei*, particularly in terms of metabolic outputs  
146 and gene expression. However, there are pronounced differences in parasite reliance on  
147 exogenous amino acids as well as carbon dissemination into pathways involved in  
148 nucleotide and lipid metabolism, as shown by stable isotope-labelled metabolomics. Using  
149 these data, we further validated these metabolic differences in *T. congolense* by  
150 pharmacological inhibition, which highlighted increased sensitivity to inhibition of  
151 mitochondrial pyruvate uptake, as well as significant resistance to inhibition of fatty acid  
152 synthesis, tested using inhibitors of fatty acid synthase and acetyl-coA synthetase. Taken  
153 together, these results suggest that *T. congolense* and *T. brucei* differ in some fundamental  
154 aspects of their core metabolism, which has important implications in terms drug sensitivity,  
155 and therefore, development of novel chemotherapeutics.

## 156 **Results**

### 157 **Comparative RNA-sequencing of *T. congolense* and *T. brucei***

158 To permit direct comparison of BSF *T. congolense* and *T. brucei* at the transcriptome level,  
159 RNAseq analysis was carried out on parasites cultured *in vitro* and trypanosome samples  
160 isolated from infected mice at first peak parasitaemia (*ex vivo*) (Fig 1). Samples were  
161 prepared using *T. congolense* (strain IL3000, *in vitro* and *ex vivo*) and pleomorphic *T. brucei*  
162 (strain STIB 247; *in vitro* and *ex vivo*), to assess similarities and differences between  
163 trypanosomes grown in culture and those from an infection (Fig 1A and 1B), and to compare  
164 and contrast the transcriptome across the species (Fig 1C and 1D). Sequencing data were  
165 aligned to the respective genome sequence with a mean overall alignment rate of  $88.0 \pm$   
166  $2.3\%$  and  $94.1 \pm 0.7\%$  for *T. brucei* and *T. congolense* reads, respectively. Resultant files  
167 were sorted and filtered for quality, and to minimize artefacts from multigene families, only  
168 uniquely aligned reads were used for downstream analyses. Read counts were normalised  
169 using transcripts per million (TPM) [53]. Orthologues were inferred between the species  
170 using Orthofinder [54], in order to compare directly TPM values for 1-to-1 orthologues, as  
171 well as sum-of-TPM values for groups containing families of paralogues (e.g. hexose  
172 transporters). These normalised read counts are henceforth referred to as orthoTPM values  
173 (S1 Table). The Orthofinder dataset (S2 Table) consisted of 6,677 orthogroups (denoted with  
174 the prefix “TbTc”), of which 5,398 (80.84%) were 1-to-1 orthologues. The Orthofinder tool  
175 was also used to predict genes only present in one of the two species (S2 Table). There are  
176 several metabolic genes that are not present in the *T. congolense* genome, including  
177 putative delta-4 and delta-6 desaturases (Tb927.10.7100 & Tb11.v5.0580), a succinate  
178 dehydrogenase subunit (SDH11; Tb927.8.6890) and guanine deaminase (Tb927.5.4560,  
179 Tb05.5K5.200 & Tb11.v5.0409), in addition to mitochondrial pyruvate carrier 1 (MPC1;  
180 Tb927.9.3780) (S2 Table).

181 Differences between four sample groups were assessed based on orthoTPM values (Fig 1;  
182 full dataset in S1 Table). There was a strong intra-species correlation between the *in vitro*  
183 and *ex vivo* conditions at the transcriptome level (*T. congolense* Pearson correlation  
184 coefficient,  $\rho = 0.765$ , Fig 1A; *T. brucei*  $\rho = 0.803$ , Fig 1B), showing that *in vitro*-derived BSF  
185 *T. congolense* and *T. brucei* closely resemble parasites isolated from infections at the  
186 transcriptome level. However, correlations between species even in the same condition were  
187 lower, implying transcriptional differences between the species (*ex vivo*:  $\rho = 0.651$ , Fig 1C; *in*  
188 *vitro*:  $\rho = 0.687$ , Fig 1D).

189 To compare data from this study to BSF *T. congolense* transcriptomics data generated by  
190 Silvester *et al.* (generated at ascending and peak parasitaemia [55]), TPM values for each

191 annotated *T. congolense* gene were compared directly (S1 Fig, S3 Table). There was good  
192 correlation between both *in vitro* and *ex vivo* *T. congolense* BSF datasets and the data from  
193 Silvester *et al.* ( $p > 0.8$ , S1 Fig), with the highest correlation being between the *ex vivo* and  
194 ascending data as expected ( $p = 0.897$ , S1 Fig), albeit the correlation between the  
195 'ascending' and 'peak parasitaemia' in Silvester *et al.* was higher ( $p = 0.979$ , S1 Fig).

## 196 ***T. congolense* metabolite consumption and output**

197 Global metabolite (metabolomics) analysis of *in vitro* culture supernatant samples provides a  
198 detailed insight into the metabolic inputs and outputs of cultured cells [56]. However, high  
199 levels of medium components can often mask subtle but significant changes in culture  
200 medium composition over time. To counteract this, a modified culture medium was designed  
201 for *T. congolense* strain IL3000, based on previous published medium formulations (SCM-3;  
202 for details see Materials and Methods) [14, 15].

203 A time course was initiated in this medium. BSF *T. congolense* IL3000 cells during  
204 exponential growth phase were inoculated into fresh medium (0 h time point). Culture  
205 supernatant samples were collected at 0, 8, 24, 32, 48 and 56 hours ( $n = 4$  at each time  
206 point) and metabolites extracted for LC-MS analysis.

207 A total of 290 putative metabolites were detected across all samples (207 after removing  
208 putative metabolites that did not map to metabolic pathways, e.g. peptides and medium  
209 components), of which 37 were matched to an authentic standard to confidently predict their  
210 identity (S4 Table).

211 80 of the 206 putative metabolites were significantly altered across the dataset (false  
212 discovery rate-adjusted  $P < 0.05$ ; one-way repeated measures ANOVA; Fig 2A and S4  
213 Table). To analyse metabolites undergoing similar changes, K-means clustering with  
214 Pearson correlation coefficient as the similarity metric was used, highlighting seven clusters  
215 with two clusters of particular interest: one containing metabolites that accumulated over  
216 time, and the other containing metabolites depleted over time (Fig. 2A).  $\text{Log}_2$  fold change  
217 ( $\text{Log}_2$  FC) between the first and final time points (0 and 56 h, respectively) was also  
218 calculated for each metabolite (S4 Table).

219 Glucose, the primary energy source for *T. brucei*, whilst clearly consumed, was not fully  
220 depleted after 56 hours in *T. congolense* culture ( $\text{Log}_2$  FC: -0.76; Fig 2A and 3A), in contrast  
221 to *T. brucei*, where 10 mM glucose is consumed by the same time-point [56]. Ribose,  
222 glucosamine, inosine and threonine were similarly depleted in *T. congolense* culture ( $\text{Log}_2$   
223 FC: -0.78, -0.97, -2.82 and -0.89, respectively).

224 In contrast, a number of metabolites accumulated in the medium (Fig 2A). The most  
225 significant of these were guanine (Log<sub>2</sub> FC: 6.34; Fig 2A and 5A), succinate (Log<sub>2</sub> FC: 5.60;  
226 Fig 2A & 3B) and (S)-malate (malate, Log<sub>2</sub> FC: 1.37; Fig 2A and 3B). Interestingly, pyruvate  
227 (Log<sub>2</sub> FC: 0.24; Fig 3B) was not excreted at the high levels relative to starting concentration  
228 consistently observed in BSF *T. brucei* culture, in both HMI-11 and in Creek's Minimal  
229 medium (CMM) [56]. Succinate and malate appear to be the primary glycolytic outputs from  
230 BSF *T. congolense*, similar to PCF *T. brucei*. Elevated levels of 2-oxoglutarate and a  
231 metabolite putatively identified as 2-oxoglutamamate were observed, which potentially  
232 originate from alanine aminotransferase activity using L-glutamate and L-glutamine,  
233 respectively, as substrates [42, 57]. Moreover, a significant build-up of N6-Acetyl-L-lysine  
234 (Log<sub>2</sub> FC: 6.30) was observed (Fig 2B). Whilst the low molecular weight of acetate means it  
235 could not be detected by the LC-MS platform used here, concentrations of this molecule  
236 were measured directly using an acetate assay in samples taken at the same time points  
237 from four independent cultures, which confirmed high levels of acetate excretion by BSF *T.*  
238 *congolense* (Fig 3F).

239 Other notable observations included the depletion of several putative  
240 lysophosphatidylcholine species at 56 hours (Fig 2A; S4 Table), coincident with increased  
241 medium levels of *sn*-glycero-3-phosphocholine, choline and choline phosphate, indicating  
242 lyso-phospholipase activity where the charged headgroup moiety of a lyso-species is  
243 cleaved from its bound fatty acid [58]. In addition, tryptophan (Log<sub>2</sub> FC: -0.74; Fig 6B; S4  
244 Table) was significantly consumed ( $P = 0.042$ ), in contrast with cysteine (Log<sub>2</sub> FC: -0.07;  $P >$   
245 0.05), despite the latter being essential to *T. brucei* [59] (S4 Table).

246 The Log<sub>2</sub> metabolite fold changes after 56 hours of culture of *T. congolense* were compared  
247 to those of *T. brucei* grown in HMI-11 (Fig 2B) [56]. A total of 90 metabolites were identified  
248 in both datasets, with some showing divergence between the two species (Fig 2B). Several  
249 metabolites only accumulated in *T. brucei* supernatant, in particular pyruvate, D-glycerate, 2-  
250 oxoglutarate and 12-hydroxydodecanoic acid (Fig 2B). Conversely, succinate, N6-acetyl-L-  
251 lysine, 4-hydroxy-4-methylglutamate, N6,N6,N6-trimethyl-L-lysine and choline only  
252 accumulated in *T. congolense* supernatant (Fig 2B). Whilst cystine (Fig 2B; 12) was depleted  
253 in *T. brucei* samples, this metabolite remained unchanged in those from *T. congolense*.

254 In summary, whilst core elements of metabolism have been conserved between BSF *T.*  
255 *congolense* and *T. brucei*, several pronounced differences in *T. congolense* metabolism  
256 were identified based solely on metabolic input and output in *in vitro* culture. An integrated  
257 analysis of the metabolomic and transcriptomic datasets was then undertaken in order to  
258 further define the metabolic differences between the two species.



## 259 **Energy metabolism**

260 As described above, RNA sequencing and culture supernatant metabolomics provided initial  
261 indications that *T. congolense* energy metabolism, specifically with respect to glucose  
262 usage, diverges substantially from that characterized in *T. brucei* BSFs (simplified map of  
263 glycolysis depicted in Fig 3G).

264 To dissect metabolic differences at the transcriptome level, pathway analysis was carried out  
265 using the TrypanoCyc database [60], which contains 186 manually curated pathways  
266 covering 422 genes or groups of multi-copy genes (S5 Table). These analyses showed  
267 broadly similar levels of gene expression of glycolytic components between BSF *T. brucei*  
268 and *T. congolense* (Fig 3G and 3I). However, the *T. brucei* *ex vivo* samples displayed a  
269 more distinct expression profile, with low transcript abundances for most glycolytic  
270 components compared to all sample groups. This is most likely the result of cells being  
271 sampled near peak parasitaemia, and so having a higher proportion of tsetse-transmissible,  
272 quiescent short stumpy forms – consistent with this there was elevated expression of stumpy  
273 markers such as the PAD array (TbTc\_0074), PIP39 (TbTc\_0700) and reduced expression  
274 of RBP10 (TbTc\_0619) (S1 Table) [61-63].

275 Transcripts associated with gluconeogenesis, the succinate shunt, and the acetate  
276 generation pathway were upregulated in BSF *T. congolense* under both *in vitro* and *ex vivo*  
277 conditions compared to BSF *T. brucei*. Key examples of this are pyruvate phosphate  
278 dikinase (PPDK), phosphoenolpyruvate carboxykinase (PEPCK), glycosomal malate  
279 dehydrogenase (gMDH) and two subunits of pyruvate dehydrogenase (PDH) (Fig 3I). PPDK  
280 was previously reported to be expressed in BSF *T. congolense*, but not BSF *T. brucei* [44],  
281 and it may be assumed that the enzyme serves a similar function in BSF *T. congolense* as it  
282 does in PCF *T. brucei*; in a mainly glycolytic role to maintain ATP/ADP balance in the  
283 glycosome. The high levels of glycosomal MDH expressions in BSF *T. congolense* contrasts  
284 with BSF *T. brucei*, where gMDH expression is reported to be mostly absent, and cytosolic  
285 MDH (cMDH) is the major isoform [64]. The RNAseq analysis also supports a previous study  
286 showing high levels of glycerol kinase expression in BSF *T. congolense* [45]. The most  
287 recent PacBio assembly of the *T. congolense* genome indicates that the parasite encodes  
288 five copies of PEPCK in tandem array (TcIL3000.A.H\_000300300,  
289 TcIL3000.A.H\_000300400, TcIL3000.A.H\_000300500, TcIL3000.A.H\_000300600 &  
290 TcIL3000.A.H\_000300700; compared to one copy in *T. brucei* – Tb927.2.4210; [65]), whilst  
291 there are only three copies of glycerol kinase in *T. congolense* (compared to five in *T.*  
292 *brucei*).

293 To confirm that the elevated levels of succinate and malate seen in *T. congolense* spent  
294 medium samples originated from glucose, LC-MS analysis using  $^{13}\text{C}$ -U-D-glucose was  
295 carried out on intracellular metabolites from cell pellet extracts. Stable isotope analysis has  
296 provided valuable insights into *T. brucei* central carbon metabolism [42], and generating *T.*  
297 *congolense* datasets enabled comparative analysis of glucose catabolism (albeit with an  
298 unavoidable difference in medium supplementation of goat serum for *T. congolense*, rather  
299 than foetal bovine serum for *T. brucei*).

300 BSF *T. congolense* was grown for 48 hours in a custom medium (Steketee's *congolense*  
301 medium; SCM-6; S6 Table), containing a total D-glucose concentration of 10 mM in a 1:1  
302 ratio of D-glucose: $^{13}\text{C}$ -U-D-glucose. Following metabolite extraction, LC-MS analysis was  
303 undertaken and the majority of glycolytic intermediates were detected, including  $^{13}\text{C}$ -labels  
304 (Fig 3H). Moreover, labelling ratios of downstream metabolites were largely similar to that of  
305 intracellular glucose, and the number of carbons found to be labelled in each metabolite  
306 matched that which would be expected in the BSF *T. brucei* glycolytic pathway (i.e. three  $^{13}\text{C}$   
307 atoms in all metabolites downstream of glyceraldehyde 3-phosphate and glycerol-3-  
308 phosphate). Similar to *T. brucei*, a high percentage of 3-carbon labelled fructose-1,6-  
309 bisphosphate (FBP) (34.8%) was observed in *T. congolense* (Fig 3H), probably a result of  
310 the "reverse" aldolase reaction occurring in the glycosome [42]. Importantly, two-carbon  
311 labelling was observed in several acetylated compounds (N-acetylornithine & N-acetyl-L-  
312 lysine; Fig 3H), confirming that acetyl groups used to generate these metabolites originate  
313 from D-glucose. Although acetyl-CoA, the product of pyruvate oxidation, was not detected  
314 for technical reasons, labelling of acetylated metabolites indicate that glucose-derived  
315 pyruvate is used to generate acetyl-CoA and subsequently acetate in the mitochondrion,  
316 similar to other trypanosomatids. Taken together, these data indicate that the flow of carbon  
317 atoms for glycolytic components in *T. congolense* is very similar to that in *T. brucei*.  
318 However, the metabolic outputs differ drastically from BSF *T. brucei* and appear to be more  
319 similar to PCF *T. brucei*.

320 To determine whether the elevated succinate in supernatants originated from glucose  
321 catabolism, metabolite labelling was corrected for the 1:1 (50%) ratio of natural glucose to  
322  $^{13}\text{C}$ -U-D-glucose, which equated to a mean percentage labelling of 43.1% (the value is less  
323 than 50% due to D-glucose in the serum). All glycolytic metabolites up to pyruvate showed  
324 >90% labelling when corrected (for glucose 6-phosphate and fructose-1,6-bisphosphate,  
325 both 3-carbon and 6-carbon labels were taken into account), although glycerol and glycerol  
326 3-phosphate exhibited 57.2% and 64.4% labelling, respectively, as these metabolites can  
327 also be obtained from catabolism of lipid precursors. Moreover, 40.1% (93.0% corrected)  
328 labelling was detected in L-alanine, suggesting that the alanine aminotransferase reaction

329 that utilizes pyruvate to generate 2-oxoglutarate and L-alanine in both BSF and PCF *T.*  
330 *brucei*, also occurs in BSF *T. congolense* [42, 66]. For both succinate and malate, 3 carbons  
331 are derived from glucose and these metabolites showed 33.6% (78.1% corrected) and  
332 26.0% (60.3% corrected) labelling, respectively. These results suggest that glucose is not  
333 the only source of intracellular succinate and malate in *T. congolense*. However, these  
334 values were higher than those reported in *T. brucei* (70% and 52% for malate and succinate,  
335 respectively [42]).

336 Whilst PCF *T. brucei* exhibit citric acid (TCA) cycle activity, this pathway is not used to  
337 catabolize glucose [35]. Similarly, no citric acid cycle intermediate isotopologues (e.g. citrate)  
338 were found when BSF *T. congolense* were incubated with <sup>13</sup>C-U-D-glucose, although small  
339 amounts of 2-carbon labelled succinate and malate were observed (Fig 3H). This is similar  
340 to BSF *T. brucei* [42], indicating that, like *T. brucei*, *T. congolense* does not appear to couple  
341 glycolysis to TCA metabolism and instead directs high amounts of pyruvate through pyruvate  
342 dehydrogenase (PDH) into acetyl-CoA and acetate. Taken together, these data suggest that  
343 BSF *T. congolense* both from *in vitro* cultures and *in vivo* infection metabolically resemble an  
344 intermediate between BSF and PCF *T. brucei*, with moderate glycolytic capacity and  
345 significant levels of succinate shunt activity (glycosomal, rather than mitochondrial; S1  
346 Table) as well as a highly active mitochondrial acetate generating pathway.

347 Previous work has shown that reduction of glucose concentrations in BSF *T. brucei* culture  
348 from 10 mM to 5 mM leads to decreased cellular motility, reduction in growth and cell body  
349 rounding morphology within 8 hours [67]. Given that glucose was not substantially depleted  
350 in *T. congolense* cultures after 56 h, we tested the effect of reduced glucose concentrations  
351 on *T. congolense* viability. Unlike *T. brucei*, *T. congolense* was able to maintain a growth  
352 rate equal to controls at concentrations as low as 2 mM (Fig 4A) when continuously  
353 passaged with no observable change in morphology or motility. To test whether glucose  
354 uptake was essential in *T. congolense*, cells were incubated with D-glucose in addition to  
355 varying concentrations of 2-deoxy-D-glucose (2DG), which can be internalised, but not  
356 metabolised further than 2-deoxy-D-glucose 6-phosphate, thereby inhibiting glycolysis (Fig  
357 4B). Incubation of *T. congolense* in medium supplemented with 2DG (in addition to 10 mM  
358 glucose) led to growth defects in a dose dependent manner, likely due to 2DG being  
359 outcompeted by glucose at lower concentrations (Fig 4B). Although the growth defect was  
360 minor in the presence of 1 mM 2DG, there was a more pronounced reduction with 5 mM  
361 2DG. When equimolar concentrations of glucose and 2DG were used, growth was repressed  
362 and cell death occurred within 48 hours (Fig 4B). *T. congolense* viability was also tested in  
363 SCM-6 in the presence of N-acetyl-D-glucosamine (GlcNAc), a sugar that inhibits glucose  
364 uptake [68] (S2 Fig). In the presence of 60 mM GlcNAc with 10 mM glucose, there was a

365 moderate, yet significant ( $P < 0.0001$  at 96 h,  $t$ -test of cell densities) growth defect in *T.*  
366 *congolense* (S2 Fig). Viability was further reduced when the same concentration GlcNAc  
367 was used alongside 2 mM glucose ( $P < 0.0001$  at 96 h,  $t$ -test of cell densities), the lowest  
368 concentration *T. congolense* could tolerate (S2 Fig). The rate of glucose consumption was  
369 measured by assaying glucose concentrations in cell culture supplemented with 4 mM  
370 glucose, and shown to be  $47.17 \pm 27.91 \text{ nmol}^{-1} \text{ min}^{-1} 10^8 \text{ cells}$  in *T. congolense*, significantly  
371 lower than the rate ( $132.18 \pm 16.31 \text{ nmol}^{-1} \text{ min}^{-1} 10^8 \text{ cells}$ ) in *T. brucei* ( $n = 4$ ,  $P = 0.0039$ ;  $t$ -  
372 test).

373 To further probe glycolytic metabolism in BSF *T. congolense*, several targets were selected  
374 for RNAi-mediated knock-down, using a tetracycline-inducible *T. congolense* line expressing  
375 T7 polymerase and Tet repressor under puromycin selection (TcoSM [69]). Given that the  
376 majority of both malate and succinate appear to originate from glucose catabolism, the effect  
377 of reducing expression levels of two proteins involved in the succinate shunt, PEPCK and  
378 PPDK (TcIL3000.A.H\_000922100 – both expressed at high levels in *T. congolense*; Fig 3I),  
379 was tested in separate experiments (Fig 4C, D). RNAi was induced by addition of 1  $\mu\text{g}/\text{mL}$   
380 tetracycline, and cell growth in culture and transcript abundance measured by qPCR were  
381 monitored every 24 hours (Fig 4C, D). Creek et al showed that PEPCK is essential in BSF *T.*  
382 *brucei*, even though the levels of succinate generated through this pathway are negligible  
383 [42]. In BSF *T. congolense*, RNAi targeting the five copies of PEPCK reduced overall  
384 *PEPCK* transcript abundance by approximately 50% (mean transcript levels of 60%, 46%  
385 and 63% compared to uninduced controls at 24, 48 and 72 h post-induction, respectively;  
386 Fig 4E), leading to a small but non-significant reduction in growth rate (Fig 4C ( $P=0.0689$ ,  $t$ -  
387 test at the 96 h time-point)). PPDK expression is not detected in BSF *T. brucei* but is  
388 expressed in the PCF stage [44]. Knock-down of PPDK in *T. congolense* did not affect  
389 parasite viability or growth rate (Fig 4D), although similar levels of transcript knockdown  
390 were observed (mean transcript levels of 67%, 64% and 50% compared to uninduced  
391 controls at 24, 48 and 72 h post-induction, respectively; Fig 4F).

392 RNAi was also used to knock down expression of the hexose transporter (HT) array,  
393 specifically those matching the THT1 and THT2 array in *T. brucei*  
394 (TcIL3000.A.H\_000260500, TcIL3000.A.H\_000260600, TcIL3000.A.H\_000794500,  
395 TcIL3000.A.H\_000794600, TcIL3000.A.H\_000794700.1), which has been shown to  
396 significantly restrict growth of BSF *T. brucei* [70]. Whilst growth rate was unaffected in BSF  
397 *T. congolense* (Fig 4G), induction of HT RNAi led to a reduction in transcript abundance at  
398 all time points (mean transcript levels of 83%, 75%, 68% and 65% compared to uninduced  
399 controls at 24, 48, 72 and 96 h post-induction, respectively; Fig 4H). Glucose uptake was  
400 decreased (mean reduction of 37% in uptake compared to uninduced controls after 72 h; Fig

401 4l), suggesting that either lower levels of glucose are sufficient for energy generation in *T.*  
402 *congolense*, or the parasite can utilize other carbon sources for ATP production. These  
403 alternatives sources could include serum components such as fatty acids or amino acids,  
404 both of which trypanosomatids have been reported to utilise [71, 72].

405 PCF *T. brucei* express most components of the electron transport chain (ETC) to generate  
406 ATP through oxidative phosphorylation, in contrast to BSF *T. brucei*, which do not detectably  
407 express any ETC components with the exception of the reversed ATPase and alternative  
408 oxidase [73]. As mentioned previously, BSF *T. congolense* is thought to express a complex I  
409 NADH dehydrogenase, but it is not known whether BSF *T. congolense* has capacity for  
410 oxidative phosphorylation. Transcriptomics analysis of the ETC was attempted, using a gene  
411 list generated by Zikova and colleagues [73], but no significant patterns could be discerned  
412 (S1 Table, S3 Fig).

### 413 **Nucleotide metabolism**

414 Metabolomic analysis of BSF *T. congolense* culture supernatants indicated a significant  
415 uptake of exogenous ribose, a contributor to nucleotide metabolism via uptake, or via the  
416 pentose phosphate pathway (PPP; Fig 5A and Fig 2A). Whilst guanosine was not detected  
417 in the supernatant, significant accumulation of guanine (Fig 5B) was observed, suggesting  
418 either excretion of this metabolite, or, hydrolysis of guanosine through parasite-secreted  
419 hydrolases/nucleosidases (previously identified in BSF *T. brucei* secretomes [74, 75]). This  
420 mechanism would enable uptake of guanine and other nucleobases through nucleobase  
421 transporters, for which multiple orthologues have been identified in the *T. congolense*  
422 genome [18] through homology with known *T. brucei* nucleobase transporters TbNT8.1 and  
423 TbNBT1 [76, 77]. In addition, there was an accumulation of xanthine, a product of  
424 xanthosine hydrolysis, and depletion of inosine, an important nucleoside composed of  
425 hypoxanthine and ribose (Fig 5C and 5D). The nucleoside cytidine and the nucleobase  
426 hypoxanthine were also detected, but appeared to remain unchanged during the time  
427 course, although the latter was a medium supplement potentially added in excess (S4  
428 Table). It is noteworthy that only a single nucleoside transporter gene (TbTc\_1072; *T.*  
429 *congolense* gene IDs: TcIL3000.A.H\_000665800 and the pseudogene  
430 TcIL3000.A.H\_000679300; S2 Table) can be identified in *T. congolense*, a syntenic  
431 homologue of TbNT10 [18], functionally characterized as a P1-type purine nucleoside  
432 transporter [78], and is thus unlikely to transport cytidine [79].

433 Purine salvage is an essential process in trypanosomatids, as they lack the *de novo*  
434 synthesis pathway for the purine ring [80], and previous analysis of cell pellets to investigate  
435 intracellular nucleotide metabolism utilizing <sup>13</sup>C-U-D-glucose in BSF *T. brucei* showed purine

436 salvage pathways incorporating 5-carbon labelled ribose derived from glucose [42] (Fig. 5F).  
437 Whilst the ribose incorporated into these nucleosides originates almost exclusively from  
438 glucose in *T. brucei* (Fig 5F), *T. congolense* appears to use far less glucose-derived ribose  
439 to make purine nucleosides such as adenosine, guanosine and inosine (Fig 5F).

440 Transcriptomics analyses indicated upregulation of genes associated with generation of  
441 adenosine nucleotides (Fig 5G; red vertical bar), especially in *ex vivo* *T. congolense*, as well  
442 as hypoxanthine-guanine phosphoribosyltransferase and uracil phosphoribosyltransferase.  
443 Upregulation of nucleoside hydrolases and phosphoribosyltransferases supports previous  
444 theories based upon genome content that *T. congolense* has a capacity for nucleobase  
445 uptake [18].

446 The purines guanosine and inosine, which incorporate glucose-derived ribose in *T. brucei*,  
447 were almost entirely unlabelled in *T. congolense* (Fig 5F). However, the phosphorylated  
448 nucleosides GMP, GDP and GTP all incorporate glucose-derived carbon atoms, presumably  
449 through ribose. Given the labelling patterns seen in adenosine, one possible explanation  
450 could be conversion of AMP to inosine monophosphate (adenosine monophosphate  
451 deaminase; TbTc\_0145), IMP to xanthosine monophosphate (IMP dehydrogenase;  
452 TbTc\_1648) and XMP to GMP (GMP synthase; TbTc\_1452). However, only one of these  
453 enzymes, GMP synthase, was expressed at higher abundance in *T. congolense* (Log<sub>2</sub> fold  
454 change: 1.56 and 2.02 for *ex vivo* and *in vitro*, respectively). Overall, incorporation of  
455 glucose-derived carbons into purine nucleosides is reduced in *T. congolense* compared to *T.*  
456 *brucei*. It should be noted that in both experiments, there was no ribose supplementation in  
457 the media

458 Of the pyrimidines, uracil and its derivatives were detected during the glucose labelling  
459 experiment (S4 Fig). Uracil is known to be the main pyrimidine salvaged by other  
460 kinetoplastids including *T. brucei* [81-83]. Whilst the majority of the uridine, UMP, UDP and  
461 UTP pools incorporate glucose-derived ribose (five <sup>13</sup>C labels), 5-carbon isotopologues of  
462 these pyrimidines were reduced in abundance in *T. congolense* compared to *T. brucei*.  
463 Instead, 2-carbon labelled isotopologues appeared to comprise the majority of uridine, uracil  
464 and their nucleotides (S4 Fig).

465 Whilst uracil biosynthesis is not essential in *T. brucei* [84], the uracil pool in *T. congolense*  
466 appears to derive almost entirely from glucose, when corrected for 50% glucose labelling  
467 (76% in *T. congolense* vs 44% in *T. brucei* [42]; S4 Fig), suggesting that this species  
468 predominantly synthesizes uracil from orotate to UMP (orotate  
469 phosphoribosyltransferase/orotidine 5-phosphate decarboxylase; TbTc\_0735) and from  
470 UMP to uracil (uracil phosphoribosyltransferase; TbTc\_4220), as can occur in *T. brucei* [42].

471 Both these genes are expressed at higher abundance in *T. congolense*, both *in vitro* and *ex*  
472 *vivo*, compared to *T. brucei* (Fig 5G, S1 Table), which could explain the increased  
473 isotopologue labelling. Uridine nucleosides (UMP, UDP, UTP) all show a similar pattern, with  
474 significant 2-carbon labelling, as well as moderate levels of 5-carbon labelling from  
475 incorporation of glucose-derived ribose (S4 Fig).

476 These data indicate that, at least under the growth conditions used here, BSF *T. congolense*  
477 favours purine nucleoside salvage in lieu of biosynthesis, in addition to *de novo* synthesis of  
478 orotate, uracil and uridine nucleosides. However, the difference in serum requirements for  
479 the two organisms is a confounding factor to the interpretation of this difference.

### 480 **Amino acid metabolism**

481 It is well established that trypanosomatid parasites scavenge amino acids, key nutrients for  
482 survival, from their hosts [85, 86]. Therefore, comparative analyses of *T. congolense* and *T.*  
483 *brucei* amino acid metabolism were undertaken. Whilst the majority of amino acids were  
484 detected during the supernatant time course, relative abundances in the medium did not  
485 vary greatly after 56 hours of *in vitro* culture (Fig 6A–C, S4 Table). The greatest reductions  
486 were observed in threonine (Log<sub>2</sub> FC after 56 hours: -0.89; Fig 6A), tryptophan (Log<sub>2</sub> FC: -  
487 0.74; Fig 6B), glutamine (Log<sub>2</sub> FC: -0.39), asparagine (Log<sub>2</sub> FC: -0.35) and phenylalanine  
488 (Log<sub>2</sub> FC: -0.35). Interestingly, cysteine, an essential factor for the *in vitro* culture of *T.*  
489 *brucei*, was not significantly consumed by 56 hours (Log<sub>2</sub> FC: -0.07; Fig 6C). However, at  
490 least low-level exogenous cysteine is still required to sustain parasite growth *in vitro*, as  
491 viability was significantly affected in the absence of cysteine (for both 1.5 mM and 1 mM vs 0  
492 mM cysteine,  $P < 0.0001$ , *t*-test of cells densities at 96 h; S5 Fig). Experiments were carried  
493 out to test the essentiality of all other individual amino acids (with the exception of glutamine,  
494 known to be an important amino donor in trypanosomatid metabolism). Using the minimal  
495 medium SCM-6, cell viability was monitored for 72 hours in the absence of specific amino  
496 acids. Removal of the following amino acids from culture medium led to defects in growth  
497 over 72 hours: asparagine, histidine, isoleucine, leucine, methionine, proline, serine, tyrosine  
498 and valine (Fig 6D–G). Whilst aspartate appeared to be depleted in spent culture  
499 supernatants (S4 Table), this also occurred in the medium only control. Furthermore,  
500 removal of aspartate did not lead to reduced cell viability or growth rate in culture (Fig 6F).  
501 Long term culture was impossible without the addition of phenylalanine and threonine,  
502 leading to a final culture formulation, SCM-7 (S6 Table) containing a total of 14 amino acids.  
503 Therefore, BSF *T. congolense* appears to require a higher number of amino acids than BSF  
504 *T. brucei*, at least *in vitro*, with CMM containing only 8 amino acids in total, including cysteine  
505 and glutamine [56]. To further probe amino acid metabolism, pathway analysis was carried  
506 out on the transcriptome (S6 Fig) and metabolome (Fig 6; S6, S7 Fig).

507 BSF *T. brucei* utilizes exogenous L-glutamine as the primary source of intracellular  
508 glutamate and 2-oxoglutarate and produce significant levels of glutamine-derived succinate  
509 [42, 85] (Fig 6I). Given the high levels of succinate excreted by *T. congolense*, stable isotope  
510 labelling was used to determine the contribution of L-glutamine to this pool. *T. congolense*  
511 was incubated for 48 hours with 1 mM <sup>13</sup>C-U-L-glutamine and cell pellets analysed by LC-  
512 MS. Results indicated the presence of biochemical activities consistent with those observed  
513 in *T. brucei*. Significant glutamine-derived carbon labelling was detected after 48 h  
514 incubation for succinate (41.3%, 48.5% corrected), glutamate (76.1%, 89.2% corrected), 2-  
515 oxoglutarate (80.5%, 94.3% corrected) and succinate semialdehyde (94.7% corrected; Fig  
516 6I). As would be anticipated, labelling of glutathione (86.1%) and trypanothione (98.4%) from  
517 glutamine through glutamate were also observed (S7 Fig). No labelling of malate or  
518 aspartate was seen in this study, despite the use of high concentrations of <sup>13</sup>C-U-L-  
519 glutamine compared to the equivalent study performed in *T. brucei* with a 50:50 ratio of <sup>13</sup>C-  
520 U-L-glutamine [85].

521 The apparent essentiality of several amino acids was also investigated using stable isotope  
522 labelling. Proline is an essential carbon source for PCF but not BSF *T. brucei* [87]. However,  
523 removal of proline from BSF *T. congolense* medium led to reduced growth (Fig 6F). RNAi-  
524 mediated knock-down of proline metabolism (specifically pyrroline-5-carboxylate  
525 dehydrogenase, TbP5CDH) in PCF *T. brucei* has highlighted the requirement of proline  
526 metabolism for mitochondrial function [87]. Indeed, both P5CDH (TbTc\_1695) and proline  
527 dehydrogenase (TbTc\_1591) expression were upregulated in *ex vivo* *T. congolense*,  
528 compared to *T. brucei*, suggesting that proline catabolism was more active (S1 Table and S6  
529 Fig). However, <sup>13</sup>C-U-L-proline labelling showed that this amino acid did not contribute to the  
530 biosynthesis of other metabolites (S8 Fig). Therefore, the apparent requirement for proline in  
531 BSF *T. congolense* may be for the purposes of polypeptide synthesis only.

532 As in *T. brucei*, glucose-derived carbon usage was detected in several amino acids in *T.*  
533 *congolense* (S6A Fig). Aspartate (a precursor for pyrimidine nucleotide biosynthesis) and  
534 alanine (a by-product of a pyruvate-utilising aminotransferase reaction) (S6A Fig) exhibited  
535 3-carbon isotopologues derived from <sup>13</sup>C-U-D-glucose. However, in *T. brucei*, a small  
536 proportion of L-asparagine labelling was observed (1.2% 3-carbon labelling) [42], whilst none  
537 was observed in *T. congolense* (S6A Fig). The metabolism of asparagine has not been  
538 studied in African trypanosomes; given the reduction of cell growth in the absence of this  
539 amino acid (Fig 6F), labelling with <sup>13</sup>C-U-L-asparagine was performed, but no other labelled  
540 metabolites were detected (S8 Fig). This indicates that, as with proline, protein synthesis is  
541 the sole role of asparagine in *T. congolense*. The reduced expression of asparagine  
542 synthetase (TbTc\_4894; TcIL3000.A.H\_000497800), which converts aspartate to asparagine



543 (S6 Fig), suggests that BSF *T. congolense* may rely upon scavenging of exogenous  
544 asparagine.

545 Serine was also shown to be essential to *T. congolense* (Fig 6F), in contrast to minimal  
546 culturing requirements for *T. brucei* [56]. <sup>13</sup>C-U-L-serine labelling indicated that *T.*  
547 *congolense* L-serine metabolism mirrors that of *T. brucei* in several aspects, such as *de*  
548 *novo* sphingolipid biosynthesis, with 70.0% 2-carbon labelling of sphinganine and  
549 downstream labelling of ceramide and sphingomyelin species (S8 Fig). Similarly,  
550 phosphatidylserine decarboxylase activity was evidenced at both transcript and metabolite  
551 levels, with 40.1% 2-carbon labelling of glycerol-phospho-ethanolamine (S1 Table; S8 Fig).  
552 However, L-serine also has a minor role in S-adenosyl-L-homocysteine detoxification, where  
553 serine-derived carbon ultimately contributes to cysteine biosynthesis. In *T. congolense*,  
554 serine-derived carbon labelling can be detected in cystathionine (18.1%) and cysteine  
555 (16.7%), through to glutathione (4.1%) and trypanothione disulfide (3-carbon labelled, 6.8%;  
556 6-carbon labelled, 0.02%; S7 Fig). Therefore, the inability to exclude L-serine from *T.*  
557 *congolense in vitro* culture media may primarily be attributable to lipid metabolism and an  
558 increased demand for serine-derived cysteine, potentially over exogenously obtained  
559 cysteine, depending on bioavailability. Indeed, metabolomics analysis of culture medium  
560 indicates that the ability of *T. congolense* to take up cysteine from its environment may be  
561 lower than in *T. brucei* (Fig 6C).

562 Although L-cysteine is primarily a source of sulphur for trypanosomatids, we also  
563 investigated the carbon contribution of this amino acid in *T. congolense*, and in particular,  
564 whether L-cysteine-derived carbon atoms contribute to the biosynthesis of glutathione and  
565 trypanothione. <sup>13</sup>C-U-L-cysteine stable isotope labelling experiments were performed (S7  
566 and S8 Fig). Direct replacement of the 1.5 mM L-cysteine present in SCM with <sup>13</sup>C-U-L-  
567 cysteine led to high levels of labelling in glutathione and trypanothione disulfide (S7B Fig).  
568 This indicates that *T. congolense* can readily take up and metabolize exogenous cysteine,  
569 even though abundance of the amino acid is not reduced significantly over 56 hours of  
570 parasite *in vitro* culture. Although no clear pattern could be observed in transcriptomic  
571 analysis of the trypanothione biosynthesis pathway, both trypanothione synthase (TRYS;  
572 TbTc\_1359) and trypanothione reductase (TRYR; TbTc\_4239) were expressed at high  
573 levels in *in vitro T. congolense* cells relative to *ex vivo* cells, indicating that under *in vitro*  
574 conditions, cells may be subjected to higher levels of oxidative stress (S7C Fig).

## 575 **Fatty acid metabolism in *T. congolense***

576 Lipids have a variety of crucial roles in trypanosomes, as a major constituent of membranes  
577 and under certain conditions, for energy [72]. BSF *T. brucei* require large quantities of

578 myristic acid in particular, for the synthesis of glycosylphosphatidylinositol (GPI) that anchors  
579 the parasite's major surface glycoprotein antigens [88]. To do this, BSF *T. brucei* both  
580 synthesises and scavenges myristic acid. Glucose labelling experiments in *T. brucei* have  
581 shown that myristic acid is partially synthesized from glucose-derived carbon through acetyl-  
582 CoA, using a system of fatty acid elongases [89] (Fig 7A). However, no fatty acid carbon  
583 labelling was detected after incubation of *T. congolense* with  $^{13}\text{C}$ -U-D-glucose (Fig 7A).  
584 Carbon dissemination was also investigated from threonine, which is used as a source of  
585 acetate, and thus, lipids [90] (Fig 7B). Similarly, no saturated lipid carbon labelling was  
586 observed, suggesting that *T. congolense* either uses alternative sources of carbon for lipid  
587 biosynthesis, or does not rely on acetate as a source of lipids in the same way as *T. brucei*  
588 [30].

589 While acetate/acetyl-CoA metabolism is highly active at the level of gene expression in *T.*  
590 *congolense* compared to *T. brucei* (Fig 7C), consistent with metabolic data, expression of  
591 acetyl-CoA synthetase (TbTc\_0318), a key enzyme in lipid biosynthesis from acetate, is  
592 reduced in both *ex vivo* and *in vitro* *T. congolense* (Fig 7C). Furthermore, an acetyl-CoA  
593 thioesterase (TbTc\_5515) that is involved in ATP synthesis-uncoupled acetate production in  
594 PCF *T. brucei* [91] is also expressed at lower levels in *T. congolense* (Fig 7B). Other  
595 enzymes involved in fatty acid biosynthesis, namely acetyl-CoA carboxylase (TbTc\_0754),  
596  $\beta$ -ketoacyl-CoA synthase (TbTc\_3372) and  $\beta$ -ketoacyl-CoA reductase (TbTc\_1241), were all  
597 expressed at lower abundance in *T. congolense* than *T. brucei*, in particular in *ex vivo* cells  
598 (Fig 7C). Of the four elongases, ELO1 (TbTc\_0159) and ELO2 (TbTc\_1882) were expressed  
599 at equal levels in BSF *T. congolense*, compared to BSF *T. brucei* (S1 Table). Whilst  
600 expression of ELO3 (TbTc\_0235) appeared to be reduced in *T. congolense* (Log<sub>2</sub> fold  
601 change of -1.98 and -1.62 compared to *T. brucei* for *in vitro* and *ex vivo*, respectively; S1  
602 Table), *T. congolense* cells expressed higher levels of ELO4 (TbTc\_0737) in both *in vitro*  
603 and *ex vivo* conditions, compared to *T. brucei* (Log<sub>2</sub> fold change: 1.39 and 1.38 for *in vitro*  
604 and *ex vivo* comparisons, respectively)

605 The variation in observed gene expression associated with the sterol pathway appeared to  
606 correlate with sample condition rather than species (Fig 7C). However, *T. congolense*  
607 transcripts for genes involved in lanosterol synthesis were reduced, especially under *in vitro*  
608 conditions (squalene synthase, SQase, TbTc\_2577; squalene monooxygenase, SM,  
609 TbTc\_3357; lanosterol synthase, LSS, TbTc\_4540; Fig 7C).

610 Fatty acid oxidation was recently confirmed to be an energy source for *T. brucei* residing in  
611 adipose tissue [72]. Transcripts associated with this pathway were less abundant in *T.*  
612 *congolense* compared to *T. brucei* under both conditions (Fig 7C), suggesting this may not

613 be an energy-generating pathway in glucose-rich culture medium, or under the *in vivo*  
614 conditions from which they were sampled. However, capacity for ATP generation from fatty  
615 acid oxidation should not be ruled out.

### 616 **Exploiting differences in metabolism for pharmacological intervention**

617 Differences in metabolism between *T. congolense* and *T. brucei* have implications for  
618 differential drug efficacy between the two species. To validate our findings in key areas of  
619 metabolism, pharmacological inhibition was attempted for specific targets in trypanosome  
620 metabolism, in order to compare inhibitory concentrations ( $EC_{50}$ ).

621 To assess whether areas of mitochondrial metabolism were more essential in BSF *T.*  
622 *congolense* than in BSF *T. brucei*, both species were treated with FCCP, an uncoupling  
623 agent that depolarises the mitochondrial membrane. However, there was no difference in  
624 sensitivity between the species ( $EC_{50}$ :  $13.0 \pm 5.0 \mu\text{M}$  and  $12.6 \pm 5.3 \mu\text{M}$  for *T. brucei* and *T.*  
625 *congolense*, respectively; Table 1). Given both metabolic and transcriptomic data indicated  
626 no increased electron transport chain activity, we also treated with the complex III inhibitor  
627 antimycin A, with again no significant differences seen between the species (Table 1). In  
628 addition, there was no change in sensitivity to azide, an inhibitor of ATP hydrolysis by the  $F_1$ -  
629 ATPase (Table 1). However, *T. congolense* appeared to be more resistant to rotenone, a  
630 complex I NADH dehydrogenase inhibitor (Table 1). Previous data inferred complex I activity  
631 in BSF *T. congolense* based on nitroblue tetrazolium staining [48]. Rotenone resistance  
632 could indicate NADH dehydrogenase activity of a rotenone-insensitive NADH  
633 dehydrogenase, such as the inner membrane space-facing NDH2 [92]. *T. congolense* also  
634 showed enhanced sensitivity to salicylhydroxamic acid (SHAM), an inhibitor of the  
635 trypanosome alternative oxidase (TAO; Table 1). Taken together, these data indicate that,  
636 like *T. brucei*, *T. congolense* does not rely on oxidative phosphorylation for ATP production,  
637 as indicated by transcriptomics analysis, and that, as previously reported, TAO is the  
638 terminal oxidase [48, 51].

639 Metabolomics and transcriptomics data indicated that *T. congolense* direct pyruvate towards  
640 mitochondrial metabolism, with high transcript levels in PDH and enzymes involved in  
641 acetate generation, compared to *T. brucei* (Fig 3 and 7). We therefore hypothesised *T.*  
642 *congolense* to be more sensitive to inhibition of mitochondrial pyruvate uptake and to  
643 investigate this further, we tested drug sensitivities for UK5099, an inhibitor of mitochondrial  
644 pyruvate transport [93]. As expected, *T. congolense* ( $EC_{50}$ :  $82.1 \mu\text{M}$ ) was significantly more  
645 sensitive ( $P = 0.0091$ , unpaired *t*-test) to UK5099 compared to *T. brucei* ( $130.0 \mu\text{M}$ ; Table 1).

646 Whilst acetate generation appears to be important in *T. congolense*, our data suggest that  
647 the acetate does not appear to be utilised for the biosynthesis of fatty acids, in contrast to

648 what has been shown for *T. brucei*. To probe this further, we compared drug sensitivity of  
649 the two species with compounds targeting fatty acid synthesis (Fig 8). Indeed, *T. congolense*  
650 was significantly more resistant than *T. brucei* to an acetyl-CoA synthetase inhibitor (ACS  
651 inhibitor; 1-(2,3-di(thiophen-2-yl)quinoxalin-6-yl)-3-(2-methoxyethyl)urea, [94]; Fig 8A; Table  
652 1), indicating that acetyl-CoA synthetase is far less essential to this species. ACS is  
653 essential to both BSF and PCF *T. brucei* [30, 95], thus indicating a key metabolic difference  
654 between the species.

655 We next compared drug sensitivity to Orlistat, an inhibitor of fatty acid synthase and  
656 phospholipase [32]. Here, a striking difference was found, with *T. congolense* exhibiting  
657 significant resistance (780-fold increase in EC<sub>50</sub>) to the compound compared to *T. brucei*  
658 (Fig 8B; Table 1), providing further evidence that *T. congolense* primarily relies on fatty acid  
659 scavenging, instead of synthesis, as predicted by the combination of metabolomics and  
660 transcriptomics.

## 661 **Discussion**

662 The protozoan parasite *T. congolense* is a principal cause of AAT, but crucially, *T. brucei*  
663 remains the dominant model for laboratory-led studies of African trypanosomes, even in the  
664 face of mounting evidence that *T. brucei* and *T. congolense* differ profoundly in many facets  
665 of their biology. In order to facilitate the identification and development of potential drug  
666 targets for *T. congolense*, a detailed understanding of the fundamental cellular metabolism,  
667 leading to an understanding of both the differences and commonalities between *T.*  
668 *congolense* and *T. brucei*, would be a significant step forward.

669 Thus, this study aimed to generate a detailed comparison of metabolism in *T. congolense*  
670 and *T. brucei*, through a combination of metabolomics, transcriptomics and gene knockdown  
671 approaches. Transcriptomic data was generated from *T. congolense* and *T. brucei* with  
672 parasite samples isolated from both *in vitro* culture and purified from *in vivo* murine infections  
673 (*ex vivo*). Crucially, there were high levels of correlation between *ex vivo* and *in vitro* *T.*  
674 *congolense* samples, indicating that the cultured form of the parasite closely resembles the  
675 *in vivo* situation, at a transcriptomic level. In contrast, there was lower inter-species  
676 correlation between *T. brucei* and *T. congolense*.

677 Our data demonstrate that BSF *T. congolense*, while possessing some metabolic similarities  
678 with BSF *T. brucei* (as expected), differs substantially in several core components, including  
679 in having a reduced reliance on glucose, excretion of distinct glycolytic end products  
680 (acetate, malate and succinate in *T. congolense* compared to pyruvate in *T. brucei*), and  
681 increased gene expression and metabolic signatures of specific mitochondrial pathways, in

682 particular pyruvate to acetate conversion. Additionally, we show increased reliance on  
683 exogenous substrates such as ribose for nucleotide synthesis as demonstrated by reduced  
684 glucose-derived carbon labelling in nucleoside species in addition to upregulation of  
685 hydrolases and phosphoribosyltransferases. Furthermore, while there is overlap in amino  
686 acid utilisation (e.g. glutamine), *T. congolense* relies on more exogenous amino acids than  
687 *T. brucei*. Surprisingly, this included serine which, in the case of *T. congolense*, appears to  
688 be important in the transsulfuration pathway that is geared towards trypanothione  
689 biosynthesis. This may also explain the observed decreased reliance on exogenous L-  
690 cysteine. Unlike *T. brucei*, *T. congolense* also requires asparagine and proline for viable *in*  
691 *vitro* culture, although carbon usage from these amino acids is minimal. Finally, *T.*  
692 *congolense* exhibits increased acetate/acetyl-CoA metabolism compared to *T. brucei*,  
693 despite a reduction in fatty acid biosynthesis through the classical trypanosomatid pathways  
694 involving acetyl-CoA synthase, acetyl-CoA carboxylase,  $\beta$ -ketoacyl-CoA synthase and  $\beta$ -  
695 ketoacyl-CoA reductase, the expression of which are reduced in *T. congolense* (both in *ex*  
696 *vivo* and *in vitro* conditions). This is further underlined by lack of glucose-derived 2-carbon  
697 labelling of fatty acids, most notably myristic acid, a key GPI anchor component of variant  
698 surface glycoproteins of *T. brucei*. However, fatty acid elongase 4, previously shown to  
699 extend exogenously scavenged arachidonic acid (C22:4) to docosatetraenoic acid (C22:4)  
700 [96], is upregulated under *in vitro* conditions, compared to *T. brucei*, which may indicate a  
701 reliance on long-chain polyunsaturated fatty acids. These findings are shown in a summary  
702 figure of *in vitro* transcriptomics data (Fig 9)

703 Analyses of culture supernatants showed that 10 mM glucose was not substantially depleted  
704 after *T. congolense* cultures reached high cell density, as would be expected from an  
705 equivalently dense *T. brucei* culture [56]. *T. brucei* requires at least 5 mM glucose in culture  
706 [67], whereas BSF *T. congolense* were viable and maintained doubling times in levels as low  
707 as 2 mM. Furthermore, confirming conclusions from one previous study on BSF *T.*  
708 *congolense* [43], the primary metabolic outputs *in vitro* were (S)-malate, succinate and  
709 acetate, in contrast to *T. brucei*, in which the main output is pyruvate, which is excreted in  
710 large amounts [42, 56]. Interestingly, we observed a reproducible reduction in pyruvate  
711 levels in *T. congolense* supernatants over time, before abundance of this metabolite  
712 returned to levels similar to those observed in negative controls. A recent study in PCF *T.*  
713 *brucei* demonstrated that these parasites can re-metabolize glycolytic end products such as  
714 pyruvate and succinate [37]. Stable isotope labelling patterns in catabolic products derived  
715 from glucose do not support cyclical TCA activity, nor re-uptake of excreted metabolites in  
716 BSF *T. congolense*. However, it would be of interest to determine whether this species can  
717 recycle the aforementioned metabolites.

718 *T. congolense* exhibits high levels of expression in genes involved in the glycosomal  
719 succinate shunt (PEPCK, glycosomal malate dehydrogenase and fumarate hydratase; Fig  
720 9). In *T. brucei* these phenotypes are associated with PCF rather than BSF; thus, to further  
721 dissect glycolytic metabolism, RNAi was employed to investigate the essentiality of PPK  
722 and PEPCK in *T. congolense*. In *T. brucei*, PPK is only expressed in the PCF stage, and is  
723 absent in the BSF stage. In contrast, BSF *T. congolense* expresses PPK at both transcript  
724 (Fig 3) and protein [44] levels, although our initial analyses suggest that the protein is not  
725 essential for growth *in vitro*. PEPCK was previously found to be essential in BSF *T. brucei*  
726 [42]; though in BSF *T. congolense*, PEPCK knock-down only led to a mild reduction in  
727 growth rate. Previous studies in PCF *T. brucei* demonstrated that individual null mutants of  
728 PEPCK and PPK showed no change in growth rate, with moderate reductions in glycolytic  
729 flux [40]. However, a PEPCK/PPK null mutant did exhibit reduced growth rates, with further  
730 data showing that PPK functions in a glycolytic direction and contributes to glycosomal  
731 ATP/ADP balance [40]. Further work is required to establish the roles of PEPCK and PPK  
732 in BSF *T. congolense*. Gene knock-out has not been previously attempted for *T. congolense*,  
733 and consistent with other studies RNAi penetrance does not appear as efficient as in *T.*  
734 *brucei* [69]. Techniques such as CRISPR/Cas9 and conditional knock-out would greatly  
735 enhance our capabilities to study this parasite.

736 Whilst the major PGK isoform in BSF *T. brucei* is expressed in the glycosome, a previous  
737 study suggested that the major isoform of phosphoglycerate kinase in BSF *T. congolense*  
738 lacks the glycosomal targeting signal present in *T. brucei*, and is thus expressed in the  
739 cytosol, akin to PCF *T. brucei* [46]. This has significant implications for glycosomal ADP/ATP  
740 balance, as the expression of cytosolic PGK in BSF *T. brucei* is lethal [39]. Taken together,  
741 these data suggest that *T. congolense* appears to carry out glycolytic metabolism in the  
742 same fashion as PCF, not BSF *T. brucei*, including in *ex vivo* cells.

743 Whilst 2-deoxy-D-glucose does cause *T. congolense* death *in vitro* and supplementation of  
744 cultures with GlcNAc also has a detrimental impact on viability, knock-down of the glucose  
745 transporter array did not affect growth, even though glucose uptake appeared to be reduced  
746 by 37% subsequent to 72 h of RNAi induction. These experiments highlight a crucial  
747 difference between BSF *T. congolense* and *T. brucei* in a pathway that has become a  
748 metabolic paradigm in the latter species. Whilst *T. brucei* requires high levels of glucose to  
749 sustain a significant glycolytic flux, *T. congolense* remains viable in significantly lower  
750 glucose concentrations, with a reduced flux, more similar to PCF *T. brucei*. However,  
751 glucose remains an essential carbon source in this species, as growth is abolished in the  
752 absence of glucose. Of particular interest is whether the parasite generates the majority of  
753 ATP from this reduced glucose intake, or if it can thrive on other carbon sources such as

754 amino acids or even fatty acids. If the latter, this adaptation could be due to the reduced  
755 bioavailability of glucose in the ruminant host bloodstream. Blood concentrations of glucose  
756 in humans are approximately 5.5 mM [97]. Glucose concentrations in ruminants are typically  
757 lower (2–4 mM [98-100]), and primary sources of energy are typically volatile fatty acids in  
758 the form of acetic, propionic and butyric acid [101, 102]. To date, products of volatile fatty  
759 acid metabolism, such as 2-methylcitrate and 2-methyl-cis-aconitase, have not been  
760 reported in *T. congolense*. As such, the ability of *T. congolense* to utilise other products only  
761 available in adult ruminant blood merits further investigation.

762 RNAseq analyses of *T. congolense* indicate high levels of expression of mitochondrial  
763 pathways associated with glucose catabolism, specifically acetate and acetyl-CoA  
764 metabolism involving pyruvate dehydrogenase, acetate:succinate CoA transferase and  
765 succinyl-CoA synthetase (Fig 9). Given that the large amounts of acetate generated by the  
766 parasite appear not to be required for fatty acid synthesis, these findings could suggest  
767 significant reliance on mitochondrial substrate level phosphorylation for growth, similar to  
768 PCF *T. brucei* cultured in glucose-rich medium [103, 104]. Interestingly, *T. congolense* does  
769 not appear to encode a homologue of MPC1, and therefore likely relies on MPC2 for  
770 pyruvate transport into the mitochondrion. The lack of multiple pyruvate transporters  
771 combined with the importance of mitochondrial pyruvate catabolism likely explains the  
772 increased sensitivity of *T. congolense* to UK5099, a mitochondrial pyruvate transport  
773 inhibitor, compared to *T. brucei*.

774 Our data are consistent with the absence of oxidative phosphorylation, based on  
775 transcriptomics and lack of sensitivity to chemical inhibition, compared to *T. brucei*.  
776 Interestingly, a previous study reported NADH dehydrogenase (complex I) activity in *T.*  
777 *congolense*, offering the possibility of ATP generation via complex V [48]. However, there  
778 was no change in rotenone sensitivity in *T. congolense*, suggesting that the NADH  
779 dehydrogenase activity may originate from a rotenone-insensitive NADH dehydrogenase  
780 such as NDH2, known to be important for acetate production in BSF *T. brucei* [92, 105, 106].

781 Rather than oxidative phosphorylation, we propose it is likelier that considerable ATP  
782 production occurs in the acetate:succinate CoA transferase – succinyl-CoA synthetase  
783 (SCS) cycle, which would explain the high levels of acetate generated by *T. congolense*, in  
784 addition to increased sensitivity to inhibition of mitochondrial uptake of pyruvate, the key  
785 metabolic precursor. Given that 2-oxoglutarate dehydrogenase complex expression appears  
786 to be less than, or equal to, that in *T. brucei* (under *in vitro* culturing conditions, Fig 9), it is  
787 likely that SCS activity occurs in the acetate-generating pathway rather than in the TCA  
788 cycle, which is not thought to be fully functional in BSF African trypanosomes [35], although

789 recent data have challenged this paradigm in PCF *T. brucei* [37]. The mechanisms proposed  
790 here bear some similarities to the scheme proposed by Dewar and colleagues for stumpy-  
791 form *T. brucei* metabolism, which also exhibit increased mitochondrial metabolism compared  
792 to BSF *T. brucei* [107].

793 In *T. brucei*, carbon atoms from glucose disseminate through multiple pathways in the cell  
794 [42] and, using stable isotope-labelled glucose, our data demonstrate that this pattern is also  
795 seen in *T. congolense*, in particular through the glycolytic pathway, suggesting some of the  
796 key metabolic differences observed are quantitative, rather than qualitative. However, there  
797 were key differences in glucose-derived carbon usage. In particular, a reduction in labelling  
798 was observed in purine nucleotides in *T. congolense*. In both species, carbon labelling is  
799 likely due to generation of ribose phosphate sugars via the PPP and these data suggest that  
800 *T. congolense* does not obtain its ribose through the pentose phosphate pathway (from  
801 glucose), to the same extent that *T. brucei* does. Interestingly, *T. congolense* appears to  
802 express higher levels of APRT1 (cytosolic) compared to APRT2 (glycosomal) to synthesise  
803 adenosine (Fig 5). This discrepancy could underpin the reduced fraction of glucose-derived  
804 purine labelling, with a reliance on ribose from alternative sources (for example,  
805 exogenously).

806 Whilst the majority of pyrimidine labelling is 5-carbons in *T. brucei*, indicating labelled ribose,  
807 there is decreased 5-carbon labelling and higher abundance of 2-carbon labelling in *T.*  
808 *congolense*, likely through uridine generated from aspartate through orotate, again  
809 highlighting a reduction in glucose-derived ribose, but conversely, an increase in glucose-  
810 derived UMP and its derivatives.

811 There was also a reduced abundance of glucose-derived fatty acid labelling in *T. congolense*  
812 relative to *T. brucei*. Coupled with a decreased abundance of acetyl-CoA synthetase mRNA,  
813 these results suggest that *T. congolense* may scavenge exogenous lipids in favour of  
814 carrying out fatty acid biosynthesis, for which it must break down extracellular lipids to their  
815 constituent parts. Indeed, supernatant metabolomics showed accumulation of both choline  
816 and choline phosphate, with a corresponding decrease in the LysoPC lipids, which appears  
817 to indicate activity of the phospholipases which *T. congolense* is known to secrete [58, 108].  
818 It is unknown whether *T. congolense* is able to generate cytosolic acetyl-CoA for fatty acid  
819 biosynthesis through the action of citrate lyase, although transcript abundance of this gene  
820 was reduced compared to *T. brucei*. Analysis of drug sensitivity supports these conclusions,  
821 as *T. congolense* is significantly less sensitive to acetyl-CoA synthetase inhibition, as well as  
822 Orlistat, and inhibitor of fatty acid synthase, suggesting that fatty acid scavenging (e.g. lipid  
823 or fatty acid transporters) could be a viable therapeutic target for this species.



824 BSF *T. brucei* growth in CMM required only cysteine and glutamine when supplemented with  
825 FBS gold, although a further 6 amino acids (Tyr, Phe, Trp, Leu, Met and Arg) were required  
826 when supplemented with standard FBS [56]. As part of this study, 14 amino acids essential  
827 for *T. congolense* growth were identified. Tryptophan and arginine, essential to *T. brucei*,  
828 were not required to sustain *T. congolense* growth in 10% goat serum. Conversely, several  
829 amino acids considered not essential to *T. brucei* were crucial for *T. congolense* growth *in*  
830 *vitro* (Asp, His, Ile, Pro, Ser and Val). Proline is a well-established carbon source for PCF *T.*  
831 *brucei* [87]. However, based on stable isotope labelling experiments, this amino acid is solely  
832 used for protein synthesis in BSF *T. congolense*, as there was no evidence of carbon  
833 dissemination from proline into the metabolome (likewise for asparagine). Unlike BSF *T.*  
834 *congolense*, BSF *T. brucei* must be able to synthesise sufficient amounts of these amino  
835 acids from alternative sources, or obtain them from the serum supplement.

836 One metabolic area of interest in trypanosomatids is trypanothione biosynthesis, a crucial  
837 pathway for parasite response to oxidative stress. Indeed, trypanothione synthase, as well  
838 as proteins involved in the trypanothione biosynthesis pathway, such as ornithine  
839 decarboxylase (targeted by Eflornithine), have long been considered prime  
840 chemotherapeutic targets due to their absence from other organisms [109]. Whilst cysteine  
841 was previously known to be a main carbon contributor to trypanothione synthesis in *T. brucei*  
842 along with glutamine and methionine [85], we show here that L-serine, an amino acid  
843 essential to *T. congolense*, also contributes to the generation of this metabolite. Interestingly,  
844 L-cysteine was not significantly depleted from *T. congolense* culture supernatants and future  
845 work should ascertain whether the presence of L-serine in medium can compensate for  
846 reduced L-cysteine levels in *T. congolense* culture.

847 The data presented here have led to the generation of a novel semi-defined medium for  
848 culturing the strain IL3000, which must be further optimized for the culture of multiple strains  
849 of *T. congolense*. Of interest is the peculiar requirement of adult bovine or goat serum for *in*  
850 *vitro* culture of *T. congolense*, rather than foetal bovine serum (FBS) which is typically used  
851 to culture *T. brucei* [15, 59]. Whilst this study made no attempts to adapt *T. congolense* to  
852 FBS-supplemented medium (indeed, even in SCM-7, growth rate is drastically reduced in  
853 the presence of FBS after 2-3 passages), this is of crucial importance, as it would allow the  
854 study of multiple species of African trypanosome under the same *in vitro* conditions. Analysis  
855 of metabolism presented here indicates that this phenomenon is likely to centre on the lipid  
856 requirements of *T. congolense*, although it remains to be seen if this requirement is for  
857 energy generation or synthesis of lipids in general. Furthermore, adult ruminant serum  
858 composition drastically differs from that of non-ruminants and of foetal ruminants [101, 102],

859 and this likely has significant implications on the extracellular environment faced by livestock  
860 trypanosomes.

861 The information presented here is a significant step in laying the foundation for fundamental  
862 understanding of metabolism for an important livestock parasite. Understanding essential  
863 areas of metabolism in both *T. brucei* and *T. congolense* enables the development of drugs  
864 effectively targeting both species. Conversely, understanding the key differences between  
865 the two species aids in dissecting drug mechanisms of action and resistance, as well as  
866 enabling a greater understanding of host-pathogen dynamics.

## 867 **Materials and Methods**

### 868 **Compounds and reagents**

869 All compounds were obtained from Sigma/Merck with the exception of: Orlistat (Cambridge  
870 Bioscience), oligomycin A (VWR International), diminazene aceturate (Cambridge  
871 BioScience) and FCCP (Abcam).

### 872 **Cell lines and *in vitro* culture**

873 In all cases, *T. congolense* strain IL3000 [48] was used (originally received from Theo Baltz,  
874 University of Bordeaux). For RNAi experiments a *T. congolense* IL3000 single marker line,  
875 TcoSM, was used [69]. For *in vitro* experiments, cells were grown at 34°C, 5% CO<sub>2</sub> and  
876 routinely cultured in either TcBSF3 [14] or HMI-93 [15], in both cases without a serum plus  
877 supplement, with 20% goat serum (Gibco). For global metabolite analysis of culture  
878 supernatant, an experimental medium (SCM-3) was used with the following components: 77  
879 mM NaCl, 1.5 mM CaCl<sub>2</sub>, 4.5 mM KCl, 0.8 mM MgSO<sub>4</sub>, 36 mM NaHCO<sub>3</sub>, 25 mM HEPES,  
880 0.05 mM bathocuproinedisulfonic acid, 0.22 mM 2-mercaptoethanol, 50 U/mL  
881 penicillin/streptomycin, 2.5 mM glucose, 1 mM pyruvate, 10 % goat serum, 10% TcBSF3  
882 [14], 1 mM each of L-cysteine and L-glutamine, and 100 µM L-tyrosine, L-phenylalanine, L-  
883 tryptophan, L-leucine, L-methionine and L-arginine. BSF *T. congolense* in exponential  
884 growth phase were centrifuged at 1,500 × *g* for 10 minutes, washed with PBS and inoculated  
885 into this medium (0 h time point).

886 For stable isotope labelling experiments, as well as experiments involving the removal or  
887 addition of specific medium components, a custom medium, Steketee's Congolense  
888 Medium-6 (SCM-6) was used (S6 Table). The final medium formulation based on this study's  
889 findings, SCM-7, is provided in S6 Table. This medium is essentially HMI-93, although i)  
890 vitamins (with the exception of folate) were removed, ii) D-glucose concentrations were  
891 modified depending on experimental procedure, but was routinely kept at 10 mM, iii) goat  
892 serum levels were reduced to 10% and, iv) of the 20 amino acids, 14 were added. Increasing

893 the temperature to 37°C led to a detrimental effect on cell viability after several passages, as  
894 previously reported [15].

895 For experiments involving *T. brucei*, either the monomorphic Lister 427 (*in vitro* experiments  
896 and growth curves) or pleomorphic STIB 247 (RNAseq experiments, both *in vitro* and *ex vivo*  
897 sample groups) strains were used. Lister 427 cells were grown in HMI-11 [110], whilst STIB  
898 247 were grown in modified HMI-9 containing 1.1% methylcellulose and 20% serum plus  
899 (Sigma) [111, 112]. In both cases, cells were incubated at 37°C, 5% CO<sub>2</sub>.

900 For both species, cell counts were carried out using a haemocytometer, and in the case of *T.*  
901 *congolense*, cells were mechanically detached from the culturing plasticware by pipetting  
902 prior to counting. Growth curves were routinely carried out in 2 mL samples incubated in 24-  
903 well plates, resuspended using a P1000. For detachment of cells from flasks, 10 mL plastic  
904 pipettes were used. In cases where cells were harvested for experiments other than those  
905 involving metabolomics, cells could also be detached by replacing the medium with PBS for  
906 incubating at room temperature for several minutes, prior to vigorously tapping the flask to  
907 detach parasites.

908 RNAi experiments using TcoSM were carried out in HMI-93 in 20 mL cultures. Cells were  
909 seeded at  $7 \times 10^5$  cells/mL and RNAi induction was initiated with the addition of 1 µg/mL  
910 tetracycline (Sigma) and  $1 \times 10^7$  cells were isolated every 24 hours for RNA analysis  
911 (outlined below) before cells were passaged

## 912 **Ethics statement**

913 All animal experiments were performed in accordance with the Animals (Scientific  
914 Procedures) Act 1986 and the University of Glasgow care and maintenance guidelines. All  
915 animal protocols and procedures were approved by The Home Office of the UK government  
916 and the University of Glasgow Ethics Committee.

## 917 **Animal experiments**

918 Adult female CD-1 mice (20–30 g body weight; Charles River Laboratories) were infected  
919 with  $5 \times 10^4$  wild-type *T. brucei* STIB 247 or  $1 \times 10^5$  wild-type *T. congolense* IL3000 by  
920 intraperitoneal injection. Parasitaemia was monitored daily by venesection of the lateral tail  
921 vein [113]. At first peak of parasitaemia ( $>10^7$  cells/mL) mice were euthanised and blood  
922 isolated. Parasites of both species were purified from blood by anion exchange using DEAE  
923 cellulose [114]. Purified cells were counted, and a total of  $1 \times 10^8$  cells were centrifuged for  
924 10 minutes at  $1,500 \times g$  prior to RNA extraction.

## 925 **RNA extraction**

926 For RNAseq experiments,  $10^8$  cells were isolated either from *in vitro* culture or from mouse  
927 infections. RNA was extracted using the QIAgen RNeasy kit (Qiagen) with an on-column  
928 DNase treatment step. Sample concentrations were analysed by Nanodrop and QuBit, and  
929 concentrations adjusted to 37 ng/ $\mu$ L of which 80  $\mu$ L (2.96  $\mu$ g) was submitted for RNAseq.

930 For RNAi time course experiments, cell pellets ( $10^7$  cells) were resuspended in 1 mL TRIzol  
931 (Invitrogen) and stored at  $-80^\circ\text{C}$ . Samples were thawed, 200  $\mu$ L chloroform was added,  
932 samples were shaken vigorously for 15 seconds and incubated at room temperature for 3  
933 minutes, prior to centrifugation at  $12,000 \times g$  for 15 minutes,  $4^\circ\text{C}$ . The aqueous layer was  
934 transferred to a fresh tube and 500  $\mu$ L isopropanol and 1  $\mu$ L Glycoblue (Invitrogen) were  
935 added. Samples were mixed by inverting, incubated at room temperature for 10 minutes and  
936 centrifuged at  $12,000 \times g$  for 10 minutes at  $4^\circ\text{C}$ . RNA pellet was washed in ice-cold 75%  
937 ethanol and centrifuged at  $12,000 \times g$  for 10 minutes at  $4^\circ\text{C}$ . After air-drying, RNA was  
938 resuspended in 20  $\mu$ L RNase-free water and concentration adjusted to 100 ng/ $\mu$ L. DNase  
939 treatment was carried out using the Ambion TURBO DNase kit (Applied Biosystems) as per  
940 manufacturer's instructions.

## 941 **Metabolomics sample preparation**

942 For metabolomics analysis of supernatants, 10 mL *T. congolense* cultures were incubated in  
943 T25 flasks in relevant media. Cells were centrifuged at  $1,500 \times g$  for 10 minutes, washed  
944 with PBS, resuspended in relevant media and density adjusted to  $1 \times 10^5$  cells/mL. At each  
945 time-point, 500  $\mu$ L medium was transferred to a 1.5 mL eppendorf tube and briefly quenched  
946 in a dry ice/ethanol bath, before centrifuging at  $1,500 \times g$  for 10 minutes at  $4^\circ\text{C}$ . A 5  $\mu$ L  
947 aliquot was then transferred to a new eppendorf containing 200  $\mu$ L metabolite extraction  
948 solvent (chloroform:methanol:water in a 1:3:1 ratio) and samples vortexed at  $4^\circ\text{C}$  for one  
949 hour. Samples were centrifuged for 5 minutes at  $13,000 \times g$  ( $4^\circ\text{C}$ ) and supernatants  
950 transferred to new eppendorfs. Samples were stored at  $-80^\circ\text{C}$  prior to analysis.

951 For analysis of intracellular metabolites, cells were grown to a final density of  $2 \times 10^6$   
952 cells/mL and a total of  $10^8$  cells isolated. Cells were quenched in 50 mL falcon tubes to  $4^\circ\text{C}$   
953 using a dry ice/ethanol bath (stirred and measured by thermometer) and all subsequent  
954 steps were carried out at  $4^\circ\text{C}$ . Cells were centrifuged at  $1,500 \times g$  for 10 minutes and if  
955 supernatant samples were required in addition to cell pellets, 5  $\mu$ L was transferred to an  
956 eppendorf containing 200  $\mu$ L extraction solvent. Cells were resuspended in residual medium  
957 before transfer to eppendorf tubes. Cells were then centrifuged ( $1,500 \times g$ , 5 minutes) and  
958 washed twice with ice-cold phosphate buffered saline (PBS) before resuspension in 200  $\mu$ L  
959 extraction solvent (chloroform:methanol:water in a 1:3:1 ratio). Samples were vortexed at

960 4°C for 1 hour, and then centrifuged for 5 minutes at 13,000 × *g*. Supernatants were  
961 transferred to clean eppendorf tubes. For all experiments, a quality control sample was  
962 generated by pooling 10 µL from each sample and samples were stored under argon gas at  
963 -80°C.

### 964 **Primers and plasmids**

965 RNAi experiments were carried out using a *T. congolense* single marker line, TcoSM [69]  
966 that expresses Tet repressor and T7 polymerase, maintained in 0.5 µg/mL puromycin, and  
967 gene specific RNAi constructs were introduced with a *T. congolense* specific plasmid, p3T7-  
968 TcoV [69]. Primers carrying a HindIII (5'-AAGCTT-forward) or an FseI (5'-GGCCGGCC-  
969 reverse) restriction site were used to amplify *TcoPEPCK*, *TcoPPDK* and *TcoHT* (S7 Table).  
970 Gene fragments were amplified using a HiFi polymerase master mix (NEB) and cloned into  
971 pGEM-T easy (Promega) and sequenced to confirm correct sequence identity of each  
972 fragment. The constructs were then digested with HindIII and FseI and ligated into the p3T7-  
973 TcoV vector using T4 DNA ligase (Promega). The final plasmid was linearised with NotI  
974 before purification by ethanol precipitation prior to electroporation into TcoSM cells.

### 975 **Transfections/electroporations**

976 *T. congolense* IL3000 electroporation experiments and selection experiments were  
977 performed as developed by [69]. A total of  $4 \times 10^7$  cells were used per transfection, including  
978 a negative (buffer only) control. A transfection buffer previously published for use with *T.*  
979 *brucei* was used for *T. congolense* transfections [115]. Cells were centrifuged at 1,500 × *g*  
980 for 10 minutes, pellets resuspended in residual medium and transferred to eppendorf tubes  
981 for a further centrifugation step. Cells were subsequently washed in transfection buffer prior  
982 to final resuspension in 100 µL buffer per transfection. Up to 12 µg linearised plasmid DNA  
983 was added to an electroporation cuvette (Sigma), and 100 µL cells were subsequently  
984 added. Electroporation was carried out using a Nucleofector II (Lonza) programme Z-001.  
985 Transfected cells were then incubated overnight in 25 mL warm medium in the absence of  
986 selective antibiotics, prior to their addition and plating out at dilutions of 1:50, 1:100 and  
987 1:200 in 96-well plates. Antibiotics were added at the following concentrations: Puromycin:  
988 0.5 µg/mL; Neomycin (G418): 0.4 µg/mL. Clones were retrieved after 7-10 days, and these  
989 were maintained in 0.25 µg/mL puromycin and 0.2 µg/mL G418.

### 990 **Drug sensitivity assays**

991 Drug sensitivity assays were carried out using the alamar blue method developed by Raz  
992 and colleagues [116]. Briefly, Compounds were diluted to 2x starting concentration in SCM-6  
993 (with 10% goat serum for *T. congolense* IL3000 or 10% FBS for *T. brucei* Lister 427) and  
994 200 µL was transferred to the first well of a solid white flat-bottomed 96-well plate. 100 µL

995 medium was then added to 23 further wells and compounds were diluted 1:2 over this series  
996 of wells, with the exception of the last well, for a negative control. Subsequently, 100  $\mu$ L cells  
997 were added at 2 $\times$  starting density ( $4 \times 10^4$  cells/mL for *T. brucei* and  $5 \times 10^5$  cells/mL for *T.*  
998 *congolense*). Plates were incubated for 48 hours (37°C or 34°C for *T. brucei* and *T.*  
999 *congolense*, respectively, 5% CO<sub>2</sub> in both cases), prior to addition of 20  $\mu$ L resazurin sodium  
1000 salt (0.49 mM in 1 $\times$  PBS, pH 7.4) to each well. Plates were then incubated for a further 24  
1001 hours before measurements of cell viability.

1002 Reduction of the resazurin salt was measured as a function of cell viability. Fluorescence of  
1003 each plate was read using a Cytation 5 imaging reader (BioTek) and GEN5 software.  
1004 Parameters were as follows:  $\lambda_{\text{excitation}} = 540$  nm and  $\lambda_{\text{emission}} = 590$  nm. Raw values were  
1005 plotted against concentrations (converted to Log<sub>10</sub> values) and normalised (0% defined as  
1006 smallest mean in the dataset; 100% defined as largest mean in the dataset) using Graphpad  
1007 Prism version 8.4.0. EC<sub>50</sub> values for each compound were calculated using a non-linear  
1008 sigmoidal dose-response curve. Each assay was performed in duplicate and each EC<sub>50</sub>  
1009 value represents a mean of three independent experiments.

### 1010 **Real-time quantitative PCR (RT-qPCR)**

1011 RNA was extracted as described above, and reverse transcription was carried out in 20  $\mu$ L  
1012 using 1  $\mu$ g RNA, using a high capacity cDNA kit (Applied Biosystems). Primers for RT-qPCR  
1013 analysis were designed using Primer 3 [117], and primer efficiency was tested using serial  
1014 dilutions of *T. congolense* IL3000 genomic DNA by plotting Ct value against Log<sub>10</sub>(DNA  
1015 concentration). Real-time PCR was carried out using the SensiFAST SYBR Hi-ROX kit  
1016 (Bioline, BIO92005). Briefly, a 20  $\mu$ L reaction was set up using 10  $\mu$ L SYBR mix, RT  
1017 template and 400 nM of each primer. Cycling conditions were: 96°C, 120 seconds, followed  
1018 by 40 cycles of 95°C for 5 seconds, 62°C for 10 seconds and 72°C for 20 seconds.  
1019 Previously published endogenous control primers for TcoTERT were used for within sample  
1020 normalisation [118], and normalised transcript level was calculated using the delta delta Ct  
1021 method [119].

### 1022 **Glucose uptake assays**

1023 For analysis of wild-type *T. congolense* and *T. brucei* glucose uptake, cells were seeded in  
1024 10 mL cultures of SCM-6 at an initial density of  $2 \times 10^5$  cells/mL (four cultures per species),  
1025 with 10 mM glucose added separately at the start of the experiment. Upon the addition of  
1026 glucose, 1 mL supernatant was immediately centrifuged (1,500  $\times$  g, 10 minutes) and  
1027 supernatant stored at -80°C. This process was repeated at 12, 15, 18, 21 and 24 h, and cell  
1028 density measured by haemocytometer. A medium-only control (4 replicates) was also  
1029 incubated alongside *in vitro* cultures. Glucose concentration of each supernatant sample

1030 was analysed using the Glucose (GO) assay kit (GAGO-20; Sigma) in a 96-well format.  
1031 Briefly, 40  $\mu$ L supernatant sample (diluted if necessary) was incubated with 80  $\mu$ L assay  
1032 reagent for 30 minutes at 37°C, after which 80  $\mu$ L 12 N sulphuric acid was added and  
1033 absorbance measured at 540 nm using a spectrophotometer. A standard curve was also run  
1034 to calculate glucose concentration. Rate of glucose consumption was calculated using a  
1035 custom script [57].

1036 For glucose consumption of the TcoHT RNAi line, the Glucose Uptake-Glo kit (Promega)  
1037 was used. RNAi was induced for 72 hours prior to carrying out the assay. Cells were  
1038 centrifuged, washed in PBS and resuspended in assay buffer (77 mM NaCl, 1.5 mM CaCl<sub>2</sub>-  
1039 2H<sub>2</sub>O, 4.5 mM KCl, 0.8 mM MgSO<sub>4</sub>-7H<sub>2</sub>O, 36 mM NaHCO<sub>3</sub>, 25 mM HEPES and 0.02 mM  
1040 bathocuproinedisulfonic acid), as it was determined *T. congolense* viability is reduced in PBS  
1041 alone. Density was adjusted to 10<sup>8</sup> cells/mL, and three 100  $\mu$ L replicates of each sample  
1042 were added to wells of a black flat-bottomed 96-well plate. The uptake reaction was started  
1043 by the addition of 50  $\mu$ L 1 mM 2-deoxy-D-glucose. Plate was shaken for 15 minutes at 34°C  
1044 prior to addition of 25  $\mu$ L stop buffer, 25  $\mu$ L neutralisation buffer and 100  $\mu$ L pre-prepared  
1045 2DG6P detection reagent. Plates were shaken in between addition of the buffers. Finally, the  
1046 plate was read with 0.3–1 second integration on a luminometer (Cytation 5 Imaging reader,  
1047 BioTek). Wild-type *T. congolense*, and *T. congolense* supplemented with glucose were used  
1048 as controls, in addition to cells without 2-deoxy-D-glucose and assays in the absence of  
1049 cells.

## 1050 **Metabolomics – Liquid chromatography mass spectrometry**

1051 Hydrophilic interaction liquid chromatography (HILIC) was carried out by Glasgow Polyomics  
1052 (Glasgow, UK), using a Dionex UltiMate 3000 RSLC system (Thermo Fischer Scientific)  
1053 coupled to a ZIC-pHILIC column (150 mm  $\times$  4.6 mm, 5  $\mu$ m column, Merck Sequant). The  
1054 column was maintained at 30°C and samples were eluted with a linear gradient (20 mM  
1055 ammonium carbonate in water and acetonitrile) over 26 minutes with a flow rate of 0.3  
1056 mL/minute.

1057 Sample injection volume was 10  $\mu$ L and samples were maintained at 4°C before injection. A  
1058 Thermo Orbitrap Exactive (Thermo Fischer Scientific) was used to generate mass spectra,  
1059 and was operated in polarity switching mode with the following settings: Resolution: 50,000;  
1060 AGC: 106; m/z range: 70–1,400; sheath gas: 40; auxiliary gas: 5; sweep gas: 1; probe  
1061 temperature: 150°C; capillary temperature: 275°C. Samples were run in both positive and  
1062 negative polarity with the following ionisation: source voltage +4.5 kV, capillary voltage +50  
1063 V, tube voltage +70 kV and skimmer voltage +20 V for positive mode; source voltage -3.5  
1064 kV, capillary voltage -50 V, tube voltage -70 V and skimmer voltage -20 V for negative mode.

1065 Mass calibration was performed for each polarity immediately prior to each analysis batch.  
1066 The calibration mass range was extended to cover small metabolites by inclusion of low-  
1067 mass contaminants with the standard Thermo calmix masses (below  $m/z$  1400),  $C_2H_6NO_2$  for  
1068 positive ion electrospray ionisation (PIESI) mode ( $m/z$  76.0393) and  $C_3H_5O_3$  for negative ion  
1069 electrospray ionisation (NIESI) mode ( $m/z$  89.0244). To enhance calibration stability, lock-  
1070 mass correction was also applied to each analytical run using these ubiquitous low-mass  
1071 contaminants. A set of authentic standards was run prior to the sample set for each  
1072 experiment.

### 1073 **Metabolomics data analysis**

1074 RAW spectra were converted to mzXML files (mzML files for fragmentation data) using  
1075 XCMS for untargeted peak detection [120]. The resultant files were further processed using  
1076 mzMatch [121] for peak matching and annotation, resulting in a tabular output that was  
1077 analysed using IDEOM with default settings [122]. For stable-isotope assisted metabolomics  
1078 experiments, mzMatch output (in .peakml format) was analysed using mzMatch-ISO to  
1079 extract all carbon isotopologue abundances from putative metabolites [123]. Data analysis of  
1080 stable isotope-labelled metabolomics was based on a 48 hour time-point in all experiments.  
1081 Data was further analysed using Microsoft Excel or Metaboanalyst v4.0 [124]. The mzXML  
1082 files from all metabolomics analyses are available in Metabolights.

### 1083 **RNA sequencing and data processing**

1084 RNA sequencing was carried out by Edinburgh Genomics (Edinburgh, UK). Libraries were  
1085 prepared from 8 samples (4x *T. brucei*, 4x *T. congolense*) using the TruSeq Stranded  
1086 mRNA kit (Illumina) and 2 × 75 bp paired-end sequencing was carried out using a HiSeq  
1087 4000 system (Illumina). Sequencing reads were aligned to the corresponding genome  
1088 sequence using HiSat2 (--no-spliced-alignment) [125]. For *T. brucei*, the TREU 927  
1089 reference genome sequence was used (v34.0 from TriTrypDB [126]), whilst a PacBio  
1090 assembly of *T. congolense* IL3000 was used for *T. congolense* [65]. The resulting SAM files  
1091 were converted to BAM files using samtools [127], and subsequently filtered for quality and  
1092 primary alignment (-q 1 -F 0x100), the latter to reduce the effects of multimapping. Read  
1093 counts were extracted from the filtered BAM files using HTSeq-count (-s reverse -f bam -t  
1094 CDS -i ID -m union -a 0 --nonunique all).

1095 For all samples, transcripts per million (TPM) values for each gene were calculated manually  
1096 using Microsoft Excel as follows: 1) Reads per kilobase (RPK) were calculated by dividing  
1097 the read counts by the length of gene in kilobases; 2) All RPK values in a sample were  
1098 summed and divided by 1 million as a scaling factor; 3) Each RPK value was divided by the  
1099 scaling factor to yield TPM values [53]. To compare transcript abundances between the two



1100 species, Orthofinder [54] was used to infer orthologue genes or gene groups. Default  
1101 parameters were used to compare the TriTrypDB v34.0 TREU 927 annotated proteins and  
1102 the PacBio *T. congolense* IL3000 annotated proteins (S2 Table). A custom MATLAB  
1103 (version R2019a) was used to combine the Orthofinder dataset and the TPM values for 1-to-  
1104 1 orthologues, as well as “sum of TPM” values for groups containing multiple genes, where  
1105 TPM value for each gene was summed, resulting in a final dataset (S1 Table). Raw RNA-  
1106 seq data is deposited at GEO. Transcriptomics data were cross-referenced with the  
1107 TrypanoCyc database ([vm-trypanocyc.toulouse.inra.fr/](http://vm-trypanocyc.toulouse.inra.fr/); [60]) to enable pathway analysis of  
1108 the data.

## 1109 **Computation**

1110 Figures were generated using Graphpad Prism version 8.4.0 ([www.graphpad.com](http://www.graphpad.com)) with the  
1111 exception of scatter plots and heatmaps, which were generated using R [128]. Heatmaps  
1112 were generated using the R packages pheatmap and ComplexHeatmap [129]; scatter plots  
1113 were generated using GGplot2 and GGally; and pathway maps were generated with  
1114 Inkscape v1.0.

## 1115 **Acknowledgements**

1116 The authors would like to thank the following people: Steve Kelly, Paul Michels & Simon  
1117 Young for very useful discussion. We thank Anne-Marie Donachie for help with *in vivo*  
1118 experiments. In addition, the authors would like to thank the following institutes: Glasgow  
1119 Polyomics for LC-MS work, Edinburgh Genomics for RNAseq, MRC PPU DNA Sequencing  
1120 and Services, Dundee, for plasmid sequencing. LM, PS, EP, HdK and MPB were funded by  
1121 BBSRC grant BB/N007492/1, and LM, PS, EP, RR and MPB by BB/S00243X/1. CG and BW  
1122 were funded by University of Nottingham Strategic Support Funds (Wellcome Trust), and  
1123 GAM by Sir Halley Stewart Medical Research Grant (R410). This article is based on  
1124 research funded in part by the Bill & Melinda Gates Foundation (Investment ID  
1125 OPP1176784) and with UK aid from the UK Government (Project 300504) through  
1126 GALVmed. The findings and conclusions contained within are those of the authors and do  
1127 not necessarily reflect positions or policies of the Bill & Melinda Gates Foundation or the UK  
1128 Government. The Roslin Institute is core funded by the BBSRC (BS/E/D/20002173).

## 1129 **Figure legends**

1130 **Figure 1: Overview of comparative transcriptomics analysis of *T. brucei* and *T.***  
1131 ***congolense*, isolated from *ex vivo* and *in vitro* conditions.** RNAseq data from *T.*  
1132 *congolense* (IL3000) and *T. brucei* (STIB247) in both *in vitro* and *ex vivo* (from mouse

1133 infections) conditions was aligned to the species' respective genome sequence and read  
1134 counts were normalised by the transcripts per million (TPM) method. To directly compare the  
1135 species, a pseudogenome was generated using the Orthofinder tool [54]. TPM values from  
1136 the 4 sample groups were plotted against each other to analyse correlation between  
1137 conditions (A and B) and between species in the same conditions (C and D). Correlation was  
1138 assessed using both Spearman's rank correlation ( $\rho$ ) and Pearson correlation ( $\rho$ ; Pearson's  
1139  $r$ ) coefficients.

1140 **Figure 2: Analysis of supernatant metabolites after *T. congolense* culture.** A heatmap  
1141 covering the 80 putative medium components judged to be significantly altered after 56  
1142 hours of *in vitro* cell culture containing *T. congolense* strain IL3000, as calculated by a one-  
1143 way repeated measures ANOVA ( $P < 0.05$ ). Peak abundances were log transformed and  
1144 mean centred and metabolites were clustered based on Pearson correlation. Two clusters of  
1145 interest were identified, which are shown in a larger format on the right. Metabolites in the  
1146 top cluster were observed to increase significantly over time, whilst those in the bottom  
1147 cluster decreased. Metabolite names follow by [\*] were matched to an authentic standard. B)  
1148 Comparison of metabolite changes in medium supernatants after 56 hours between *T.*  
1149 *brucei* [56] and *T. congolense* (S4 Table). Relative changes in metabolite abundance were  
1150 calculated as  $\text{Log}_2$  fold change of 56 h vs 0 h. Key differences are highlighted numerically: 1,  
1151 guanine; 2, N6-acetyl-L-lysine; 3, succinate; 4, 4-hydroxy-4-methylglutamate; 5, N6,N6,N6-  
1152 trimethyl-L-lysine; 6, choline; 7, 2-oxoglutarate; 8, L-1-pyrroline-3-hydroxy-5-carboxylate; 9,  
1153 D-glycerate; 10, pyruvate; 11, 12-hydroxydodecanoic acid; 12, L-cystine; 13, diacetyl; 14,  
1154 [PC (18:0)] 1-octadecanoyl-sn-glycero-3-phosphocholine; 15, LysoPC(17:0); 16, [PC (16:0)]  
1155 1-hexadecanoyl-sn-glycero-3-phosphocholine; 17, inosine; 18, [PC (16:1)] 1-(9Z-  
1156 hexadecenoyl)-sn-glycero-3-phosphocholine; 19, [FA trihydroxy(18:1)] 9S,12S,13S-  
1157 trihydroxy-10E-octadecenoic acid; 20, inosine.

1158 **Figure 3: Energy metabolism in *T. congolense*.** A-E) Supernatant metabolomics analysis  
1159 of metabolites involved in glycolytic metabolism in *T. congolense*. Grey bars indicate a  
1160 negative medium control incubated for 56 hours. F) A commercial kit was used to measure  
1161 acetate concentration during *T. congolense* culture, with supernatant samples analysed at  
1162 the same time points as the supernatant metabolomics experiment. G) A simplified overview  
1163 of the glycolytic pathway. Typically, the succinate shunt is only active in PCF *T. brucei*, with  
1164 low levels of activity in BSF *T. brucei*. Numbers refer to the following proteins: 1, glucose  
1165 transporters; 2, hexokinase; 3, glucose 6-phosphate isomerase; 4, phosphofructokinase; 5,  
1166 aldolase; 6, triosephosphate isomerase; 7, glycerol 3-phosphate dehydrogenase; 8, glycerol  
1167 kinase; 9, glyceraldehyde 3-phosphate dehydrogenase; 10, phosphoglycerate kinase; 11,  
1168 phosphoglycerate mutase and enolase; 12, phosphoenolpyruvate carboxykinase; 13, malate

1169 dehydrogenase; 14, fumarate hydratase; 15, NADH-dependent fumarate reductase; 16,  
1170 pyruvate kinase; 17, alanine aminotransferase; 18, pyruvate dehydrogenase complex; 19,  
1171 acetate:succinate CoA-transferase and acetyl-CoA thioesterase. H) Tracing glucose derived  
1172 carbon usage through glycolytic metabolism. *T. congolense* were incubated with a 50:50 mix  
1173 of <sup>12</sup>C-D-glucose:<sup>13</sup>C-U-D-glucose before cell pellets were isolated for metabolomics  
1174 analysis. Results were compared to those generated in *T. brucei* by Creek and colleagues  
1175 [42]. Colours indicate the number of <sup>13</sup>C atoms in each metabolite. I) Comparative analysis  
1176 of transcript level activity of glycolysis in *T. brucei* and *T. congolense* from both *in vitro* and  
1177 *ex vivo* conditions. Gene IDs: HK1 & 2, hexokinase, TbTc\_0341; GPI, glucose 6-phosphate  
1178 isomerase, TbTc\_1840; PFK, phosphofructokinase, TbTc\_1399; ALDA, aldolase,  
1179 TbTc\_0358; TPI, Triosephosphate isomerase, TbTc\_1075; GPDH, glycerol 3-phosphate  
1180 dehydrogenase, TbTc\_2722; GK, glycerol kinase, TbTc\_0392; GAPDH, glyceraldehyde 3-  
1181 phosphate dehydrogenase, TbTc\_0377; PGK, phosphoglycerate kinase, TbTc\_6030; PGKA,  
1182 phosphoglycerate kinase A, TbTc\_0241; PGKB/C, phosphoglycerate kinase B & C,  
1183 TbTc\_0240, ENO1, enolase, TbTc\_0465; ENO2, enolase, putative, TbTc\_3614, PK1,  
1184 pyruvate kinase 1, TbTc\_0372; FBPase, fructose-1,6-bisphosphatase, TbTc\_1967; PEPCK,  
1185 phosphoenolpyruvate carboxykinase, TbTc\_0348; gMDH, glycosomal malate  
1186 dehydrogenase, TbTc\_0642, FH, fumarate hydratase, TbTc\_0242; Frd, NADH-dependent  
1187 fumarate reductase, TbTc\_0141; PPDK, pyruvate phosphate dikinase, TbTc\_1304; AAT,  
1188 alanine aminotransferase, TbTc\_0675; PDH E1 $\alpha$ , pyruvate dehydrogenase E1 alpha  
1189 subunit, TbTc\_4169; PDH E1 $\beta$ , pyruvate dehydrogenase E1 beta subunit, TbTc\_5437.

1190 **Figure 4: *In vitro* analysis of glycolytic metabolism.** To further probe glycolytic  
1191 metabolism in *T. congolense*, novel RNAi technology was employed to knock-down key  
1192 glycolytic and gluconeogenic steps. A) *T. congolense* remains viable in reduced glucose  
1193 concentrations. A growth defect was only observed when glucose concentrations were  
1194 reduced to <2 mM. B) Supplementation with increased concentrations of 2-deoxy-D-glucose  
1195 leads to *T. congolense* cell death (red dotted line indicates detection limit by  
1196 haemocytometer). C) Growth analysis of RNAi-mediated knock-down of PEPCK in *T.*  
1197 *congolense* IL3000 single marker induced with 1  $\mu$ g/mL tetracycline. D) Growth analysis of  
1198 RNAi-mediated knock-down of PPDK in *T. congolense* IL3000 single marker induced with 1  
1199  $\mu$ g/mL tetracycline. E-F) Transcript abundance over time, following tetracycline-mediated  
1200 RNAi induction of PEPCK and PPDK. G) Knock-down of the entire glucose transporter (HT)  
1201 array does not affect *in vitro* cell viability. H) Normalised HT mRNA abundance over time  
1202 after RNAi induction. I) Changes in glucose uptake in RNAi-induced cells were detected via  
1203 an enzyme-linked luminescence assay coupled to 2-deoxy-D-glucose uptake over a period

1204 of 30 minutes. The assay was carried out 72-hours post-induction. Of the three RNAi lines, 2  
1205 showed a significant reduction in glucose uptake capability (\* $P < 0.05$ ; \*\*\* $P < 0.001$ )

1206 **Figure 5: Nucleotide metabolism in *T. congolense*.** Supernatant analysis of *T.*  
1207 *congolense* *in vitro* cultures showing changes in abundance of D-ribose (A), guanine (B),  
1208 xanthine (C) and inosine (D) over 56 hours. Grey bar indicates a negative medium control  
1209 group E) Simplified overview of purine salvage and synthesis in trypanosomatids adapted  
1210 from [130]. Numbers indicate the following enzymes: 1, APRT; 2, AD; 3, HGPRT; 4, IMPD;  
1211 5, HGXPRT; 6, GMPR; 7, GMPS; 8, HGPRT. Red cross indicates guanine deaminase,  
1212 which is not encoded/annotated in the *T. congolense* genome. F) Comparison of glucose-  
1213 derived purine carbon labelling in *T. congolense* and *T. brucei* [42]. Colours indicate the  
1214 number of  $^{13}\text{C}$  atoms in each metabolite. D) Comparative RNAseq analysis of *T. congolense*  
1215 and *T. brucei* under both *in vitro* and *ex vivo* conditions. Gene IDs from top to bottom: P121-  
1216 PWY (adenine/adenosine salvage): IMPDH1, inosine-5'-monophosphate dehydrogenase,  
1217 TbTc\_1648; ADSS, adenylosuccinate synthetase, TbTc\_1142; APRT-1, cytosolic adenine  
1218 phosphoribosyltransferase, TbTc\_3522; HGPRT, hypoxanthine-guanine  
1219 phosphoribosyltransferase, TbTc\_0726; GMPR, GMP reductase, TbTc\_4627; HGXPRT,  
1220 hypoxanthine-guanine-xanthine phosphoribosyltransferase, TbTc\_3696; APRT-2,  
1221 glycosomal adenine phosphoribosyltransferase, TbTc\_5918; ADSL, adenylosuccinate lyase,  
1222 TbTc\_1986. PWY0-162 (pyrimidine biosynthesis): DHODH, dihydroorotate dehydrogenase  
1223 (fumarate), TbTc\_0620; PYR1A-B, glutamine hydrolysing carbomoyl phosphate synthase,  
1224 TbTc\_1631; PYR2, aspartate carbamoyltransferase, TbTc\_1630; PYR3, dihydroorotase,  
1225 TbTc\_3801; CTPS, cytidine triphosphate synthase, TbTc\_0920; OMPDC/OPRT, orotidine-5-  
1226 monophosphate decarboxylase/orotate phosphoribosyltransferase, TbTc\_0735; CMF40a,  
1227 nucleoside diphosphate kinase, TbTc\_5784. PWY0-163 (pyrimidine salvage): UP, uridine  
1228 phosphorylase, TbTc\_5794; CDA, cytidine deaminase, TbTc\_3318; UPRT, uracil  
1229 phosphoribosyltransferase, TbTc\_4220; NDPK, nucleoside diphosphate kinase, TbTc\_0593;  
1230 CMF40a, nucleoside diphosphate kinase, TbTc\_5784; NDPK3, nucleoside diphosphate  
1231 kinase 3, TbTc\_2560.

1232 **Figure 6: Amino acid metabolism in *T. congolense* IL3000.** A-C) Analysis of indicated  
1233 amino acids in *T. congolense* IL3000 culture supernatants over a 56 h time course. Grey  
1234 bars indicate a negative medium control group. D-F) Growth curves in SCM-6 excluding one  
1235 amino acid at a time, to determine those essential to *T. congolense* viability. In each  
1236 experiment, full SCM-6 was used as a positive control. Legends indicate which amino acid  
1237 was removed in each experiment. G) Growth analysis of SCM-6 and SCM-7, the latter  
1238 containing only amino acids deemed essential, compared to HMI-93 [110]. H) Simplified map  
1239 of intracellular glutamine metabolism. Numbers refer to the following enzymes: 1,

1240 glutaminase; 2, glutamate decarboxylase; 3, 4-aminobutyrate aminotransferase; 4, succinate  
1241 semialdehyde dehydrogenase; 5, glutamate dehydrogenase; 6, 2-oxoglutarate  
1242 dehydrogenase; 7, Succinyl-CoA synthetase; 8, isocitrate dehydrogenase; 9 & 10,  
1243 aconitase. I) Carbon utilisation from L-glutamine was analysed in *T. congolense* (100% <sup>13</sup>C-  
1244 U-L-glutamine) and compared to that in *T. brucei* (50:50 ratio of L-glutamine and <sup>13</sup>C-U-L-  
1245 glutamine) [85].

1246 **Figure 7: Fatty acid metabolism in *T. congolense*.** A) Glucose-derived <sup>13</sup>C carbon  
1247 labelling of saturated fatty acids in *T. congolense* and *T. brucei* [42]. Colours correspond to  
1248 the number of <sup>13</sup>C labels detected in each metabolite. B) L-threonine-derived saturated fatty  
1249 acid <sup>13</sup>C labelling in *T. congolense*. Fatty acid systematic names and numbers: lauric acid:  
1250 dodecanoic acid, C12:0; myristic acid: tetradecanoic acid, C14:0; palmitic acid:  
1251 hexadecanoic acid, C16:0; nonadecyclic acid: nonadecanoic acid, C19:0. C) Transcriptomics  
1252 analysis of acetate and lipid metabolism. Gene names and IDs: ACH, acetyl-CoA hydrolase,  
1253 TbTc\_5515; ACS, acetyl-CoA synthetase, TbTc\_0318; AKCT, 2-amino-3-ketobutyrate-CoA  
1254 ligase, TbTc\_6236; TDH, L-threonine 3-dehydrogenase, TbTc\_5991; PDHe1 $\alpha$ , pyruvate  
1255 dehydrogenase E1  $\alpha$  subunit, TbTc\_4169; PDHe1 $\beta$ , pyruvate dehydrogenase E1  $\beta$  subunit;  
1256 SCS $\alpha$ , succinyl-CoA synthetase  $\alpha$  subunit, TbTc\_0813; PPK, pyruvate phosphate dikinase,  
1257 TbTc\_1304; PDHe2, dihydrolipoamide acetyltransferase, TbTc\_1015; PDHe3, pyruvate  
1258 dehydrogenase E3, TbTc\_4765; PYK1, pyruvate kinase, TbTc\_0372; BKR,  $\beta$ -ketoacyl-ACP  
1259 reductase, TbTc\_1241; BKS,  $\beta$ -ketoacyl synthase, TbTc\_3372; ACC, acetyl-CoA  
1260 carboxylase, TbTc\_0754; HMGCL, hydroxymethylglutaryl-CoA lyase, TbTc\_6160; FPPS,  
1261 farnesyl pyrophosphate synthase, TbTc\_5375; LSS, lanosterol synthase, TbTc\_4540; MVK,  
1262 mevalonate kinase, TbTc\_3761; SM, squalene monooxygenase, TbTc\_3357; MDD,  
1263 mevalonate diphosphate decarboxylase, TbTc\_0546; SMT, sterol 24-c methyltransferase,  
1264 TbTc\_0387; CYP51A1, lanosterol 14 $\alpha$  demethylase, TbTc\_4837; SQase, squalene  
1265 synthase, TbTc\_2577; SPPS, solanesyl-diphosphate synthase, TbTc\_3025; IDI, isopentenyl-  
1266 diphosphate delta-isomerase, TbTc\_1099; PTase, prenyltransferase, TbTc\_1352; GGTase-  
1267 II $\beta$ , geranylgeranyl transferase type II  $\beta$  subunit, TbTc\_0680; SCP2, 3-ketoacyl-CoA  
1268 thiolase, TbTc\_4024; PMVK, phosphomevalonate kinase, TbTc\_3039; HMGR, 3-hydroxy-3-  
1269 methylglutaryl-CoA reductase, TbTc\_3189; LACS5, fatty acyl-CoA synthetase, TbTc\_0099;  
1270 ACSL\_0688, long-chain-fatty-acid-CoA ligase, TbTc\_0688; ECHD, enoyl-CoA hydratase,  
1271 TbTc\_3283; ACS3/ACS4, fatty acyl-CoA synthetase 3 & 4, TbTc\_0101; ACS1, fatty acyl-  
1272 CoA synthetase 1, TbTc\_0100; ACS2, fatty acyl-CoA synthetase 2, TbTc\_0102; ECI\_4184,  
1273 3,2-trans-enoyl-CoA isomerase, TbTc\_4184; ACSL\_2381, long-chain-fatty-acid-CoA ligase,  
1274 TbTc\_2381; TFE $\alpha$ 1, enoyl-CoA hydratase/enoyl-CoA isomerase, TbTc\_3362; SCP2, 3-

1275 ketoacyl-CoA thiolase, TbTc\_4024; ECI\_0360, 3,2-trans-enoyl-CoA isomerase, TbTc\_0360;  
1276 ACAD, acyl-CoA dehydrogenase, TbTc\_4954.

1277 **Figure 8: Pharmacological inhibition of fatty acid synthesis in *T. brucei* and *T.***  
1278 ***congolense*.** Dose-response curves to determine differential sensitivity of the two species of  
1279 parasite to inhibition of an ACS inhibitor (panel A) and Orlistat (B).

1280 **Figure 9: Summary of *T. congolense* and *T. brucei* in vitro transcriptome.** Log<sub>2</sub> fold  
1281 change (*T. congolense*/*T. brucei*) was calculated for each gene (for ratio changes, see the key  
1282 on the bottom-left). Dashed lines represent transport processes. Genes: 1, hexose  
1283 transporters, TbTc\_0095; 2, hexokinase, TbTc\_0341; 3, glucose-6-phosphate isomerase,  
1284 TbTc\_1840; 4, phosphofructokinase, TbTc\_1399; 5, fructose-1,6-bisphosphatase,  
1285 TbTc\_1967; 6, aldolase, TbTc\_0358; 7, triosephosphate isomerase, TbTc\_1075; 8, glycerol-  
1286 3-phosphate dehydrogenase, TbTc\_2722; 9, glycerol kinase, TbTc\_0392; 10,  
1287 glyceraldehyde 3-phosphate dehydrogenase, TbTc\_0377; 11, phosphoglycerate kinase,  
1288 TbTc\_0240; 12, phosphoglycerate mutase, TbTc\_5039; 13, enolase, TbTc\_0465; 14,  
1289 pyruvate kinase 1, TbTc\_0372; 15, alanine aminotransferase, TbTc\_0675; 16, pyruvate  
1290 phosphate dikinase, TbTc\_1304; 17, Phosphoenolpyruvate carboxykinase, TbTc\_0348; 18,  
1291 glycosomal malate dehydrogenase, TbTc\_0642; 19, glycosomal fumarate hydratase,  
1292 TbTc\_0242; 20, glycosomal NADH-dependent fumarate reductase, TbTc\_0140; 21, glucose-  
1293 6-phosphate dehydrogenase, TbTc\_0931; 22, 6-phosphogluconolactonase, TbTc\_4165; 23,  
1294 6-phosphogluconate dehydrogenase, TbTc\_2025; 24, ribulose-5-phosphate epimerase,  
1295 TbTc\_4356; 25, ribose 5-phosphate isomerase, TbTc\_3090; 26, transketolase, TbTc\_1701;  
1296 27, transaldolase, TbTc\_1823; 28, ribokinase, TbTc\_5212; 29, malic enzyme, TbTc\_0296;  
1297 30, Mitochondrial pyruvate carrier 2, TbTc\_2668; 31, FAD-dependent glycerol-3-phosphate  
1298 dehydrogenase, TbTc\_2282; 32, NADH dehydrogenase (NDH2), TbTc\_5033; 33, Alternative  
1299 oxidase, TbTc\_6589; 34, mitochondrial fumarate hydratase, TbTc\_0243; 35, mitochondrial  
1300 NADH-dependent fumarate reductase, TbTc\_0141; 36, mitochondrial malate  
1301 dehydrogenase, TbTc\_0256; 37, citrate synthase, TbTc\_0486; 38, aconitase, TbTc\_5765;  
1302 39, isocitrate dehydrogenase, TbTc\_0510; 40, 2-oxoglutarate dehydrogenase E1  
1303 component, TbTc\_2864; 41, 2-oxoglutarate dehydrogenase E1 component, TbTc\_3111; 42,  
1304 2-oxoglutarate dehydrogenase E2 component, TbTc\_3057; 43, succinyl-CoA synthetase  $\alpha$ ,  
1305 TbTc\_0813; 44, succinyl-CoA ligase  $\beta$ , TbTc\_3392; 45, glutamine synthetase, TbTc\_2226;  
1306 46, glutamate dehydrogenase, TbTc\_0872; 47, pyruvate dehydrogenase E1  $\alpha$  subunit,  
1307 TbTc\_4169; 48, pyruvate dehydrogenase E1  $\beta$  subunit, TbTc\_5437; 49, dihydrolipoamide  
1308 acetyltransferase, TbTc\_1015; 50, pyruvate dehydrogenase complex E3, TbTc\_4765; 51, L-  
1309 threonine 3-dehydrogenase, TbTc\_5991; 52, 2-amino-3-ketobutyrate coenzyme A ligase,  
1310 TbTc\_6236; 53, Acetyl-CoA hydrolase (ACH), TbTc\_5515; 54, Succinyl-CoA:3-ketoacid

1311 coenzyme A transferase (ASCT), TbTc\_0236; 55, Acyl carrier protein, TbTc\_5262; 56, beta-  
1312 ketoacyl-ACP synthase, TbTc\_3372; 57, beta-ketoacyl-ACP reductase, TbTc\_1241; 58,  
1313 Trans-2-enoyl-ACP reductase 1, TbTc\_5269; 59, acetyl-CoA synthetase, TbTc\_0318; 60,  
1314 acetyl-CoA carboxylase, TbTc\_0754; 61, Fatty acid elongase (ELO1), TbTc\_0159; 62, Fatty  
1315 acid elongase (ELO2), TbTc\_1882; 63, Fatty acid elongase (ELO3), TbTc\_0235; 64,  
1316 elongation of very long chain fatty acids protein (ELO4), TbTc\_0737; 65, aspartate  
1317 aminotransferase, TbTc\_0799; 66, aspartate carbamoyltransferase, TbTc\_1630; 67,  
1318 dihydroorotase, TbTc\_3801; 68, dihydroorotate dehydrogenase, TbTc\_0620; 69, orotidine-5-  
1319 phosphate decarboxylase/orotate phosphoribosyltransferase, TbTc\_0735; 70, uracil  
1320 phosphoribosyltransferase, TbTc\_4220; 71, Adenine phosphoribosyltransferase (APRT-2),  
1321 TbTc\_3522; 72, inosine-adenosine-guanosine-nucleoside hydrolase, TbTc\_4998; 73,  
1322 adenosine kinase, TbTc\_1024; 74, AMP deaminase, TbTc\_5808; 75, hypoxanthine-guanine  
1323 phosphoribosyltransferase (HGPRT), TbTc\_0726; 76, inosine-guanine nucleoside hydrolase,  
1324 TbTc\_0808; 77, inosine-5'-monophosphate dehydrogenase, TbTc\_1648; 78, Hypoxanthine-  
1325 guanine-xanthine phosphoribosyltransferase (HGXPRT), TbTc\_3696; 79, GMP reductase,  
1326 TbTc\_4627; 80, GMP synthase, TbTc\_1452. Abbreviations: PUFA, polyunsaturated fatty  
1327 acid.

1328 **S1 figure: comparative analysis of published *T. congolense* RNAseq data and data**  
1329 **generated in this study.** Scatter matrix of *T. congolense* datasets from this study compared  
1330 to ascending and peak parasitaemia *in vivo* transcriptomics data generated by Silvester and  
1331 colleagues [55]. TPM values were calculated for each gene in the *T. congolense* genome  
1332 and Log<sub>2</sub> TPM was plotted. Lower panels: Scatter plots of individual comparisons of the 4  
1333 datasets. Red dots correspond to genes associated with glycolysis; Diagonal panels: sample  
1334 names; Upper panels: Pearson correlation coefficients for comparisons of entire datasets  
1335 (black), glycolytic pathway (“Glyc”, green) and proteins with predicted transmembrane  
1336 domains (“Trans”, red).

1337 **S2 figure: Growth of *T. congolense* IL3000 in absence or presence of N-acetyl-D-**  
1338 **glucosamine.** Parasites were cultured in SCM-6 supplemented with 10 mM or 2 mM  
1339 glucose in the presence or absence of 60 mM GlcNAc and density monitored by  
1340 haemocytometer every 24 hours.

1341 **S3 figure: Comparative transcriptomics analysis of the electron transport chain in *T.***  
1342 ***congolense* and *T. brucei*.** A heatmap of all ETC complexes based on a table generated by  
1343 Zikova and colleagues [73]. Heatmaps are divided into the alternative oxidases (AOX),  
1344 NADH dehydrogenase 2 (NDH2), complex I, II, III, IV and ATPase (complex V).

1345 **S4 figure: Stable isotope labelled (<sup>13</sup>C)-glucose derived pyrimidine labelling.**

1346 Comparative analysis of glucose-derived pyrimidine labelling in *T. congolense* and *T. brucei*  
1347 (taken from [42]).

1348 **S5 figure: Effect of cysteine exclusion on *T. congolense* growth.** Parasites were grown

1349 in SCM-6 supplemented with 1.5 mM, 1.0 mM or absence of L-cysteine. Cell density was  
1350 monitored every 24 hours.

1351 **S6 figure: Comparison of amino acid metabolism in *T. congolense* and *T. brucei*.** A)

1352 glucose-derived carbon labelling of amino acids B) Transcriptomics pathway analysis. Gene

1353 IDs: A) ARG+POLYAMINE-SYN: AdoMetDC\_3193, AdoMet decarboxylase, TbTc\_3193;

1354 ODC, ornithine decarboxylase, TbTc\_5903; AdoMetDC\_0696, AdoMet decarboxylase,

1355 TbTc\_0696; SpSyn, spermidine synthase, TbTc\_1034. B) ASPASN-PWY: cASAT, cytosolic

1356 aspartate aminotransferase, TbTc\_0799; ASNS, asparagine synthetase, TbTc\_4894;

1357 mASAT, mitochondrial aspartate aminotransferase, TbTc\_5877. C) GLUCAT-PWY: OGDH-

1358 E1, 2-oxoglutarate dehydrogenase E1, TbTc\_2864; GDH, glutamate dehydrogenase,

1359 TbTc\_0872; SCS $\alpha$ , succinyl-CoA synthetase, TbTc\_0813; SUCLG2, succinyl-CoA ligase,

1360 TbTc\_3392; OGDH-E2, 2-oxoglutarate dehydrogenase E2, TbTc\_3057. D) ILEUDEG-PWY:

1361 ECH, enoyl-CoA hydratase, TbTc\_3283; BCAAT, branched-chain amino acid

1362 aminotransferase, TbTc\_0559; SCP2, 3-ketoacyl-CoA thiolase, TbTc\_4024. E) LEUDEG-

1363 PWY: ECH, enoyl-CoA hydratase, TbTc\_3283; BCKDH $\alpha$ , 2-oxoisovalerate dehydrogenase

1364  $\alpha$ , TbTc\_1182; BCKDH $\beta$ , 2-oxoisovalerate dehydrogenase  $\beta$ , TbTc\_0682; AUH,

1365 methylglutaconyl-CoA hydratase, TbTc\_5348; HMGCL, hydroxymethylglutaryl-CoA lyase,

1366 TbTc\_6160; BCAAT, branched-chain amino acid aminotransferase, TbTc\_0559; MCC $\beta$ , 3-

1367 methylcrotonyl-CoA carboxylase  $\beta$ , TbTc\_5385; MCC $\alpha$ , 3-methylcrotonyl-CoA carboxylase

1368  $\alpha$ , TbTc\_1670; SCP2, 3-ketoacyl-CoA thiolase, TbTc\_4024; IVDH, isovaleryl-CoA

1369 dehydrogenase, TbTc\_3112. F) PWY0-781: cASAT, cytosolic aspartate aminotransferase,

1370 TbTc\_0799; MTR - 5-methyltetrahydropteroyltriglutamate-homocysteine S-

1371 methyltransferase, TbTc\_5805; NMNAT, nicotinamide/nicotinic acid mononucleotide

1372 adenyltransferase, TbTc\_4133; NADSYN, NAD<sup>+</sup> synthase, TbTc\_2404; mASAT,

1373 mitochondrial aspartate aminotransferase, TbTc\_5877; METK1, AdoMet synthase,

1374 TbTc\_0178. G) PWY1V8-11: AKCT, 2-amino-3-ketobutyrate-CoA ligase, TbTc\_6236; TDH,

1375 L-threonine dehydrogenase, TbTc\_5991. H) VALDEG-PWY: ECH, enoyl-CoA hydratase,

1376 TbTc\_3283; HOPR, 2-hydroxy-3-oxopropionate reductase, TbTc\_2903; BCAAT, branched-

1377 chain amino acid aminotransferase, TbTc\_0559. I) PROLINE-DEG2-PWY: P5CDH, delta-1-

1378 pyrroline-5-carboxylate dehydrogenase, TbTc\_1695; GDH, glutamate dehydrogenase,

1379 TbTc\_0872; ProDH, proline dehydrogenase, TbTc\_1591.



1380 **S7 figure: Carbon utilisation for trypanothione biosynthesis in *T. congolense*.**

1381 Metabolomics and transcriptomics analyses were carried out to analyse trypanothione  
1382 biosynthesis. A) A simplified map of trypanothione biosynthesis as known in *T. brucei*.  
1383 Numbers refer to the following enzymes: 1, S-adenosyl-L-methionine synthase, METK1; 2,  
1384 S-adenosyl-L-methionine decarboxylase, AdoMetDC; 3, spermidine synthase, SpSyn; 4,  
1385 methyltransferase reaction, MTase; 5, S-adenosyl-L-homocysteine dehydrolase,  
1386 AdoHycase; 6, cystathionine beta synthase, CBS; 7, cystathione gamma lyase, CTH; 8,  
1387 glutaminase/amidase, AM; 9, gamma-glutamylcysteine synthetase, GCS; 10, glutathione  
1388 synthetase, GSS; 11, ornithine decarboxylase, ODC; 12, spermidine synthase, SpSyn; 13,  
1389 glutathionylspermidine synthase, GSP; 14, trypanothione synthetase, TRYS; 15,  
1390 tryparedoxin peroxidase, TXN1b; 16, trypanothione reductase, TRYR. B) Isotopologue  
1391 labelling experiments using 100% <sup>13</sup>C-L-serine, <sup>13</sup>C-L-glutamine, <sup>13</sup>C-L-methionine or <sup>13</sup>C-L-  
1392 cysteine, showing the abundance of carbon labelling derived from these amino acids in  
1393 components of the trypanothione biosynthesis pathway. C) Transcriptomics analysis using  
1394 the following TrypanoCyc pathways: PWY1V8-6 (trypanothione biosynthesis),  
1395 HOMOCYSDESGR-PWY1 (homocysteine degradation/cysteine biosynthesis) &  
1396 METHIONINE-DEG1-PWY (methionine degradation I). GeneIDs: TNX1b, tryparedoxin 1b,  
1397 TbTc\_0324; TRYS, trypanothione synthetase, TbTc\_1359; SpSyn, Spermidine synthase,  
1398 TbTc\_1034; TRYR, trypanothione reductase, TbTc\_4239; AdoMetDC\_0696, S-  
1399 adenosylmethionine decarboxylase, TbTc0696; GCS, gamma-glutamylcysteine synthetase,  
1400 TbTc\_3424; METK1, S-adenosylmethionine synthetase, TbTc\_0178; GSS, glutathione  
1401 synthetase, TbTc\_3678; AdoMetDC\_3193, S-adenosylmethionine decarboxylase,  
1402 TbTc\_3193; AM, amidase, TbTc\_5549; ODC, ornithine decarboxylase, TbTc\_5903; CTH,  
1403 cystathione gamma lyase, TbTc\_1051; CBS, cystathionine beta synthase, TbTc\_0413;  
1404 AdoHycase, S-adenosylhomocysteine hydrolase, TbTc\_0685; METK1, S-  
1405 adenosylmethionine synthase, TbTc\_0178.

1406 **S8 Figure: Analysis of LC-MS utilising stable isotope labelled amino acids.** Percentage  
1407 total labelling of metabolites identified in data from 6 stable isotope labelling experiments  
1408 using <sup>13</sup>C-L-asparagine, <sup>13</sup>C-L-cysteine, <sup>13</sup>C-L-glutamine, <sup>13</sup>C-L-methionine, <sup>13</sup>C-L-proline and  
1409 <sup>13</sup>C-L-serine. Colour intensity correlates to the total fraction of the metabolite that was <sup>13</sup>C-  
1410 labeled.

1411 **Supplementary Data**

1412 **S1 Table:** RNAseq dataset – *T. congolense ex vivo*, *T. congolense in vitro*, *T. brucei ex vivo*,  
1413 *T. brucei in vitro*, Silvester *et al* dataset

1414 **S2 Table:** Orthofinder output comparing *T. congolense* TriTrypDB (v34.0), *T. congolense*  
1415 Liverpool pacbio, *T. brucei* TriTrypDB (v34.0) and other trypanosomatids

1416 **S3 Table:** RNAseq dataset – *T. congolense* only, Pacbio assembly, single genes.

1417 **S4 Table:** Supernatant metabolomics dataset for *in vitro* cultured *T. congolense* over a  
1418 period of 56 hours. Metabolites highlighted in yellow were confidently predicted using a set  
1419 of metabolite standards run alongside the experimental samples. Results of statistical  
1420 analysis by means of a one-way repeated measures ANOVA (false discovery rate-adjusted  
1421 P value, FDR) is also shown for metabolites that were taken forward for downstream  
1422 analysis

1423 **S5 Table:** TrypanoCyc pathways and linked Orthogroup gene IDs

1424 **S6 Table:** Formulation of Steketee's congolense medium (SCM)-6 & -7

1425 **S7 table:** List of primers used in this study

1426

Compound	Target	<i>T. congolense</i> EC <sub>50</sub> Mean ± SEM	<i>T. brucei</i> EC <sub>50</sub> Mean ± SEM	Fold change (Tc/Tb)	P value (t-test)
Antimycin	Complex III	271.2 ± 143.5 μM	144.2 ± 18.1 μM	1.9	0.4295
FCCP	Uncoupling agent	12.6 ± 5.3 μM	13.0 ± 5.0 μM	1.0	0.9592
Azide	F <sub>1</sub> -ATPase	432.3 ± 127.9 μM	235.0 ± 6.0 μM	1.8	0.1982
Oligomycin	Complex V (F <sub>0</sub> ATPase)	33.9 ± 14.1 nM	197.6 ± 39.0 nM	0.2	0.0169
Rotenone	Complex I	27.4 ± 1.4 μM	7.4 ± 0.9 μM	3.7	0.0003
SHAM	TAO	14.4 ± 0.5 μM	26.0 ± 1.5 μM	0.6	0.0004
UK5099	Pyruvate transport	82.1 ± 8.8 μM	130.0 ± 5.0 μM	0.6	0.0091
ACS inhibitor	Acetyl-CoA synthetase	57.7 ± 15.2 μM	7.1 ± 2.4 μM	8.1	0.0304
Orlistat	Fatty acid synthase/lipases	15.6 ± 2.5 μM	0.02 ± 0.01 μM	780.0	0.0033
Diminazene	Kinetoplast	50.0 ± 5.6 nM	32.0 ± 0.5 nM	1.6	0.0425

1427 **Table 1: Comparative analysis of sensitivity to metabolic inhibitors in *T. congolense***  
 1428 **and *T. brucei*.** Abbreviations: SHAM, salicylhydroxamic acid; LCFA, long-chain fatty acid

1429

## 1430 References

- 1431 1. Morrison LJ, Vezza L, Rowan T, Hope JC. Animal African Trypanosomiasis: Time to  
1432 Increase Focus on Clinically Relevant Parasite and Host Species. *Trends Parasitol.*  
1433 2016;32(8): 599-607. doi: 10.1016/j.pt.2016.04.012.
- 1434 2. Auty H, Torr SJ, Michoel T, Jayaraman S, Morrison LJ. Cattle trypanosomosis: the  
1435 diversity of trypanosomes and implications for disease epidemiology and control. *Rev*  
1436 *Sci Tech.* 2015;34(2): 587-98.
- 1437 3. Giordani F, Morrison LJ, Rowan TG, HP DEK, Barrett MP. The animal trypanosomiasis  
1438 and their chemotherapy: a review. *Parasitology.* 2016;143(14): 1862-89. doi:  
1439 10.1017/S0031182016001268.
- 1440 4. Shaw AP, Cecchi G, Wint GR, Mattioli RC, Robinson TP. Mapping the economic  
1441 benefits to livestock keepers from intervening against bovine trypanosomosis in Eastern  
1442 Africa. *Prev Vet Med.* 2014;113(2): 197-210. doi: 10.1016/j.prevetmed.2013.10.024.
- 1443 5. Chitanga S, Marcotty T, Namangala B, Van den Bossche P, Van Den Abbeele J,  
1444 Delespaux V. High prevalence of drug resistance in animal trypanosomes without a  
1445 history of drug exposure. *PLoS Negl Trop Dis.* 2011;5(12): e1454. doi:  
1446 10.1371/journal.pntd.0001454.
- 1447 6. Delespaux V, Dinka H, Masumu J, Van den Bossche P, Geerts S. Five-fold increase in  
1448 *Trypanosoma congolense* isolates resistant to diminazene aceturate over a seven-year  
1449 period in Eastern Zambia. *Drug Resist Updat.* 2008;11(6): 205-9. doi:  
1450 10.1016/j.drug.2008.10.002.
- 1451 7. Geerts S, Holmes PH, Eisler MC, Diall O. African bovine trypanosomiasis: the problem  
1452 of drug resistance. *Trends Parasitol.* 2001;17(1): 25-8.
- 1453 8. Diall O, Cecchi G, Wanda G, Argiles-Herrero R, Vreysen MJB, Cattoli G, et al.  
1454 Developing a Progressive Control Pathway for African Animal Trypanosomosis. *Trends*  
1455 *Parasitol.* 2017;33(7): 499-509. doi: 10.1016/j.pt.2017.02.005.
- 1456 9. Barrett MP, Burchmore RJ, Stich A, Lazzari JO, Frasc AC, Cazzulo JJ, et al. The  
1457 trypanosomiasis. *Lancet.* 2003;362(9394): 1469-80. doi: 10.1016/S0140-  
1458 6736(03)14694-6.
- 1459 10. Alsford S, Kawahara T, Glover L, Horn D. Tagging a *T. brucei* RRNA locus improves  
1460 stable transfection efficiency and circumvents inducible expression position effects. *Mol*  
1461 *Biochem Parasitol.* 2005;144(2): 142-8. doi: 10.1016/j.molbiopara.2005.08.009.
- 1462 11. Rico E, Jeacock L, Kovarova J, Horn D. Inducible high-efficiency CRISPR-Cas9-  
1463 targeted gene editing and precision base editing in African trypanosomes. *Sci Rep.*  
1464 2018;8(1): 7960. doi: 10.1038/s41598-018-26303-w.

- 1465 12. Gibson W. The origins of the trypanosome genome strains *Trypanosoma brucei brucei*  
1466 TREU 927, *T. b. gambiense* DAL 972, *T. vivax* Y486 and *T. congolense* IL3000. *Parasit*  
1467 *Vectors*. 2012;5: 71. doi: 10.1186/1756-3305-5-71.
- 1468 13. Kay C, Peacock L, Gibson W. *Trypanosoma congolense*: In Vitro Culture and  
1469 Transfection. *Curr Protoc Microbiol*. 2019;53(1): e77. doi: 10.1002/cpmc.77.
- 1470 14. Coustou V, Guegan F, Plazolles N, Baltz T. Complete in vitro life cycle of *Trypanosoma*  
1471 *congolense*: development of genetic tools. *PLoS Negl Trop Dis*. 2010;4(3): e618. doi:  
1472 10.1371/journal.pntd.0000618.
- 1473 15. Hirumi H, Hirumi K. In vitro cultivation of *Trypanosoma congolense* bloodstream forms in  
1474 the absence of feeder cell layers. *Parasitology*. 1991;102 Pt 2: 225-36.
- 1475 16. Rotureau B, Van Den Abbeele J. Through the dark continent: African trypanosome  
1476 development in the tsetse fly. *Front Cell Infect Microbiol*. 2013;3: 53. doi:  
1477 10.3389/fcimb.2013.00053.
- 1478 17. Silvester E, Young J, Ivens A, Matthews KR. Interspecies quorum sensing in co-  
1479 infections can manipulate trypanosome transmission potential. *Nat Microbiol*.  
1480 2017;2(11): 1471-9. doi: 10.1038/s41564-017-0014-5.
- 1481 18. Jackson AP, Allison HC, Barry JD, Field MC, Hertz-Fowler C, Berriman M. A cell-  
1482 surface phylome for African trypanosomes. *PLoS Negl Trop Dis*. 2013;7(3): e2121. doi:  
1483 10.1371/journal.pntd.0002121.
- 1484 19. Jackson AP, Berry A, Aslett M, Allison HC, Burton P, Vavrova-Anderson J, et al.  
1485 Antigenic diversity is generated by distinct evolutionary mechanisms in African  
1486 trypanosome species. *Proc Natl Acad Sci U S A*. 2012;109(9): 3416-21. doi:  
1487 10.1073/pnas.1117313109.
- 1488 20. Silva Pereira S, Casas-Sanchez A, Haines LR, Ogugo M, Absolomon K, Sanders M, et  
1489 al. Variant antigen repertoires in *Trypanosoma congolense* populations and  
1490 experimental infections can be profiled from deep sequence data using universal protein  
1491 motifs. *Genome Res*. 2018;28(9): 1383-94. doi: 10.1101/gr.234146.118.
- 1492 21. Silva Pereira S, de Almeida Castilho Neto KJG, Duffy CW, Richards P, Noyes H, Ogugo  
1493 M, et al. Variant antigen diversity in *Trypanosoma vivax* is not driven by recombination.  
1494 *Nat Commun*. 2020;11(1): 844. doi: 10.1038/s41467-020-14575-8.
- 1495 22. Tihon E, Imamura H, Dujardin JC, Van Den Abbeele J, Van den Broeck F. Discovery  
1496 and genomic analyses of hybridization between divergent lineages of *Trypanosoma*  
1497 *congolense*, causative agent of Animal African Trypanosomiasis. *Mol Ecol*. 2017;26(23):  
1498 6524-38. doi: 10.1111/mec.14271.
- 1499 23. Creek DJ, Barrett MP. Determination of antiprotozoal drug mechanisms by  
1500 metabolomics approaches. *Parasitology*. 2014;141(1): 83-92. doi:  
1501 10.1017/S0031182013000814.

- 1502 24. Haanstra JR, Gerding A, Dolga AM, Sorgdrager FJH, Buist-Homan M, du Toit F, et al.  
1503 Targeting pathogen metabolism without collateral damage to the host. *Sci Rep.* 2017;7:  
1504 40406. doi: 10.1038/srep40406.
- 1505 25. Vincent IM, Ehmann DE, Mills SD, Perros M, Barrett MP. Untargeted Metabolomics To  
1506 Ascertain Antibiotic Modes of Action. *Antimicrob Agents Chemother.* 2016;60(4): 2281-  
1507 91. doi: 10.1128/AAC.02109-15.
- 1508 26. Bringaud F, Biran M, Millerioux Y, Wargnies M, Allmann S, Mazet M. Combining reverse  
1509 genetics and nuclear magnetic resonance-based metabolomics unravels trypanosome-  
1510 specific metabolic pathways. *Mol Microbiol.* 2015;96(5): 917-26. doi:  
1511 10.1111/mmi.12990.
- 1512 27. Creek DJ, Anderson J, McConville MJ, Barrett MP. Metabolomic analysis of  
1513 trypanosomatid protozoa. *Mol Biochem Parasitol.* 2012;181(2): 73-84. doi:  
1514 10.1016/j.molbiopara.2011.10.003.
- 1515 28. Allmann S, Bringaud F. Glycosomes: A comprehensive view of their metabolic roles in  
1516 *T. brucei*. *Int J Biochem Cell Biol.* 2017;85: 85-90. doi: 10.1016/j.biocel.2017.01.015.
- 1517 29. Haanstra JR, van Tuijl A, Kessler P, Reijnders W, Michels PA, Westerhoff HV, et al.  
1518 Compartmentation prevents a lethal turbo-explosion of glycolysis in trypanosomes. *Proc*  
1519 *Natl Acad Sci U S A.* 2008;105(46): 17718-23. doi: 10.1073/pnas.0806664105.
- 1520 30. Mazet M, Morand P, Biran M, Bouyssou G, Courtois P, Daulouede S, et al. Revisiting  
1521 the central metabolism of the bloodstream forms of *Trypanosoma brucei*: production of  
1522 acetate in the mitochondrion is essential for parasite viability. *PLoS Negl Trop Dis.*  
1523 2013;7(12): e2587. doi: 10.1371/journal.pntd.0002587.
- 1524 31. Millerioux Y, Mazet M, Bouyssou G, Allmann S, Kiema TR, Bertiaux E, et al. De novo  
1525 biosynthesis of sterols and fatty acids in the *Trypanosoma brucei* procyclic form: Carbon  
1526 source preferences and metabolic flux redistributions. *PLoS Pathog.* 2018;14(5):  
1527 e1007116. doi: 10.1371/journal.ppat.1007116.
- 1528 32. Yang PY, Wang M, Liu K, Ngai MH, Sheriff O, Lear MJ, et al. Parasite-based screening  
1529 and proteome profiling reveal orlistat, an FDA-approved drug, as a potential anti  
1530 *Trypanosoma brucei* agent. *Chemistry.* 2012;18(27): 8403-13. doi:  
1531 10.1002/chem.201200482.
- 1532 33. Lamour N, Riviere L, Coustou V, Coombs GH, Barrett MP, Bringaud F. Proline  
1533 metabolism in procyclic *Trypanosoma brucei* is down-regulated in the presence of  
1534 glucose. *J Biol Chem.* 2005;280(12): 11902-10. doi: 10.1074/jbc.M414274200.
- 1535 34. Tielens AG, Van Hellemond JJ. Differences in energy metabolism between  
1536 trypanosomatidae. *Parasitol Today.* 1998;14(7): 265-72.

- 1537 35. van Weelden SW, Fast B, Vogt A, van der Meer P, Saas J, van Hellemond JJ, et al.  
1538 Procyclic *Trypanosoma brucei* do not use Krebs cycle activity for energy generation. *J*  
1539 *Biol Chem.* 2003;278(15): 12854-63. doi: 10.1074/jbc.M213190200.
- 1540 36. van Hellemond JJ, Opperdoes FR, Tielens AG. The extraordinary mitochondrion and  
1541 unusual citric acid cycle in *Trypanosoma brucei*. *Biochem Soc Trans.* 2005;33(Pt 5):  
1542 967-71. doi: 10.1042/BST20050967.
- 1543 37. Villafraz O, Biran M, Pineda E, Plazolles N, Cahoreau E, Ornitz R, et al. Fly stage  
1544 trypanosomes recycle glucose catabolites and TCA cycle intermediates to stimulate  
1545 growth in near physiological conditions. 2020: 2020.12.17.423221. doi:  
1546 10.1101/2020.12.17.423221 %J bioRxiv.
- 1547 38. Colasante C, Robles A, Li CH, Schwede A, Benz C, Voncken F, et al. Regulated  
1548 expression of glycosomal phosphoglycerate kinase in *Trypanosoma brucei*. *Mol*  
1549 *Biochem Parasitol.* 2007;151(2): 193-204. doi: 10.1016/j.molbiopara.2006.11.003.
- 1550 39. Blattner J, Helfert S, Michels P, Clayton C. Compartmentation of phosphoglycerate  
1551 kinase in *Trypanosoma brucei* plays a critical role in parasite energy metabolism. *Proc*  
1552 *Natl Acad Sci U S A.* 1998;95(20): 11596-600.
- 1553 40. Deramchia K, Morand P, Biran M, Millerioux Y, Mazet M, Wargnies M, et al. Contribution  
1554 of pyruvate phosphate dikinase in the maintenance of the glycosomal ATP/ADP balance  
1555 in the *Trypanosoma brucei* procyclic form. *J Biol Chem.* 2014;289(25): 17365-78. doi:  
1556 10.1074/jbc.M114.567230.
- 1557 41. van Grinsven KW, Van Den Abbeele J, Van den Bossche P, van Hellemond JJ, Tielens  
1558 AG. Adaptations in the glucose metabolism of procyclic *Trypanosoma brucei* isolates  
1559 from tsetse flies and during differentiation of bloodstream forms. *Eukaryot Cell.*  
1560 2009;8(8): 1307-11. doi: 10.1128/EC.00091-09.
- 1561 42. Creek DJ, Mazet M, Achcar F, Anderson J, Kim DH, Kamour R, et al. Probing the  
1562 metabolic network in bloodstream-form *Trypanosoma brucei* using untargeted  
1563 metabolomics with stable isotope labelled glucose. *PLoS Pathog.* 2015;11(3):  
1564 e1004689. doi: 10.1371/journal.ppat.1004689.
- 1565 43. Agosin M, Von Brand T. Studies on the carbohydrate metabolism of *Trypanosoma*  
1566 *congolense*. *Exp Parasitol.* 1954;3(6): 517-24.
- 1567 44. Bringaud F, Baltz D, Baltz T. Functional and molecular characterization of a glycosomal  
1568 PPI-dependent enzyme in trypanosomatids: pyruvate, phosphate dikinase. *Proc Natl*  
1569 *Acad Sci U S A.* 1998;95(14): 7963-8.
- 1570 45. Ohashi-Suzuki M, Yabu Y, Ohshima S, Nakamura K, Kido Y, Sakamoto K, et al.  
1571 Differential kinetic activities of glycerol kinase among African trypanosome species:  
1572 phylogenetic and therapeutic implications. *J Vet Med Sci.* 2011;73(5): 615-21.

- 1573 46. Parker HL, Hill T, Alexander K, Murphy NB, Fish WR, Parsons M. Three genes and two  
1574 isozymes: gene conversion and the compartmentalization and expression of the  
1575 phosphoglycerate kinases of *Trypanosoma (Nannomonas) congolense*. *Mol Biochem*  
1576 *Parasitol.* 1995;69(2): 269-79.
- 1577 47. Vickerman K. The fine structure of *Trypanosoma congolense* in its bloodstream phase. *J*  
1578 *Protozool.* 1969;16(1): 54-69.
- 1579 48. Bienen EJ, Webster P, Fish WR. *Trypanosoma (Nannomonas) congolense*: changes in  
1580 respiratory metabolism during the life cycle. *Exp Parasitol.* 1991;73(4): 403-12.
- 1581 49. Ebiloma GU, Ayuga TD, Balogun EO, Gil LA, Donachie A, Kaiser M, et al. Inhibition of  
1582 trypanosome alternative oxidase without its N-terminal mitochondrial targeting signal  
1583 (DeltaMTS-TAO) by cationic and non-cationic 4-hydroxybenzoate and 4-  
1584 alkoxybenzaldehyde derivatives active against *T. brucei* and *T. congolense*. *Eur J Med*  
1585 *Chem.* 2018;150: 385-402. doi: 10.1016/j.ejmech.2018.02.075.
- 1586 50. Fueyo Gonzalez FJ, Ebiloma GU, Izquierdo Garcia C, Bruggeman V, Sanchez  
1587 Villamanan JM, Donachie A, et al. Conjugates of 2,4-Dihydroxybenzoate and  
1588 Salicylhydroxamate and Lipocations Display Potent Antiparasite Effects by Efficiently  
1589 Targeting the *Trypanosoma brucei* and *Trypanosoma congolense* Mitochondrion. *J Med*  
1590 *Chem.* 2017;60(4): 1509-22. doi: 10.1021/acs.jmedchem.6b01740.
- 1591 51. Steiger RF, Steiger E, Trager W, Schneider I. *Trypanosoma congolense*: partial cyclic  
1592 development in a *Glossina* cell system and oxygen consumption. *J Parasitol.*  
1593 1977;63(5): 861-7.
- 1594 52. Hsu HH, Araki M, Mochizuki M, Hori Y, Murata M, Kahar P, et al. A Systematic  
1595 Approach to Time-series Metabolite Profiling and RNA-seq Analysis of Chinese Hamster  
1596 Ovary Cell Culture. *Sci Rep.* 2017;7: 43518. doi: 10.1038/srep43518.
- 1597 53. Wagner GP, Kin K, Lynch VJ. Measurement of mRNA abundance using RNA-seq data:  
1598 RPKM measure is inconsistent among samples. *Theory Biosci.* 2012;131(4): 281-5. doi:  
1599 10.1007/s12064-012-0162-3.
- 1600 54. Emms DM, Kelly S. OrthoFinder: solving fundamental biases in whole genome  
1601 comparisons dramatically improves orthogroup inference accuracy. *Genome Biol.*  
1602 2015;16: 157. doi: 10.1186/s13059-015-0721-2.
- 1603 55. Silvester E, Ivens A, Matthews KR. A gene expression comparison of *Trypanosoma*  
1604 *brucei* and *Trypanosoma congolense* in the bloodstream of the mammalian host reveals  
1605 species-specific adaptations to density-dependent development. *PLoS Negl Trop Dis.*  
1606 2018;12(10): e0006863. doi: 10.1371/journal.pntd.0006863.
- 1607 56. Creek DJ, Nijagal B, Kim DH, Rojas F, Matthews KR, Barrett MP. Metabolomics guides  
1608 rational development of a simplified cell culture medium for drug screening against



- 1609 Trypanosoma brucei. Antimicrob Agents Chemother. 2013;57(6): 2768-79. doi:  
1610 10.1128/AAC.00044-13.
- 1611 57. Kim DH, Achcar F, Breitling R, Burgess KE, Barrett MP. LC-MS-based absolute  
1612 metabolite quantification: application to metabolic flux measurement in trypanosomes.  
1613 Metabolomics. 2015;11(6): 1721-32. doi: 10.1007/s11306-015-0827-2.
- 1614 58. Nok AJ, Esievo KA, Ibrahim S, Ukoha AI, Ikediobi CO. Phospholipase A2 from  
1615 Trypanosoma congolense: characterization and haematological properties. Cell  
1616 Biochem Funct. 1993;11(2): 125-30. doi: 10.1002/cbf.290110208.
- 1617 59. Duszenko M, Ferguson MA, Lamont GS, Rifkin MR, Cross GA. Cysteine eliminates the  
1618 feeder cell requirement for cultivation of Trypanosoma brucei bloodstream forms in vitro.  
1619 J Exp Med. 1985;162(4): 1256-63.
- 1620 60. Shameer S, Logan-Klumpler FJ, Vinson F, Cottret L, Merlet B, Achcar F, et al.  
1621 TrypanoCyc: a community-led biochemical pathways database for Trypanosoma brucei.  
1622 Nucleic Acids Res. 2015;43(Database issue): D637-44. doi: 10.1093/nar/gku944.
- 1623 61. Szoor B, Ruberto I, Burchmore R, Matthews KR. A novel phosphatase cascade  
1624 regulates differentiation in Trypanosoma brucei via a glycosomal signaling pathway.  
1625 Genes Dev. 2010;24(12): 1306-16. doi: 10.1101/gad.570310.
- 1626 62. Mugo E, Clayton C. Expression of the RNA-binding protein RBP10 promotes the  
1627 bloodstream-form differentiation state in Trypanosoma brucei. PLoS Pathog.  
1628 2017;13(8): e1006560. doi: 10.1371/journal.ppat.1006560.
- 1629 63. Dean S, Marchetti R, Kirk K, Matthews KR. A surface transporter family conveys the  
1630 trypanosome differentiation signal. Nature. 2009;459(7244): 213-7. doi:  
1631 10.1038/nature07997.
- 1632 64. Aranda A, Maugeri D, Uttaro AD, Oppendoes F, Cazzulo JJ, Nowicki C. The malate  
1633 dehydrogenase isoforms from Trypanosoma brucei: subcellular localization and  
1634 differential expression in bloodstream and procyclic forms. Int J Parasitol. 2006;36(3):  
1635 295-307. doi: 10.1016/j.ijpara.2005.09.013.
- 1636 65. Abbas AH, Silva Pereira S, D'Archivio S, Wickstead B, Morrison LJ, Hall N, et al. The  
1637 Structure of a Conserved Telomeric Region Associated with Variant Antigen Loci in the  
1638 Blood Parasite Trypanosoma congolense. Genome Biol Evol. 2018;10(9): 2458-73. doi:  
1639 10.1093/gbe/evy186.
- 1640 66. Spitznagel D, Ebikeme C, Biran M, Nic a' Bhaird N, Bringaud F, Henehan GT, et al.  
1641 Alanine aminotransferase of Trypanosoma brucei--a key role in proline metabolism in  
1642 procyclic life forms. FEBS J. 2009;276(23): 7187-99. doi: 10.1111/j.1742-  
1643 4658.2009.07432.x.

- 1644 67. Natesan SK, Peacock L, Leung KF, Gibson W, Field MC. Evidence that low endocytic  
1645 activity is not directly responsible for human serum resistance in the insect form of  
1646 African trypanosomes. *BMC Res Notes*. 2010;3: 63. doi: 10.1186/1756-0500-3-63.
- 1647 68. Ebikeme CE, Peacock L, Coustou V, Riviere L, Bringaud F, Gibson WC, et al. N-acetyl  
1648 D-glucosamine stimulates growth in procyclic forms of *Trypanosoma brucei* by inducing  
1649 a metabolic shift. *Parasitology*. 2008;135(5): 585-94. doi: 10.1017/S0031182008004241.
- 1650 69. Awuah-Mensah G, McDonald J, Steketee PC, Autheman D, Whipple S, D'Archivio S, et  
1651 al. Reliable, scalable functional genetics in bloodstream-form *Trypanosoma congolense*  
1652 in vitro and in vivo. *PLoS Pathog*. 2020;Forthcoming.
- 1653 70. Kovarova J, Nagar R, Faria J, Ferguson MAJ, Barrett MP, Horn D. Gluconeogenesis  
1654 using glycerol as a substrate in bloodstream-form *Trypanosoma brucei*. *PLoS Pathog*.  
1655 2018;14(12): e1007475. doi: 10.1371/journal.ppat.1007475.
- 1656 71. Tielens AG, van Hellemond JJ. Surprising variety in energy metabolism within  
1657 *Trypanosomatidae*. *Trends Parasitol*. 2009;25(10): 482-90. doi:  
1658 10.1016/j.pt.2009.07.007.
- 1659 72. Trindade S, Rijo-Ferreira F, Carvalho T, Pinto-Neves D, Guegan F, Aresta-Branco F, et  
1660 al. *Trypanosoma brucei* Parasites Occupy and Functionally Adapt to the Adipose Tissue  
1661 in Mice. *Cell Host Microbe*. 2016;19(6): 837-48. doi: 10.1016/j.chom.2016.05.002.
- 1662 73. Zikova A, Verner Z, Nenarokova A, Michels PAM, Lukes J. A paradigm shift: The  
1663 mitoproteomes of procyclic and bloodstream *Trypanosoma brucei* are comparably  
1664 complex. *PLoS Pathog*. 2017;13(12): e1006679. doi: 10.1371/journal.ppat.1006679.
- 1665 74. Geiger A, Hirtz C, Becue T, Bellard E, Centeno D, Gargani D, et al. Exocytosis and  
1666 protein secretion in *Trypanosoma*. *BMC Microbiol*. 2010;10: 20. doi: 10.1186/1471-  
1667 2180-10-20.
- 1668 75. Manivel G, Meyyazhagan A, Durairaj DR, Piramanayagam S. Genome-wide analysis of  
1669 Excretory/Secretory proteins in *Trypanosoma brucei brucei*: Insights into functional  
1670 characteristics and identification of potential targets by immunoinformatics approach.  
1671 *Genomics*. 2019;111(5): 1124-33. doi: 10.1016/j.ygeno.2018.07.007.
- 1672 76. Henriques C, Sanchez MA, Tryon R, Landfear SM. Molecular and functional  
1673 characterization of the first nucleobase transporter gene from African trypanosomes.  
1674 *Mol Biochem Parasitol*. 2003;130(2): 101-10. doi: 10.1016/s0166-6851(03)00167-1.
- 1675 77. Burchmore RJ, Wallace LJ, Candlish D, Al-Salabi MI, Beal PR, Barrett MP, et al.  
1676 Cloning, heterologous expression, and in situ characterization of the first high affinity  
1677 nucleobase transporter from a protozoan. *J Biol Chem*. 2003;278(26): 23502-7. doi:  
1678 10.1074/jbc.M301252200.
- 1679 78. Munday JC, Rojas Lopez KE, Eze AA, Delespaux V, Van Den Abbeele J, Rowan T, et  
1680 al. Functional expression of TcoAT1 reveals it to be a P1-type nucleoside transporter

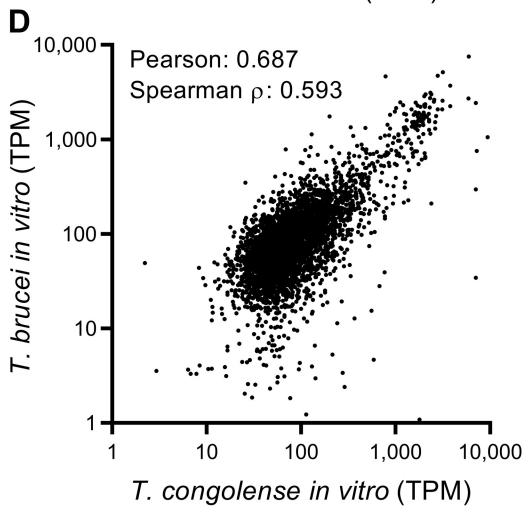
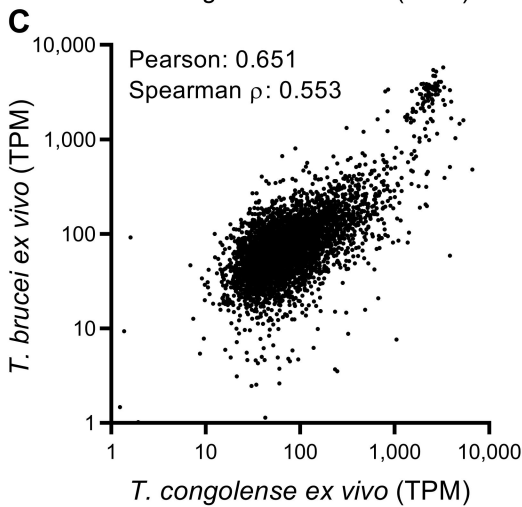
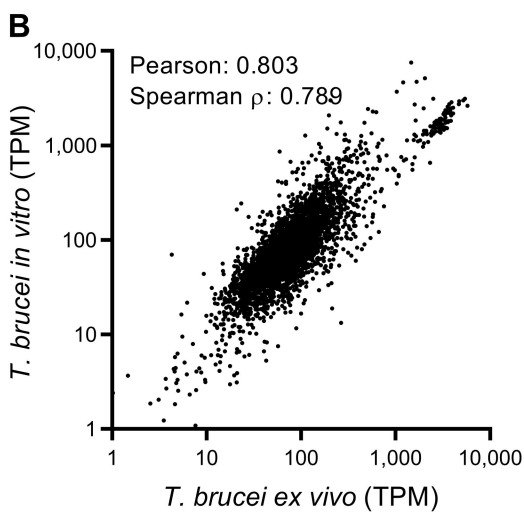
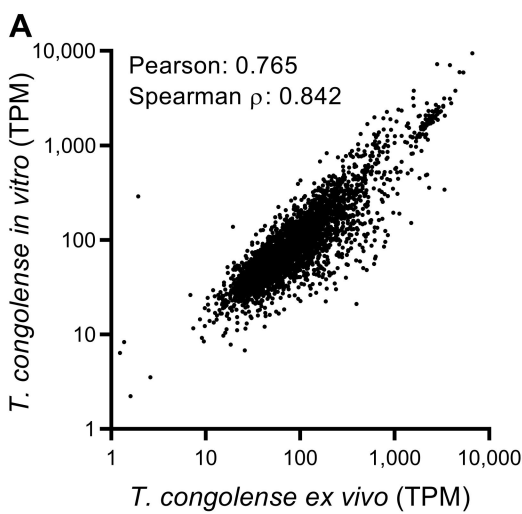
- 1681 with no capacity for diminazene uptake. *Int J Parasitol Drugs Drug Resist.* 2013;3: 69-  
1682 76. doi: 10.1016/j.ijpddr.2013.01.004.
- 1683 79. Al-Salabi MI, Wallace LJ, Luscher A, Maser P, Candlish D, Rodenko B, et al. Molecular  
1684 interactions underlying the unusually high adenosine affinity of a novel *Trypanosoma*  
1685 *brucei* nucleoside transporter. *Mol Pharmacol.* 2007;71(3): 921-9. doi:  
1686 10.1124/mol.106.031559.
- 1687 80. de Koning HP, Bridges DJ, Burchmore RJ. Purine and pyrimidine transport in  
1688 pathogenic protozoa: from biology to therapy. *FEMS Microbiol Rev.* 2005;29(5): 987-  
1689 1020. doi: 10.1016/j.femsre.2005.03.004.
- 1690 81. Papageorgiou IG, Yakob L, Al Salabi MI, Diallinas G, Soteriadou KP, De Koning HP.  
1691 Identification of the first pyrimidine nucleobase transporter in *Leishmania*: similarities  
1692 with the *Trypanosoma brucei* U1 transporter and antileishmanial activity of uracil  
1693 analogues. *Parasitology.* 2005;130(Pt 3): 275-83. doi: 10.1017/s0031182004006626.
- 1694 82. Gudin S, Quashie NB, Candlish D, Al-Salabi MI, Jarvis SM, Ranford-Cartwright LC, et  
1695 al. *Trypanosoma brucei*: a survey of pyrimidine transport activities. *Exp Parasitol.*  
1696 2006;114(2): 118-25. doi: 10.1016/j.exppara.2006.02.018.
- 1697 83. de Koning HP, Jarvis SM. A highly selective, high-affinity transporter for uracil in  
1698 *Trypanosoma brucei brucei*: evidence for proton-dependent transport. *Biochem Cell*  
1699 *Biol.* 1998;76(5): 853-8. doi: 10.1139/bcb-76-5-853.
- 1700 84. Ali JA, Tagoe DN, Munday JC, Donachie A, Morrison LJ, de Koning HP. Pyrimidine  
1701 biosynthesis is not an essential function for *Trypanosoma brucei* bloodstream forms.  
1702 *PLoS One.* 2013;8(3): e58034. doi: 10.1371/journal.pone.0058034.
- 1703 85. Johnston K, Kim DH, Kerkhoven EJ, Burchmore R, Barrett MP, Achcar F. Mapping the  
1704 metabolism of five amino acids in bloodstream form *Trypanosoma brucei* using U-(13)C-  
1705 labelled substrates and LC-MS. *Biosci Rep.* 2019;39(5). doi: 10.1042/BSR20181601.
- 1706 86. Marchese L, Nascimento JF, Damasceno FS, Bringaud F, Michels PAM, Silber AM. The  
1707 Uptake and Metabolism of Amino Acids, and Their Unique Role in the Biology of  
1708 Pathogenic *Trypanosomatids*. *Pathogens.* 2018;7(2). doi: 10.3390/pathogens7020036.
- 1709 87. Mantilla BS, Marchese L, Casas-Sanchez A, Dyer NA, Ejeh N, Biran M, et al. Proline  
1710 Metabolism is Essential for *Trypanosoma brucei brucei* Survival in the Tsetse Vector.  
1711 *PLoS Pathog.* 2017;13(1): e1006158. doi: 10.1371/journal.ppat.1006158.
- 1712 88. Paul KS, Jiang D, Morita YS, Englund PT. Fatty acid synthesis in African trypanosomes:  
1713 a solution to the myristate mystery. *Trends Parasitol.* 2001;17(8): 381-7. doi:  
1714 10.1016/s1471-4922(01)01984-5.
- 1715 89. Stephens JL, Lee SH, Paul KS, Englund PT. Mitochondrial fatty acid synthesis in  
1716 *Trypanosoma brucei*. *J Biol Chem.* 2007;282(7): 4427-36. doi:  
1717 10.1074/jbc.M609037200.

- 1718 90. Millerioux Y, Ebikeme C, Biran M, Morand P, Bouyssou G, Vincent IM, et al. The  
1719 threonine degradation pathway of the *Trypanosoma brucei* procyclic form: the main  
1720 carbon source for lipid biosynthesis is under metabolic control. *Mol Microbiol.*  
1721 2013;90(1): 114-29. doi: 10.1111/mmi.12351.
- 1722 91. Millerioux Y, Morand P, Biran M, Mazet M, Moreau P, Wargnies M, et al. ATP synthesis-  
1723 coupled and -uncoupled acetate production from acetyl-CoA by mitochondrial  
1724 acetate:succinate CoA-transferase and acetyl-CoA thioesterase in *Trypanosoma*. *J Biol*  
1725 *Chem.* 2012;287(21): 17186-97. doi: 10.1074/jbc.M112.355404.
- 1726 92. Surve SV, Jensen BC, Heestand M, Mazet M, Smith TK, Bringaud F, et al. NADH  
1727 dehydrogenase of *Trypanosoma brucei* is important for efficient acetate production in  
1728 bloodstream forms. *Mol Biochem Parasitol.* 2017;211: 57-61. doi:  
1729 10.1016/j.molbiopara.2016.10.001.
- 1730 93. Stafkova J, Mach J, Biran M, Verner Z, Bringaud F, Tachezy J. Mitochondrial pyruvate  
1731 carrier in *Trypanosoma brucei*. *Mol Microbiol.* 2016;100(3): 442-56. doi:  
1732 10.1111/mmi.13325.
- 1733 94. Comerford SA, Huang Z, Du X, Wang Y, Cai L, Witkiewicz AK, et al. Acetate  
1734 dependence of tumors. *Cell.* 2014;159(7): 1591-602. doi: 10.1016/j.cell.2014.11.020.
- 1735 95. Riviere L, Moreau P, Allmann S, Hahn M, Biran M, Plazolles N, et al. Acetate produced  
1736 in the mitochondrion is the essential precursor for lipid biosynthesis in procyclic  
1737 trypanosomes. *Proc Natl Acad Sci U S A.* 2009;106(31): 12694-9. doi:  
1738 10.1073/pnas.0903355106.
- 1739 96. Lee SH, Stephens JL, Paul KS, Englund PT. Fatty acid synthesis by elongases in  
1740 trypanosomes. *Cell.* 2006;126(4): 691-9. doi: 10.1016/j.cell.2006.06.045.
- 1741 97. Danaei G, Finucane MM, Lu Y, Singh GM, Cowan MJ, Paciorek CJ, et al. National,  
1742 regional, and global trends in fasting plasma glucose and diabetes prevalence since  
1743 1980: systematic analysis of health examination surveys and epidemiological studies  
1744 with 370 country-years and 2.7 million participants. *Lancet.* 2011;378(9785): 31-40. doi:  
1745 10.1016/S0140-6736(11)60679-X.
- 1746 98. Cozzi G, Ravarotto L, Gottardo F, Stefani AL, Contiero B, Moro L, et al. Short  
1747 communication: reference values for blood parameters in Holstein dairy cows: effects of  
1748 parity, stage of lactation, and season of production. *J Dairy Sci.* 2011;94(8): 3895-901.  
1749 doi: 10.3168/jds.2010-3687.
- 1750 99. Jackson PGG, Cockcroft PD. Appendix 2: Laboratory Reference Values: Haematology.  
1751 *Clinical Examination of Farm Animals*2002. p. 302-.
- 1752 100. Mair B, Drillich M, Klein-Jobstl D, Kanz P, Borchardt S, Meyer L, et al. Glucose  
1753 concentration in capillary blood of dairy cows obtained by a minimally invasive lancet

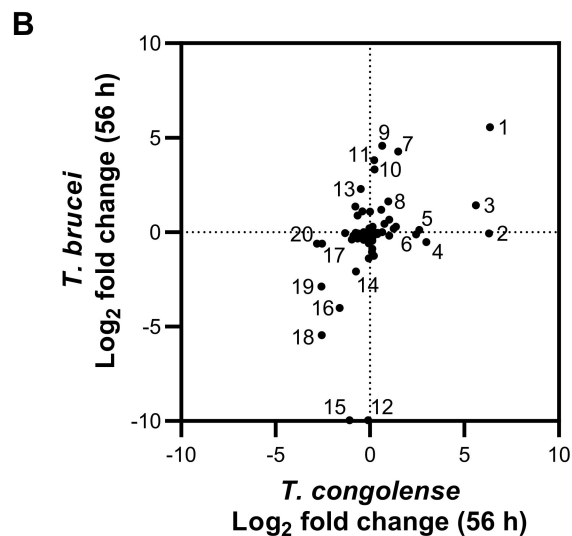
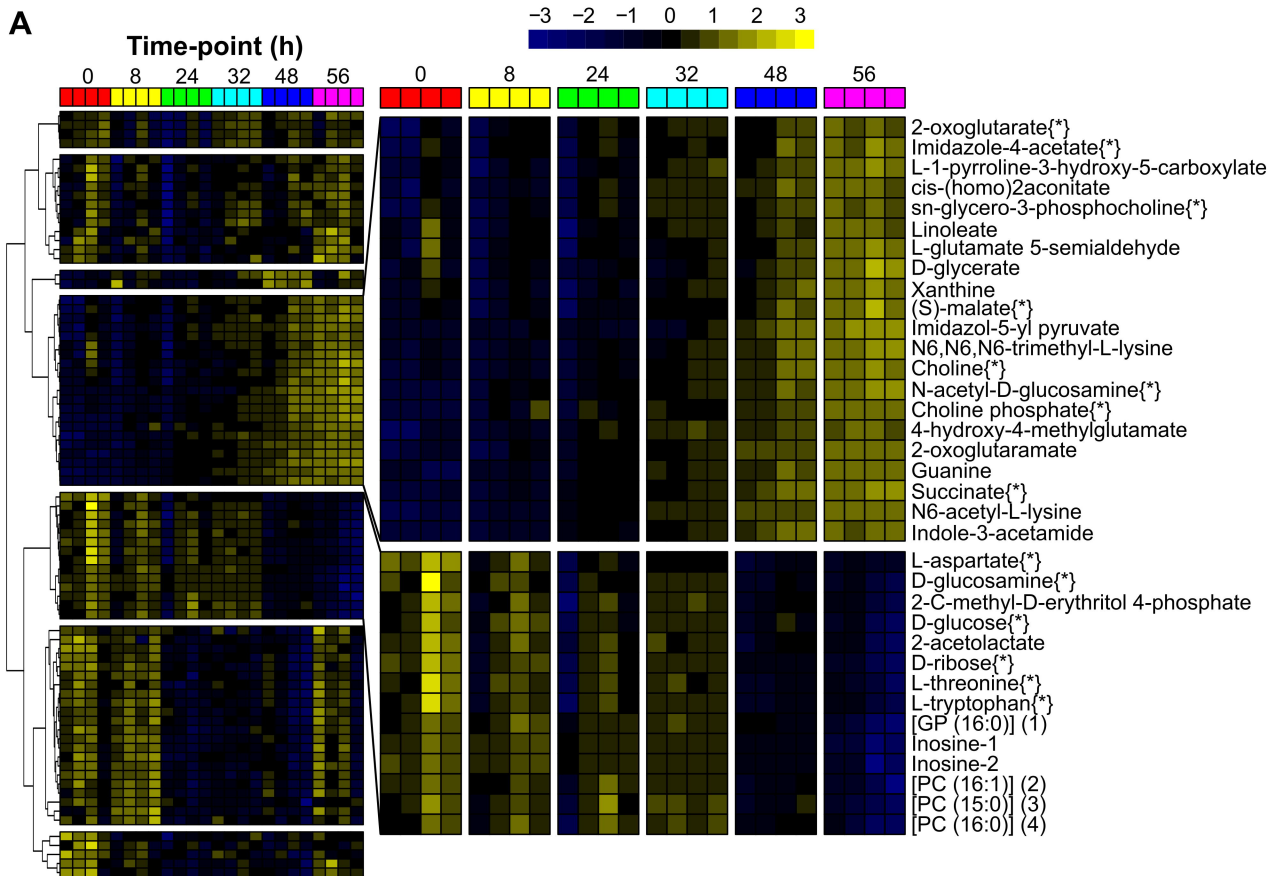
- 1754 technique and determined with three different hand-held devices. *BMC Vet Res.*  
1755 2016;12: 34. doi: 10.1186/s12917-016-0662-3.
- 1756 101. Nafikov RA, Beitz DC. Carbohydrate and lipid metabolism in farm animals. *J Nutr.*  
1757 2007;137(3): 702-5. doi: 10.1093/jn/137.3.702.
- 1758 102. Puppel K, Kuczynska B. Metabolic profiles of cow's blood; a review. *J Sci Food Agric.*  
1759 2016;96(13): 4321-8. doi: 10.1002/jsfa.7779.
- 1760 103. Bochud-Allemann N, Schneider A. Mitochondrial substrate level phosphorylation is  
1761 essential for growth of procyclic *Trypanosoma brucei*. *J Biol Chem.* 2002;277(36):  
1762 32849-54. doi: 10.1074/jbc.M205776200.
- 1763 104. Mochizuki K, Inaoka DK, Mazet M, Shiba T, Fukuda K, Kurasawa H, et al. The  
1764 ASCT/SCS cycle fuels mitochondrial ATP and acetate production in *Trypanosoma*  
1765 *brucei*. *Biochim Biophys Acta Bioenerg.* 2020;1861(11): 148283. doi:  
1766 10.1016/j.bbabi.2020.148283.
- 1767 105. Verner Z, Skodova I, Polakova S, Durisova-Benkovicova V, Horvath A, Lukes J.  
1768 Alternative NADH dehydrogenase (NDH2): intermembrane-space-facing counterpart of  
1769 mitochondrial complex I in the procyclic *Trypanosoma brucei*. *Parasitology.* 2013;140(3):  
1770 328-37. doi: 10.1017/S003118201200162X.
- 1771 106. Fang J, Beattie DS. Novel FMN-containing rotenone-insensitive NADH  
1772 dehydrogenase from *Trypanosoma brucei* mitochondria: isolation and characterization.  
1773 *Biochemistry.* 2002;41(9): 3065-72. doi: 10.1021/bi015989w.
- 1774 107. Dewar CE, MacGregor P, Cooper S, Gould MK, Matthews KR, Savill NJ, et al.  
1775 Mitochondrial DNA is critical for longevity and metabolism of transmission stage  
1776 *Trypanosoma brucei*. *PLoS Pathog.* 2018;14(7): e1007195. doi:  
1777 10.1371/journal.ppat.1007195.
- 1778 108. Tizard IR, Mellors A, Holmes WL, Nielsen K. The generation of phospholipase A and  
1779 hemolytic fatty acids by autolysing suspensions of *Trypanosoma congolense*.  
1780 *Tropenmed Parasitol.* 1978;29(1): 127-33.
- 1781 109. Field MC, Horn D, Fairlamb AH, Ferguson MAJ, Gray DW, Read KD, et al. Anti-  
1782 trypanosomatid drug discovery: an ongoing challenge and a continuing need. *Nat Rev*  
1783 *Microbiol.* 2017;15(7): 447. doi: 10.1038/nrmicro.2017.69.
- 1784 110. Hirumi H, Hirumi K. Axenic culture of African trypanosome bloodstream forms.  
1785 *Parasitol Today.* 1994;10(2): 80-4.
- 1786 111. Vassella E, Kramer R, Turner CM, Wankell M, Modes C, van den Bogaard M, et al.  
1787 Deletion of a novel protein kinase with PX and FYVE-related domains increases the rate  
1788 of differentiation of *Trypanosoma brucei*. *Mol Microbiol.* 2001;41(1): 33-46.

- 1789 112. Hirumi H, Hirumi K. Continuous cultivation of *Trypanosoma brucei* blood stream  
1790 forms in a medium containing a low concentration of serum protein without feeder cell  
1791 layers. *J Parasitol.* 1989;75(6): 985-9.
- 1792 113. Herbert WJ, Lumsden WH. *Trypanosoma brucei*: a rapid "matching" method for  
1793 estimating the host's parasitemia. *Exp Parasitol.* 1976;40(3): 427-31. doi: 10.1016/0014-  
1794 4894(76)90110-7.
- 1795 114. Lanham SM, Godfrey DG. Isolation of salivarian trypanosomes from man and other  
1796 mammals using DEAE-cellulose. *Exp Parasitol.* 1970;28(3): 521-34. doi: 10.1016/0014-  
1797 4894(70)90120-7.
- 1798 115. Schumann Burkard G, Jutzi P, Roditi I. Genome-wide RNAi screens in bloodstream  
1799 form trypanosomes identify drug transporters. *Mol Biochem Parasitol.* 2011;175(1): 91-  
1800 4. doi: 10.1016/j.molbiopara.2010.09.002.
- 1801 116. Raz B, Iten M, Grether-Buhler Y, Kaminsky R, Brun R. The Alamar Blue assay to  
1802 determine drug sensitivity of African trypanosomes (*T.b. rhodesiense* and *T.b.*  
1803 *gambiense*) in vitro. *Acta Trop.* 1997;68(2): 139-47. doi: 10.1016/s0001-706x(97)00079-  
1804 x.
- 1805 117. Untergasser A, Cutcutache I, Koressaar T, Ye J, Faircloth BC, Remm M, et al.  
1806 Primer3--new capabilities and interfaces. *Nucleic Acids Res.* 2012;40(15): e115. doi:  
1807 10.1093/nar/gks596.
- 1808 118. Tihon E, Imamura H, Van den Broeck F, Vermeiren L, Dujardin JC, Van Den Abbeele  
1809 J. Genomic analysis of Isometamidium Chloride resistance in *Trypanosoma congolense*.  
1810 *Int J Parasitol Drugs Drug Resist.* 2017;7(3): 350-61. doi: 10.1016/j.ijpddr.2017.10.002.
- 1811 119. Livak KJ, Schmittgen TD. Analysis of relative gene expression data using real-time  
1812 quantitative PCR and the 2<sup>-</sup>(Delta Delta C(T)) Method. *Methods.* 2001;25(4): 402-8. doi:  
1813 10.1006/meth.2001.1262.
- 1814 120. Smith CA, Want EJ, O'Maille G, Abagyan R, Siuzdak G. XCMS: processing mass  
1815 spectrometry data for metabolite profiling using nonlinear peak alignment, matching, and  
1816 identification. *Anal Chem.* 2006;78(3): 779-87. doi: 10.1021/ac051437y.
- 1817 121. Scheltema RA, Jankevics A, Jansen RC, Swertz MA, Breitling R. PeakML/mzMatch:  
1818 a file format, Java library, R library, and tool-chain for mass spectrometry data analysis.  
1819 *Anal Chem.* 2011;83(7): 2786-93. doi: 10.1021/ac2000994.
- 1820 122. Creek DJ, Jankevics A, Burgess KE, Breitling R, Barrett MP. IDEOM: an Excel  
1821 interface for analysis of LC-MS-based metabolomics data. *Bioinformatics.* 2012;28(7):  
1822 1048-9. doi: 10.1093/bioinformatics/bts069.
- 1823 123. Chokkathukalam A, Jankevics A, Creek DJ, Achcar F, Barrett MP, Breitling R.  
1824 mzMatch-ISO: an R tool for the annotation and relative quantification of isotope-labelled

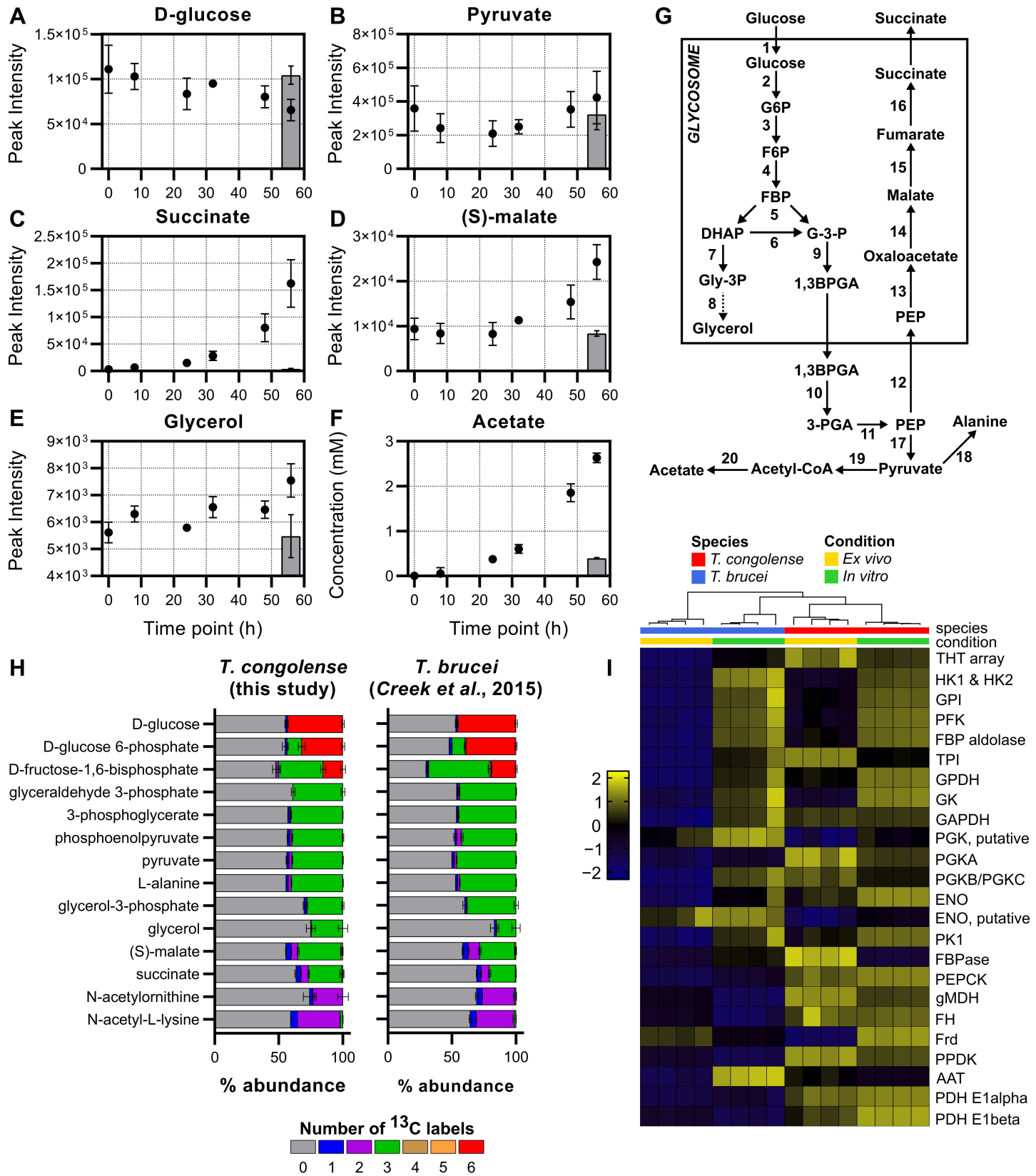
- 1825 mass spectrometry data. *Bioinformatics*. 2013;29(2): 281-3. doi:  
1826 10.1093/bioinformatics/bts674.
- 1827 124. Chong J, Xia J. Using MetaboAnalyst 4.0 for Metabolomics Data Analysis,  
1828 Interpretation, and Integration with Other Omics Data. *Methods Mol Biol*. 2020;2104:  
1829 337-60. doi: 10.1007/978-1-0716-0239-3\_17.
- 1830 125. Kim D, Langmead B, Salzberg SL. HISAT: a fast spliced aligner with low memory  
1831 requirements. *Nat Methods*. 2015;12(4): 357-60. doi: 10.1038/nmeth.3317.
- 1832 126. Aslett M, Aurrecochea C, Berriman M, Brestelli J, Brunk BP, Carrington M, et al.  
1833 TriTrypDB: a functional genomic resource for the Trypanosomatidae. *Nucleic Acids Res*.  
1834 2010;38(Database issue): D457-62. doi: 10.1093/nar/gkp851.
- 1835 127. Li H, Handsaker B, Wysoker A, Fennell T, Ruan J, Homer N, et al. The Sequence  
1836 Alignment/Map format and SAMtools. *Bioinformatics*. 2009;25(16): 2078-9. doi:  
1837 10.1093/bioinformatics/btp352.
- 1838 128. Team. RC. R: A language and environment for statistical computing.: R Foundation  
1839 for Statistical Computing, Vienna, Austria.; 2013.
- 1840 129. Gu Z, Eils R, Schlesner M. Complex heatmaps reveal patterns and correlations in  
1841 multidimensional genomic data. *Bioinformatics*. 2016;32(18): 2847-9. doi:  
1842 10.1093/bioinformatics/btw313.
- 1843 130. Dolezelova E, Teran D, Gahura O, Kotrbova Z, Prochazkova M, Keough D, et al.  
1844 Evaluation of the *Trypanosoma brucei* 6-oxopurine salvage pathway as a potential  
1845 target for drug discovery. *PLoS Negl Trop Dis*. 2018;12(2): e0006301. doi:  
1846 10.1371/journal.pntd.0006301.
- 1847

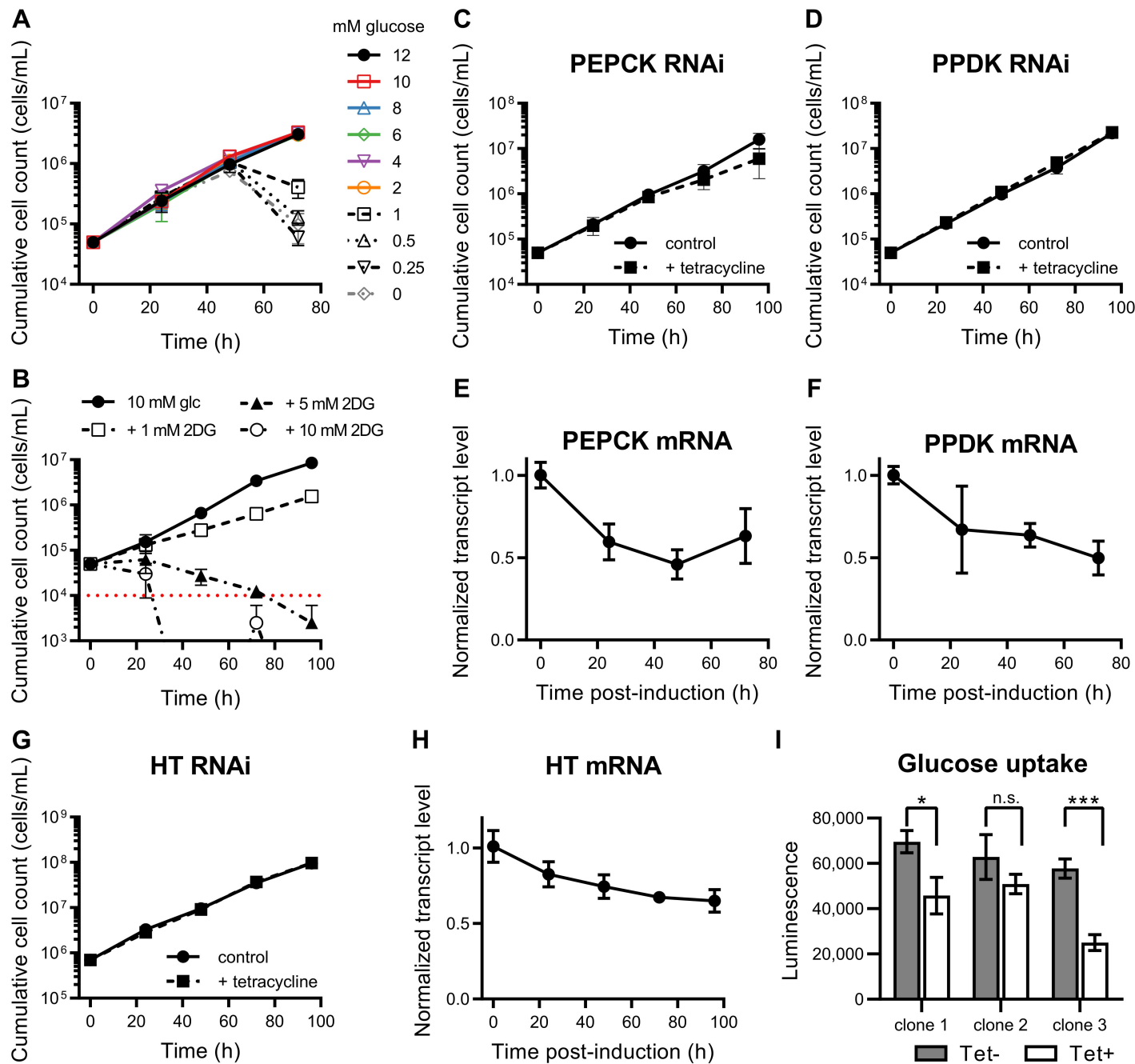


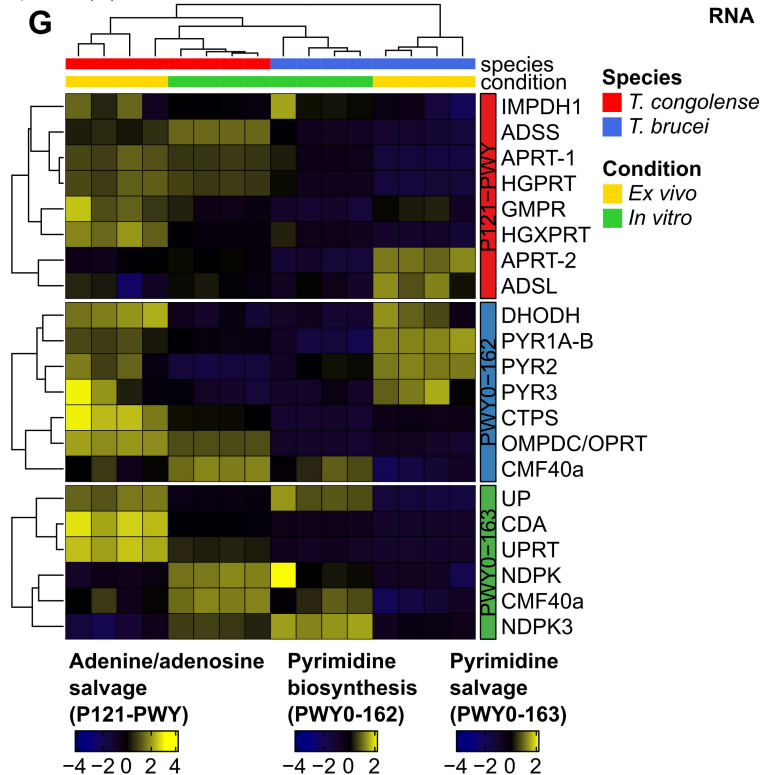
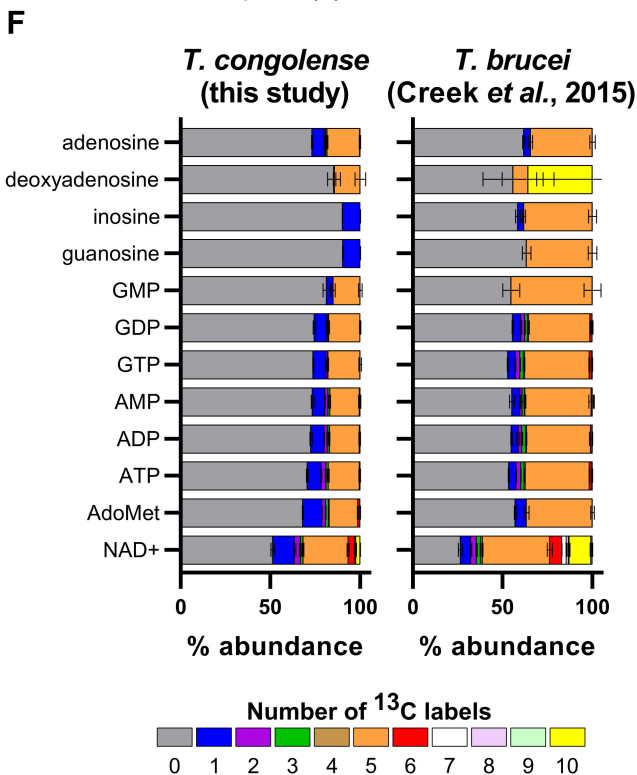
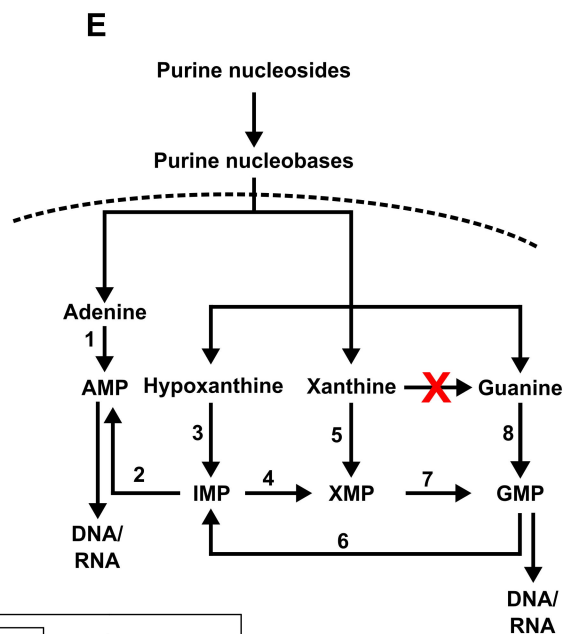
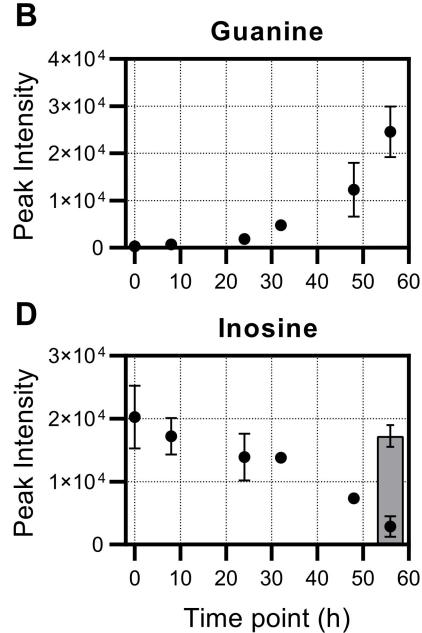
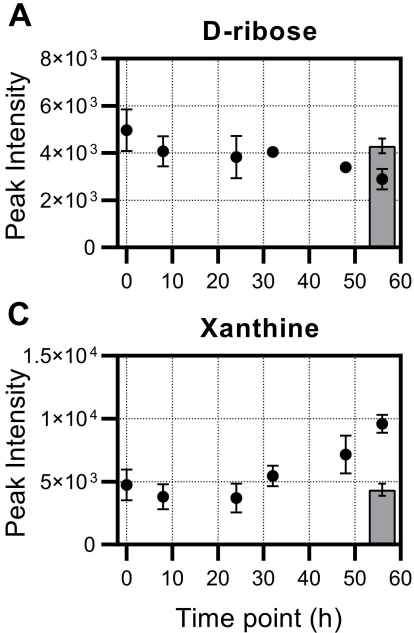


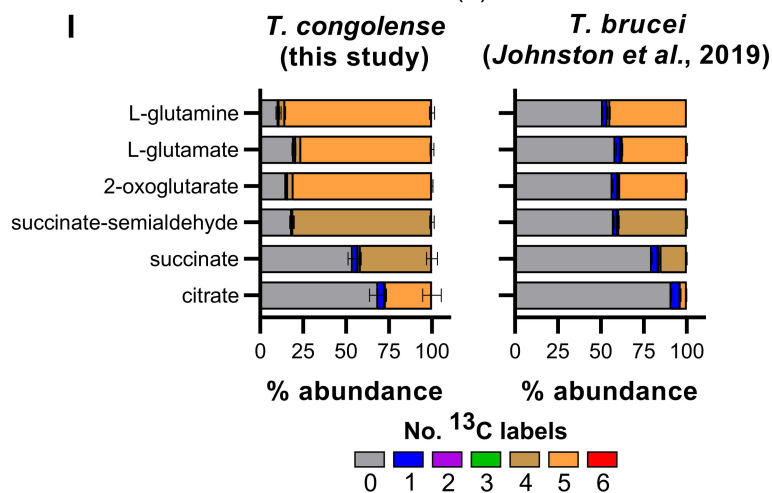
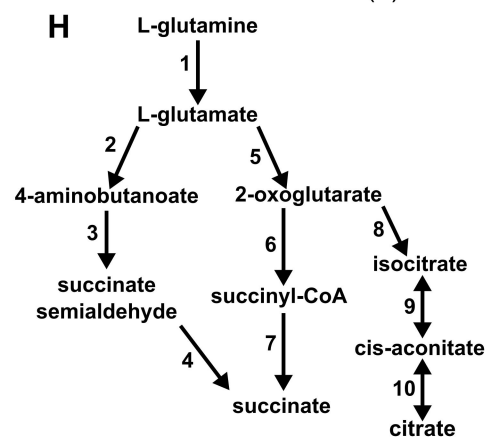
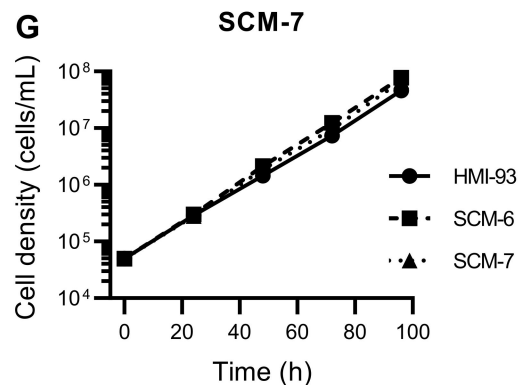
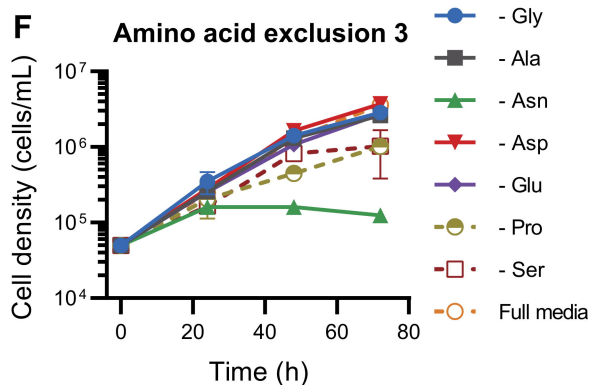
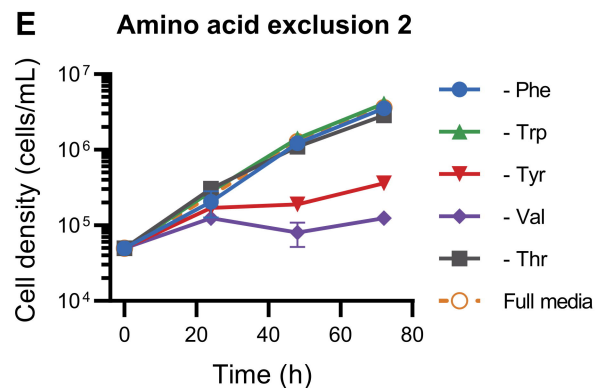
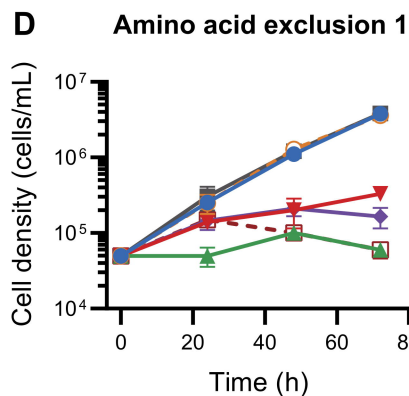
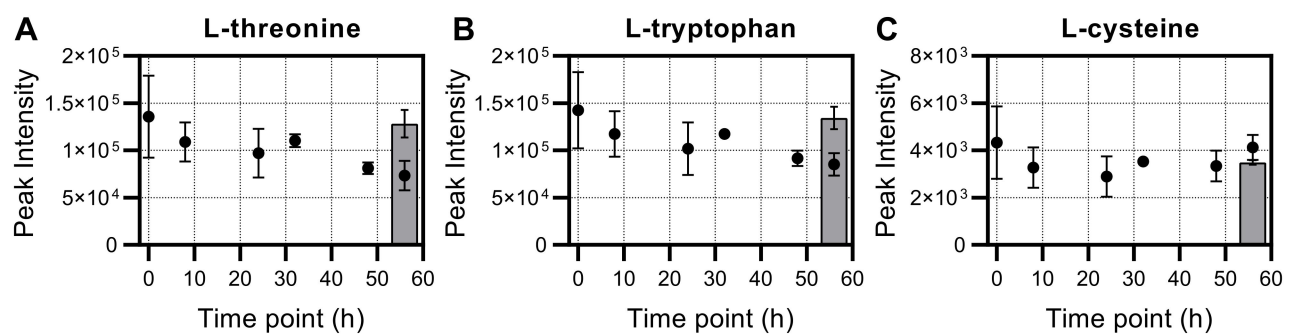


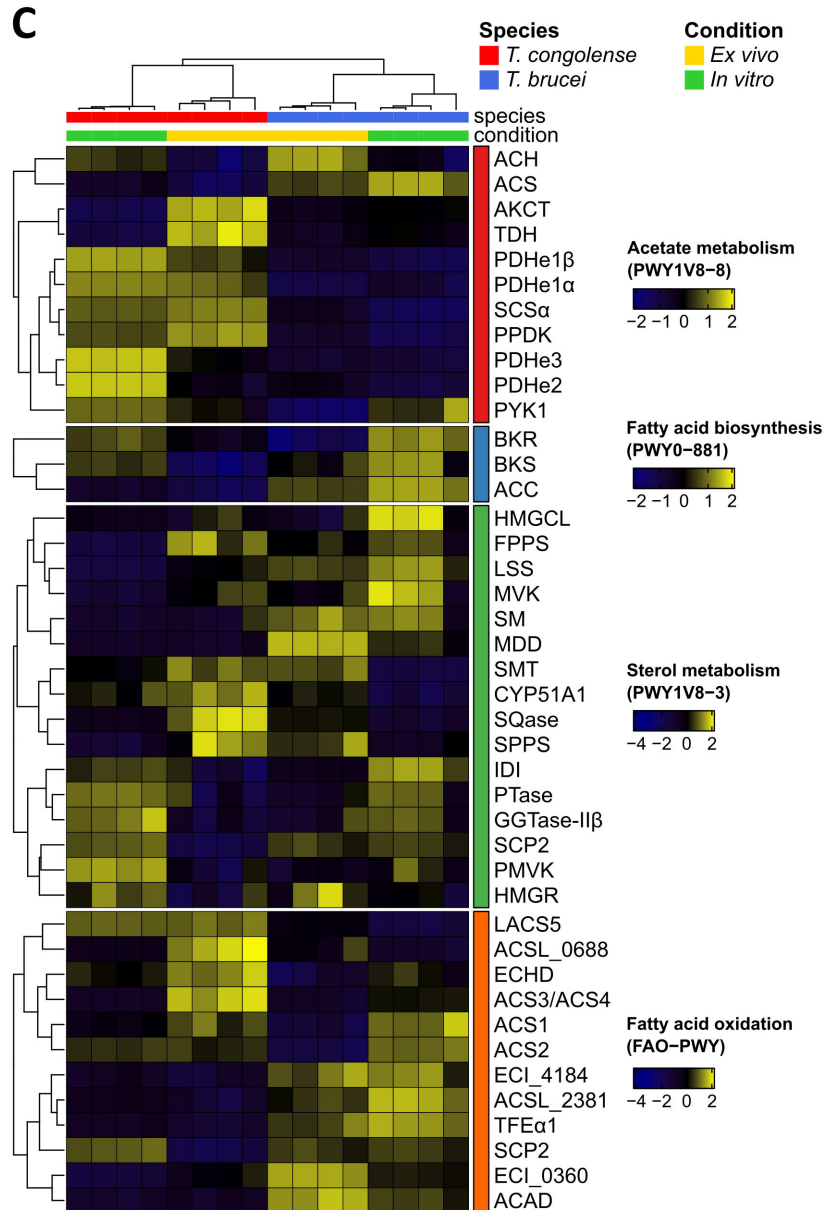
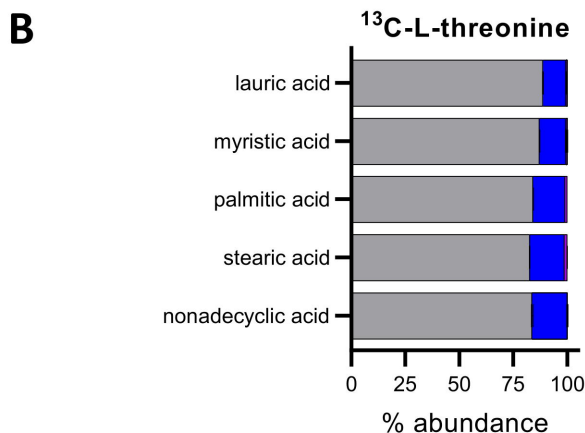
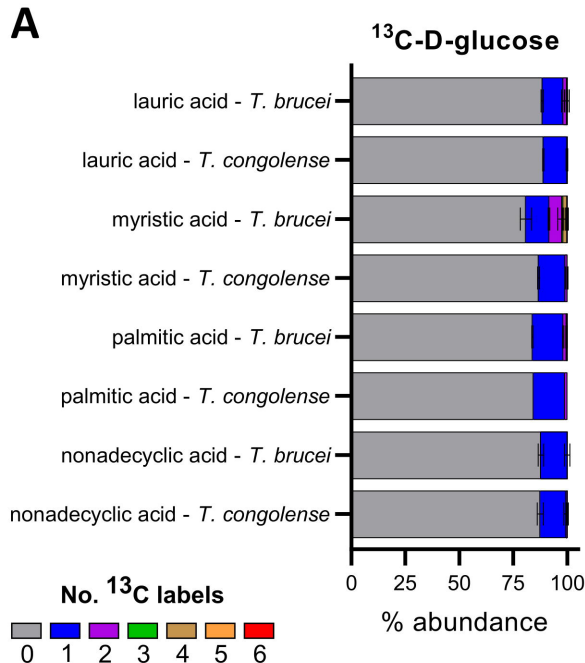
1. Guanine
2. N6-acetyl-L-lysine
3. Succinate
4. 4-hydroxy-4-methylglutamate
5. N6,N6,N6-trimethyl-L-lysine
6. Choline
7. 2-oxoglutarate
8. L-1-pyrroline-3-hydroxy-5-carboxylate
9. D-glycerate
10. Pyruvate
11. 12-hydroxydodecanoic acid
12. L-cystine
13. Diacetyl
14. PC(18:0)
15. LysoPC(17:0)
16. PC(16:0)
17. Inosine
18. PC(16:1)
19. FA trihydroxyl(18:1)
20. Inosine

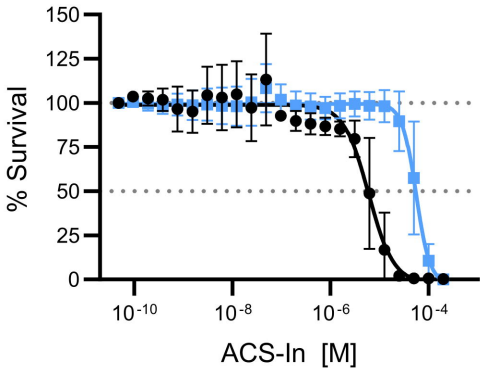
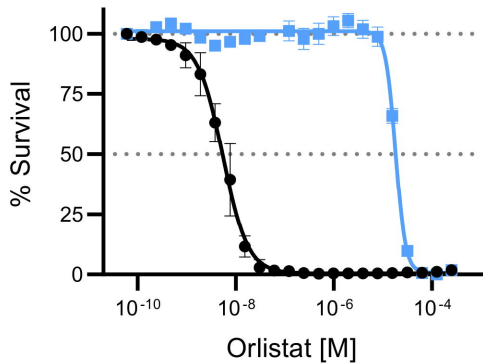


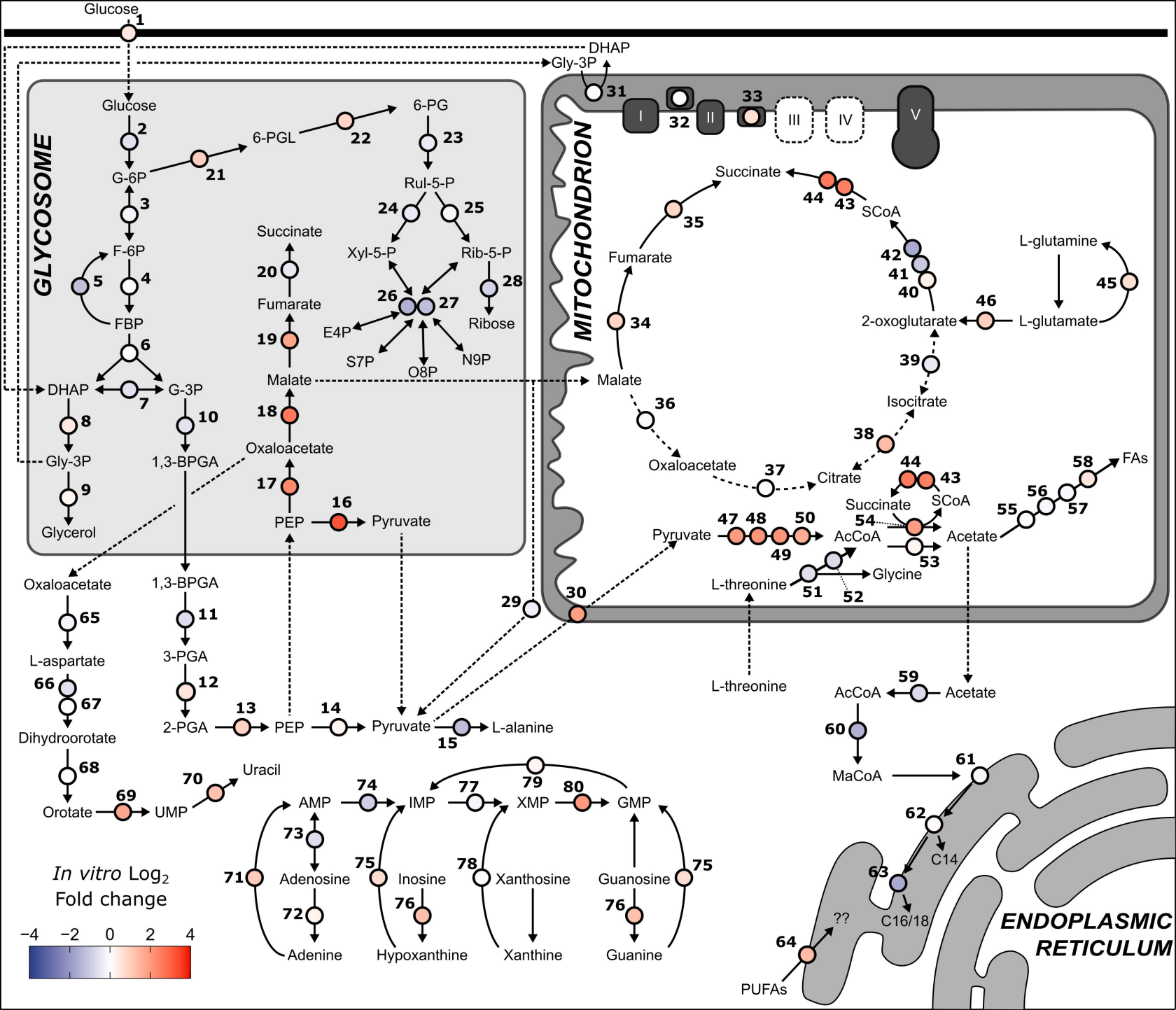




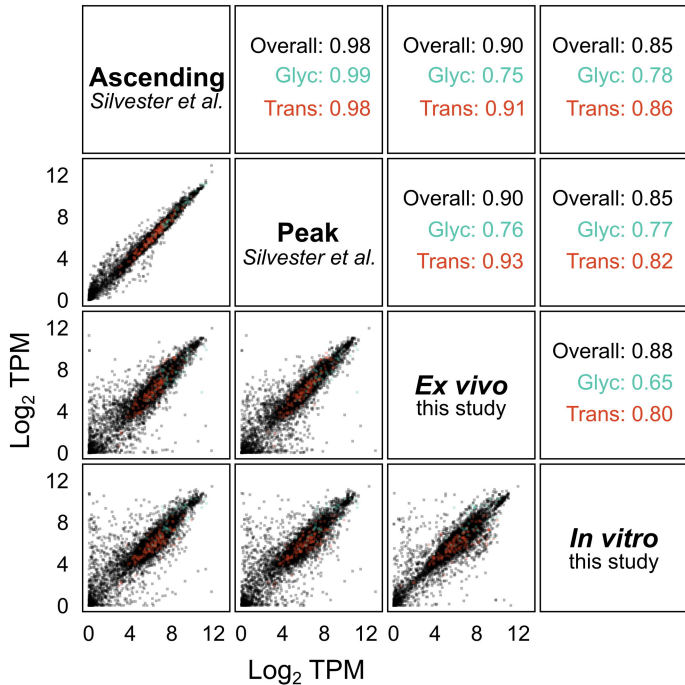


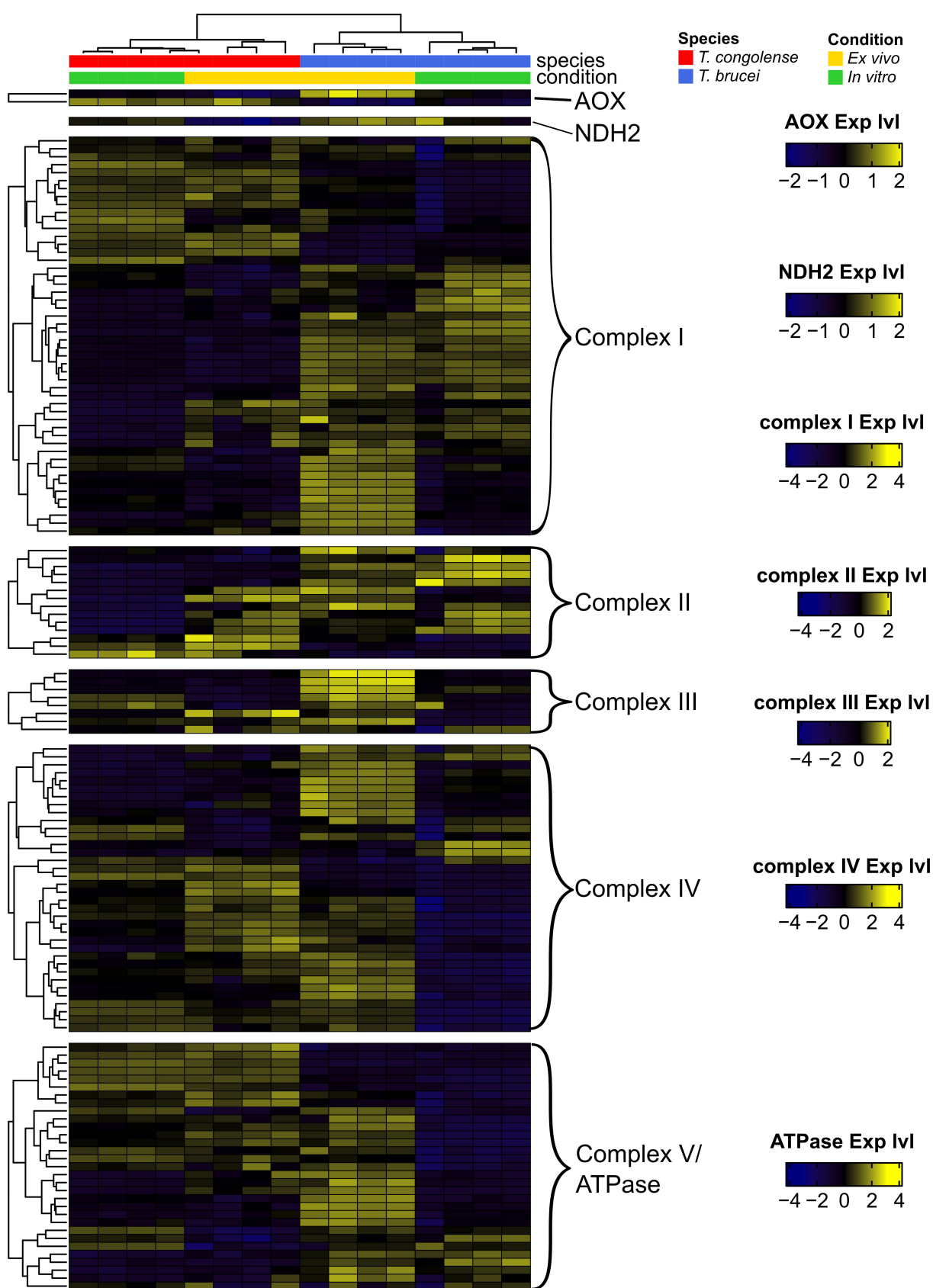


**A****ACS inhibitor**● *T. brucei*■ *T. congolense***B****Orlistat**

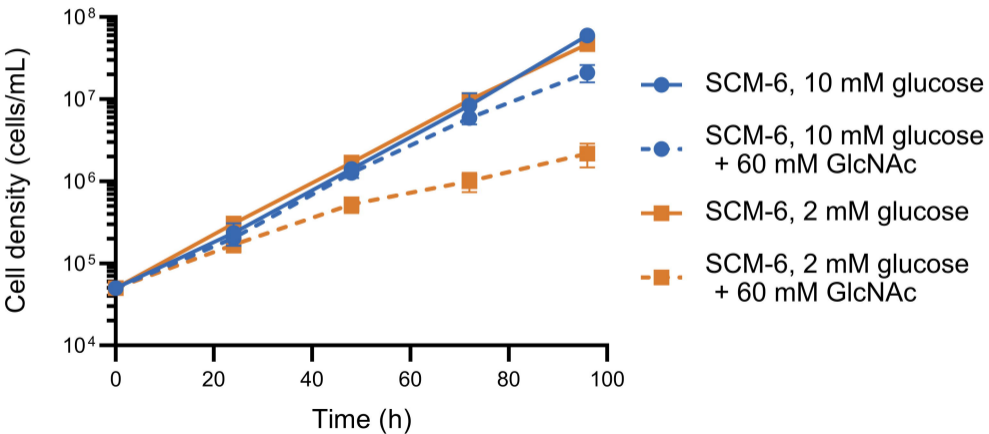






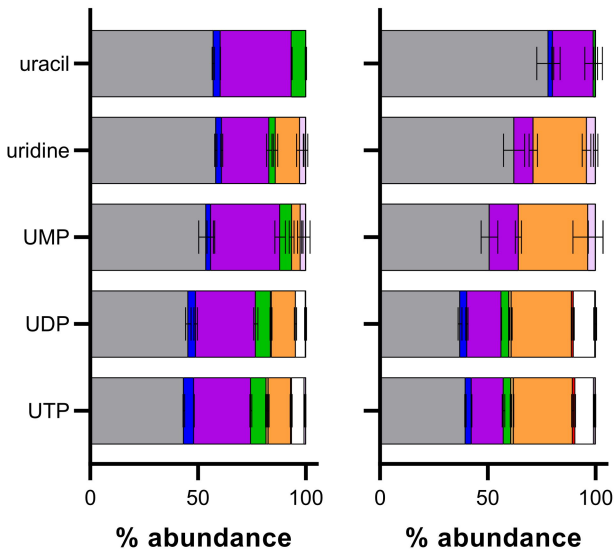


# *T. congolense* growth ± N-acetyl-D-glucosamine



*T. congolense*  
(this study)

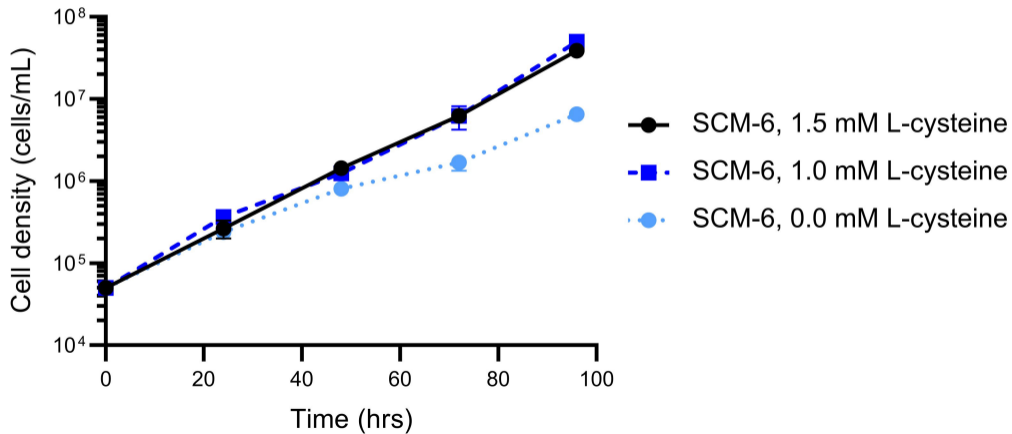
*T. brucei*  
(Creek et al., 2015)

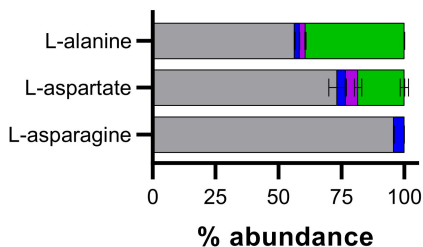
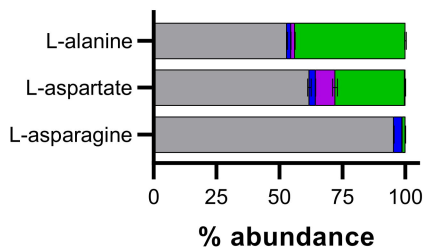


No. <sup>13</sup>C labels



# *T. congolense* growth ± L-cysteine



**A*****T. congolense***  
**(this study)*****T. brucei***  
**(Creek et al., 2015)****Number of <sup>13</sup>C labels****B**